

**FEASIBILITY STUDY OF A CONTROLLABLE
MECHANICAL SEAL FOR REACTOR COOLANT
PUMPS**

A Thesis
Presented to
The Academic Faculty

by

John Wilson Payne

In Partial Fulfillment
of the Requirements for the Degree
Master of Science in the
Woodruff School of Mechanical Engineering

Georgia Institute of Technology
May 2013

**FEASIBILITY STUDY OF A CONTROLLABLE
MECHANICAL SEAL FOR REACTOR COOLANT
PUMPS**

Approved by:

Dr. Richard Salant, Advisor
Woodruff School of Mechanical Engineering
Georgia Institute of Technology

Dr. Jeffrey Streater
Woodruff School of Mechanical Engineering
Georgia Institute of Technology

Dr. Scott Bair
Woodruff School of Mechanical Engineering
Georgia Institute of Technology

Date Approved: 28 March 2013

ACKNOWLEDGEMENTS

The author wishes to acknowledge the vital contributions of several individuals during his Master's studies. First, Dr. Richard Salant, for his advice, expertise, and mentoring, as well as for his assistance during the writing of this thesis. In addition, Dr. Wayne Book, for his assistance in the design of the proposed control systems. Also, Dr. Jeffrey Streater and Dr. Scott Bair, for their participation in the reading committee and approval of the thesis.

The author thanks his family, especially his wife, Jennifer Payne, for her constant love and support and her patience throughout the process of graduate school. Also, his parents, John and Helen Payne, for their support in every manner possible for over 23 years.

Finally, the author wishes to express his thanks to Mr. Gary Boles of the Electric Power Research Institute and the many participants in EPRI Technical Advisory Group meetings over the course of this project. This project was funded by the Electric Power Research Institute, under grant EP-P39081/C17361.

TABLE OF CONTENTS

ACKNOWLEDGEMENTS	iii
LIST OF TABLES	vii
LIST OF FIGURES	viii
NOMENCLATURE	xi
SUMMARY	xiii
I INTRODUCTION	1
1.1 Objectives	2
II BACKGROUND	4
2.1 Mechanical Seal Theory	4
2.1.1 General Characteristics of Mechanical Seals	4
2.1.2 The Face Gap	5
2.1.3 The Floating Face	6
2.1.4 Hydrostatic Seals	8
2.1.5 Production of Coning	12
2.1.6 Hydrodynamic Seals	12
2.2 The Nuclear Reactor Coolant Pump Seals	13
2.3 Causes of Abnormal Seal Leakoff	15
2.3.1 Electrophoresis	16
2.3.2 Particulate Contamination	18
2.3.3 Reactor Coolant Pump Transients	18
2.3.4 Temperature and Pressure Excursions	19
2.4 Abnormal Seal Leakoff Mitigation Strategies	20
2.4.1 Changing Seal Injection Water Temperature	21
2.4.2 Seal Injection Filter Replacement to Alter Reactor Coolant System Chemistry	22
2.5 Previous Controllable Seals	24

III	PROPOSED CONTROLLABLE SEALS AND SEAL MODELING	30
3.1	Proposed Controllable Seals	30
3.1.1	Motivation	30
3.1.2	Proposal	30
3.2	Modeling	31
3.2.1	Purpose	31
3.2.2	Methods	31
3.2.3	Language and Scripting	33
3.3	Geometry and Materials	33
3.3.1	Dimension Approximation	33
3.3.2	Materials	35
3.3.3	Hydraulic Actuation Geometry	37
3.3.4	Piezoelectric Actuation Geometry	38
3.4	Fluid Mechanics Analysis	40
3.5	Deformation Analysis	44
3.6	Force Balance	47
3.7	Iteration Process	47
3.8	Potential Control Systems	50
3.8.1	Hydraulic Control System	51
3.8.2	Piezoelectric Control System	52
IV	RESULTS	54
4.1	Hydraulic Actuation Results - Varying Leakage Rates	54
4.1.1	Stainless Steel Face	55
4.1.2	Carbon Graphite Face	62
4.2	Piezoelectric Actuation Results - Varying Leakage Rates	69
4.2.1	Full Piezoelectric Seal Face	70
4.2.2	Piezoelectric Seal Face with Carbon Graphite Layer	70
4.3	Hydraulic and Piezoelectric Results - Restoring Nominal Leakage Rates	73

4.3.1	Steel Hydraulic Seal	74
4.3.2	Carbon Graphite Hydraulic Seal	76
4.3.3	Piezoelectric Seal	79
4.3.4	Piezoelectric Seal with Graphite Layer	81
4.4	Stress Results	83
V	CONCLUSION	86
5.1	Future Work	88
	APPENDIX A — WESTINGHOUSE REACTOR COOLANT PUMP AND SEAL ASSEMBLY DIAGRAMS	90
	REFERENCES	95

LIST OF TABLES

3.1	Seal Face Dimensions	33
3.2	Elastic Properties of Modeled Materials	36
3.3	Relative Dielectric Constants of Modeled PZT-4	36
4.1	Stainless Steel, Base Coning Leakage Study	58
4.2	Stainless Steel, Increased Closing Force Leakage Study	59
4.3	Stainless Steel, Reduced Pre-Coning Leakage Study	61
4.4	Carbon Graphite Base Case	64
4.5	Carbon Graphite, Reduced Closing Force Leakage Study	66
4.6	Carbon Graphite, Increased Closing Force Leakage Study	67
4.7	Full Piezoelectric Seal Leakage Study	71
4.8	Piezoelectric Seal with Carbon Graphite Layer Leakage Study	72
4.9	Stainless Steel, Restoring Nominal Leakage Rate	76
4.10	Carbon Graphite, Restoring Nominal Leakage Rate	77
4.11	Full Piezoelectric Seal, Restoring Nominal Leakage Rate	79
4.12	Piezoelectric Seal with Carbon Graphite Layer, Restoring Nominal Leakage Rate	81

LIST OF FIGURES

2.1 Schematic of a General Mechanical Seal [5]	5
2.2 Forces Acting on a Floating Seal Face [5]	6
2.3 Positive Coning of Seal Faces [5]	8
2.4 Sealed Pressure Distribution with Varied Coning [5]	10
2.5 Controllable Seal Schematic for Boiler Feedwater Pump [14]	25
2.6 Transient Performance in Uncontrolled Seal [14]	26
2.7 Transient Performance in Controlled Seal [14]	27
2.8 Controllable Seal for LOX Turbopump [15]	27
2.9 Duty Cycle for LOX Turbopump Seal [16]	28
2.10 Controllable Seal Performance for Fixed Leakage Rate [16]	28
2.11 Controllable Seal Performance for Fixed Face Temperature [16]	29
3.1 Hydraulic Actuation Seal Model (dimensions in mm)	37
3.2 Piezoelectric Actuation Seal Model (dimensions in mm)	39
3.3 Piezoelectric Actuation Seal Model with Carbon Graphite Coating (dimensions in mm)	39
3.4 Typical Sealed Pressure Distribution	44
3.5 Typical ABAQUS Hydraulic Deformation Output (mm)	45
3.6 Typical ABAQUS Piezoelectric Deformation Output (mm)	46
3.7 Typical Film Thickness Distribution	46
3.8 Computational Procedure	49
3.9 Proposed Hardware-Based Hydraulic Control System	52
3.10 Proposed Software-Based Hydraulic Control System	53
3.11 Proposed Piezoelectric Control System	53
4.1 Typical Film Thickness and Pre-Coning for Steel Face	56
4.2 Typical Sealed Pressure Distribution for Steel Face	57
4.3 Leakage Rate vs. Cavity 1 Pressure, Steel, Base Case	58
4.4 Leakage Rate vs. Cavity 1 Pressure, Steel, Increased Closing Force	60

4.5	Leakage Rate vs. Cavity 1 Pressure, Steel, Reduced Pre-Coning . . .	61
4.6	Typical Film Thickness Distribution for Carbon Graphite Seal Face .	63
4.7	Typical Sealed Pressure Distribution for Carbon Graphite Seal Face .	63
4.8	Leakage Rate vs. Cavity 1 Pressure, Carbon Graphite, Base Case . .	65
4.9	Leakage Rate vs. Cavity 1 Pressure, Carbon Graphite, Reduced Clos- ing Force	66
4.10	Leakage Rate vs. Cavity 1 Pressure, Carbon Graphite, Increased Clos- ing Force	68
4.11	Typical Film Thickness Distribution for Piezoelectric Seal Face	69
4.12	Typical Sealed Pressure Distribution for Piezoelectric Seal Face . . .	70
4.13	Leakage Rate vs. Voltage, Full Piezoelectric Seal Face	71
4.14	Leakage Rate vs. Voltage, Piezoelectric Seal Face with Carbon Graphite Layer	72
4.15	Steel, Control Pressure to Restore Nominal Leakage Rate vs. Closing Force	75
4.16	Steel, Control Pressure to Restore Nominal Leakage Rate vs. Uncon- trolled Leakage Rate	75
4.17	Carbon Graphite, Control Pressure to Restore Nominal Leakage Rate vs. Closing Force	78
4.18	Carbon Graphite, Control Pressure to Restore Nominal Leakage Rate vs. Uncontrolled Leakage Rate	78
4.19	Piezoelectric Voltage to Restore Nominal Leakage Rate vs. Closing Force, Full Piezoelectric Seal	80
4.20	Piezoelectric Voltage to Restore Nominal Leakage Rate vs. Uncor- rected Leakage Rate, Full Piezoelectric Seal	80
4.21	Piezoelectric Voltage to Restore Nominal Leakage Rate vs. Closing Force, Piezoelectric Seal with Carbon Graphite Layer	82
4.22	Piezoelectric Voltage to Restore Nominal Leakage Rate vs. Uncor- rected Leakage Rate, Piezoelectric Seal with Carbon Graphite Layer .	82
4.23	Von Mises Effective Stress at Maximum Control Pressures, Steel Hy- draulic Seal	84
4.24	Von Mises Effective Stress at Maximum Control Pressures, Carbon Graphite Hydraulic Seal	85

4.25 Von Mises Effective Stress at 5000 V, Piezoelectric Seal with Carbon Graphite Layer	85
A.1 Westinghouse Reactor Coolant Pump and Motor Assembly [4]	91
A.2 Sectional View of Westinghouse RCP [4]	92
A.3 Typical Westinghouse #1 Seal [4]	93
A.4 Flow Diagram Sectional, RCP Models 93-A1 and 100 [4]	94

NOMENCLATURE

A'	Area of rear of floating face
A_f	Area of sealing surface of floating face
a_i	TDMA method coefficient
b_i	TDMA method coefficient
c_i	TDMA method coefficient
d	Piezoelectric strain-charge relation matrix
d_i	TDMA method coefficient
Δf	Difference between opening and closing force
$F_{closing}$	Closing Force
$F_{contact}$	Contact force
$F_{opening}$	Opening Force
F_{spring}	Spring force on rear of floating face
h	Film thickness
h_1	Film thickness at r_{coning}
h_2	Film thickness at outer radius in a dual-taper seal
h_{avg}	Average Film Thickness
h_m	Minimum film thickness (located at inner radius of seal face)
N_B	Seal Balance Ratio
Δp	Pressure drop across seal face
p	Sealed pressure distribution in face gap
P_1, P_2, P_3	Control pressures in seal face cavities, left to right
P_i	Numerical value of sealed pressure distribution at i^{th} node
p_s	Sealed Pressure
Q	Leakage Rate
r	Radial coordinate

r_b	Balance radius of seal face
r_{coning}	Radius at which coning angle changes in a dual-taper seal
r_i	Inner radius of seal face
r_o	Outer radius of seal face
U	Relative tangential velocity between seal faces
v_θ	Relative circumferential velocity
v_r	Relative radial velocity
X_i	TDMA recurrence relation coefficient
Y_i	TDMA recurrence relation coefficient

Greek Symbols:

α_1	First coning angle in a dual-taper seal
α_2	Second coning angle in a dual-taper seal
δ	Coning
θ	Circumferential coordinate
μ	Viscosity of sealed fluid

SUMMARY

In a nuclear power plant, one of the most important systems for both safety and performance is the reactor cooling system. The cooling system is generally driven by one or more very large centrifugal pumps. Most reactor coolant pumps utilize a multi-stage mechanical face seal system for fluid containment. As a result, these seal systems are critical to safe, continued operation of a nuclear reactor. Without adequate sealing, loss of coolant volume can occur, and a reactor may be forced to shut down, costing the operating utility significantly until it can be brought online again.

The main advantage of mechanical face seals is their self-adjusting properties. These seals are tuned so that they automatically adjust to varying fluid conditions to provide adequate leakage control. Because of the enormous pressures, complicated water chemistry, and possible large temperature transients, the mechanical seals inside a reactor coolant pump must be some of the most robust seals available. In addition, their long service life and continuous operation demand durability and the capability to adjust to a wide range of conditions. However, over time, wear, chemical deposition, or changing operating conditions can alter the face gap, which is the critical geometry between the sealing faces of a seal. An altered face gap can lead to undesirable conditions of too much or not enough leakage, which must be maintained within a certain range to provide lubrication and cooling to the seal faces without resulting in uncontrolled coolant volume loss. Nuclear power plants operate within strict leakage ranges, and long-term effects causing undesirable leakage can eventually necessitate a reactor shutdown if the seal cannot self-adjust to control the leakage.

This document will examine possible causes of undesirable leakage rates in a

commonly-used reactor coolant pump assembly. These causes will be examined to determine the conditions which promote them, the physical explanation for their effect on the operation of a mechanical seal, and possible methods of mitigation of both the cause and its effect. These findings are based on previous publications by utilities and technical and incident reports from reactor stations which detail actual incidents of abnormal seal performance and their root causes as determined by the utilities. Next, a method of increasing the ability of a mechanical seal to adapt to a wider range of conditions will be proposed. This method involves modifying an existing seal face to include a method of active control. This active control focuses on deliberately deforming one face of the mechanical sealing face pair. This deformation alters the face gap in order to make the fluid conditions inside the face gap more preferable, generating more or less leakage as desired. Two methods of actuation, hydraulic pressure and piezoelectric deformation, will be proposed.

Finally, a model of the actively controlled seal faces will be introduced. This model includes a method of numerically solving the Reynolds equation to determine the fluid mechanics that drive the lubrication problem in the seal face and coupling the solution with a deformation analysis in a finite element model of a seal face. The model solves iteratively until a converged solution of a sealed pressure distribution, a resulting face deformation, and a calculated leakage rate is reached. The model includes a study of the effects of induced deformation in the seal via both hydraulic and piezoelectric actuation and the ability of this deformation to control the leakage rate.

CHAPTER I

INTRODUCTION

Nuclear power plants rely on cooling systems to ensure safe, continuous operation of the nuclear reactor. Because of the large amount of heat generated by the fission reaction, the cooling systems demand a large volumetric flow of water to maintain a safe temperature. The cooling water is usually supplied by one or more large centrifugal pumps. In order to maintain pump pressure and restrict water volume loss, the pumps typically utilize a multi-stage mechanical face seal system. These seals must operate with large pressure drops, potentially harsh water chemistry, and possible high temperature excursions during their service life. As such, the seals used in nuclear reactor coolant pumps (RCPs) must be some of the most robust seals available.

Mechanical seals are chosen for RCP sealing needs because of their self-adjusting properties. These seals are designed to adjust automatically to varying fluid conditions to provide the required sealing behavior. Over the service life of an RCP seal, it must operate continuously within a specified range of leakage rates. The designed leakage rate serves to lubricate the gap between the seal faces, or the face gap, while minimizing overall fluid loss. This lubrication prevents the seal faces from coming into contact, which can cause accelerated wear and damage, jeopardizing sealing integrity, and serves to cool the sealing components. The leakage rate of a mechanical seal is dependent on a variety of factors, including seal geometry and operating conditions. Two of the most important characteristics of a seal system are the face gap, or the average distance between the two seal faces, and the coning, or the taper of the face gap from the inner diameter of the seal ring to the outer diameter. In addition, the

face gap and the coning are dependent on one another.

Nuclear power stations can experience difficulties over the service life of a seal due to a number of factors. Due to continuous operation and long service lives, seal systems can experience gradual deviation from normal leakage rates. Most often, these deviations are caused by an altered face gap. Over time, wear or chemical deposition can alter the face geometry of the seals, changing the behavior of the lubricating film and altering the face gap to produce too little or too much fluid leakage. If the leakage rate cannot be returned to an acceptable range, the nuclear reactor may be required to perform an unplanned shutdown and replacement of the seal faces, which is extremely costly to the operating utility. Therefore, utilities are interested in extending both the service life of seal systems and the ability of those systems to adjust to changing reactor coolant system conditions.

1.1 Objectives

This document will examine causes of undesirable seal operation in a commonly-used reactor coolant pump assembly. These causes will be examined to determine the conditions which promote them, the underlying interactions which explain how they cause undesirable seal behavior, and possible methods for preventing or mitigating their impact. These findings are based on publications by utilities and technical and incident reports from nuclear power stations which record actual incidents of abnormal seal performance and the causes of that performance, as determined by the utilities. Incidents of seal failure often happen at two times: during reactor startup, when the seal fails to reach a steady state of satisfactory operation, and during continuous operation, when the seal started up correctly but experienced either gradual departure from normal leakage rates or catastrophic failure due to sudden loss of sealing integrity. Both types of failures will be examined, but the proposed solution will focus on correcting or preventing failures during continuous operation.

Next, a method of increasing the ability of a mechanical seal to adapt to reactor coolant system conditions will be introduced. This method involves modifying an existing seal face to include a method of active control. This active control is intended to induce a deformation in one face of the sealing face pair by actuation. This deformation alters the face gap in order to make the fluid conditions in the face gap more preferable, generating more or less leakage as desired. Two methods of actuation, hydraulic actuation by pressurizing a void in the seal face and piezoelectric actuation by polarizing a piezoelectric element, will be proposed.

Finally, a model of the actively controlled seal faces will be introduced. This model includes a numerical solution of the Reynolds equation to characterize the lubrication problem in the seal face and solve for the pressure distribution across the face gap. Also, a finite-element solution of the deformation of the seal face is included. The fluid mechanics and deformation solutions are coupled to characterize the effects of the sealed pressure and the active control on the leakage rate. The model will solve iteratively to reach a converged solution of the sealed pressure distribution, the resulting face deformation, and the calculated leakage rate. The active control methods are examined to determine the extent to which they can control the deformation of the seal face, and thus also the leakage rate produced by the seal.

CHAPTER II

BACKGROUND

2.1 Mechanical Seal Theory

2.1.1 General Characteristics of Mechanical Seals

Mechanical seals, or face seals, are devices used to restrict fluid flow out of a pressurized compartment in a rotating mechanism. A mechanical seal contains two annular faces which fit around a rotating shaft. One face is known as the runner or the rotor. This face is fixed to the shaft and rotates with it. The other face is known as the seal ring or the stator. This face is fixed to the device housing and does not rotate. Axially, one face is flexibly mounted, usually with a spring, such that it can travel along the shaft axis, and the other face is fixed. Designs vary, such that either the rotor or the stator can be the “floating” face in the axial direction. Together, the two faces make up a mating pair. The seal faces restrict leakage by operating in close proximity to one another, so that any leakage through the seal assembly must be through the interface between the two faces, known as the face gap.

Secondary seals such as O-rings physically block gaps between the shaft, the housing, and the respective seal faces mounted to each, preventing leakage by those routes. A generalized mechanical seal is illustrated in Figure 2.1. The spring serves to close the face gap when the system is not rotating and to provide a component of the closing force when the system is rotating. While the shaft is rotating, the sealing interface is lubricated by a relatively small amount of fluid leakage through the interface. Finally, many seals contain anti-rotation pins to prevent the seal faces from rotating in undesirable directions.

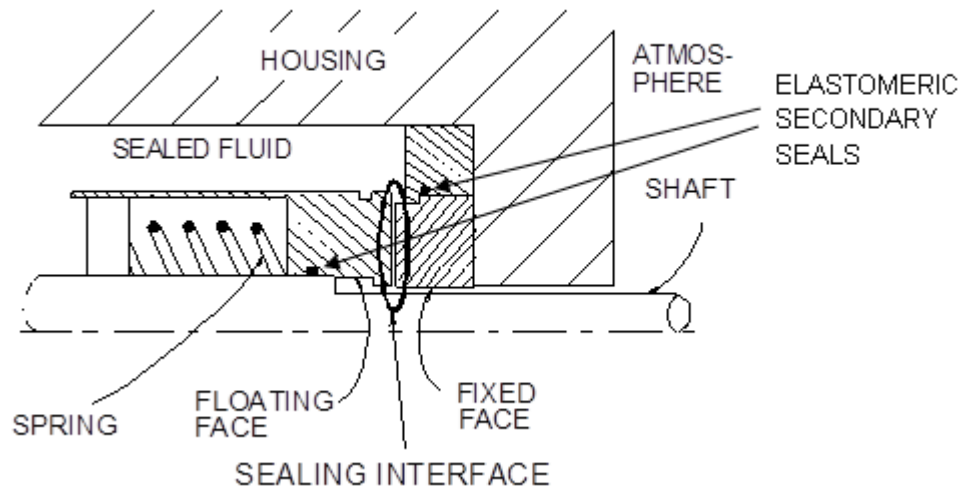


Figure 2.1: Schematic of a General Mechanical Seal [5]

2.1.2 The Face Gap

The sealing interface, also known as the face gap, is the most critical component of a mechanical seal. The seal faces move relative to one another and are in close operation, so careful design and operation is necessary to maintain optimum sealing conditions in the face gap. In some seals, a full-film lubrication regime, in which the faces do not contact each other, is desired, and in other seals, mixed lubrication, with partial asperity contact, is desired. The operating conditions of the seal will dictate which lubrication regime is chosen. For full-film lubrication, the face gap must be greater than three times the root mean square roughness of the seal faces; a smaller face gap will result in mixed lubrication. Full-film lubrication maximizes seal life by eliminating wear caused by face contact during normal operation, but results in a higher leakage rate. Mixed lubrication reduces the leakage rate, but wear and failures may occur more frequently due to sliding contact in the faces.

2.1.3 The Floating Face

The axial position of the floating seal face determines the average fluid film thickness. This film thickness influences all other behaviors in the face gap. These behaviors include heat generation rate, fluid pressure, contact area, wear rate, and leakage rate. The floating face's axial position is determined by the forces acting on it; an equilibrium position is reached when the sum of axial forces is zero. Forces that act to close the face gap are closing forces and forces that widen the face gap are opening forces.

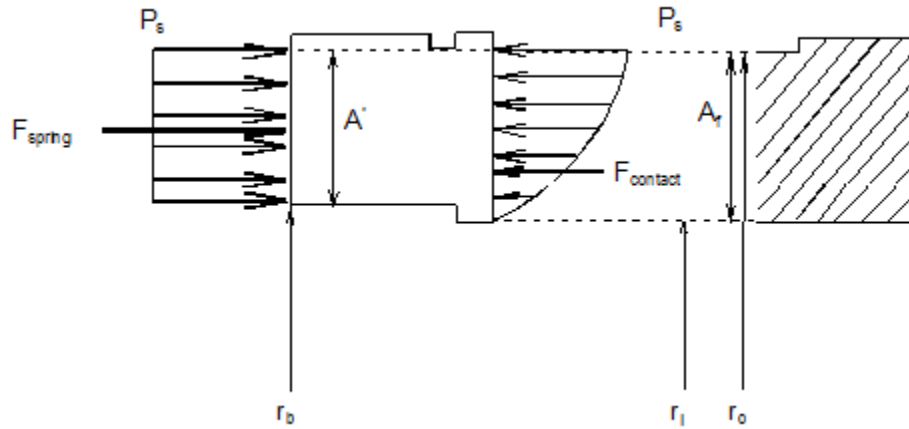


Figure 2.2: Forces Acting on a Floating Seal Face [5]

Figure 2.2 shows a schematic of forces acting on the floating seal face. The closing forces include a spring force and the pressure exerted by the sealed fluid acting on the rear side of the floating face. Generally, the force exerted by the pressure dominates this arrangement. For moderate to high pressures, the spring force is generally negligible versus the pressure force. The closing force is characterized by

$$F_{closing} = F_{spring} + A'p_s \quad (2.1)$$

where A' is the effective area of the rear of the floating face and p_s is the sealed

pressure. Another method of expressing the closing force involves the balance ratio, or the ratio between the backside area of the seal face (A') and the area of the seal face that makes up the face gap (A_f). The balance ratio for a spring-loaded seal pressurized at the outer diameter is

$$N_B = \frac{A'}{A_f} = \frac{r_0^2 - r_b^2}{r_0^2 - r_i^2} \quad (2.2)$$

The balance ratio is a function of the seal geometry only, and for most seals is between 0.65 and 0.90. In terms of the balance ratio, the closing force is then given by

$$F_{closing} = F_{spring} + p_s N_B A_f \quad (2.3)$$

The closing force is simple to obtain for a specific seal design and is generally constant during seal operation. The opening force, however, is difficult to calculate and varies during seal operation. It is this opening force that adjusts to achieve an equilibrium position for the floating face. The opening force is characterized by

$$F_{opening} = \int_{A_f} p \, dA + F_{contact} \quad (2.4)$$

Axial equilibrium of the floating face is reached when the opening and closing forces are equal

$$F_{spring} + p_s N_B A_f = \int_{A_f} p \, dA + F_{contact} \quad (2.5)$$

The sealed pressure distribution and contact forces depend on the axial location of the floating face and on mechanical and thermal deformations, all of which influence the film thickness distribution. These dependencies create difficulty in solving equation 2.5.

It is important to note that elastomeric elements such as secondary seal O-rings can cause axial forces due to friction. Typically, these friction forces are negligible compared to sealed pressure forces and contact forces, but they can be responsible for some abnormal seal behavior. Over time, the elastomer may age and become less flexible, causing a larger friction force that creates a “dragging” effect on the floating face, restricting its axial motion. Also, since the friction force always opposes axial motion of the floating face, a large enough friction force can cause a hysteresis behavior, such that the seal behaves differently as sealed pressure increases than it does when sealed pressure decreases.

2.1.4 Hydrostatic Seals

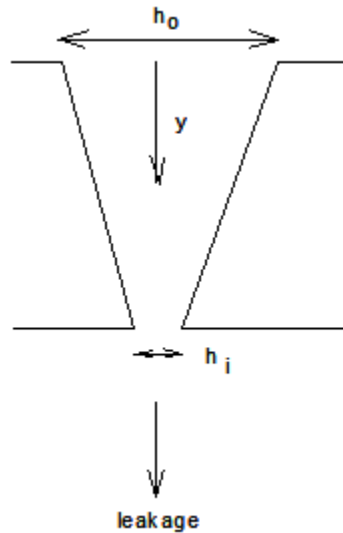


Figure 2.3: Positive Coning of Seal Faces [5]

Most commercial mechanical seals are hydrostatic seals, which means that the pressure distribution in the face gap is derived from only the sealed pressure and does not directly depend on the relative motion of the seal faces. In order to avoid pressure generation by relative motion, the seal faces in a hydrostatic seal are axisymmetric. The film thickness in a hydrostatic seal varies only with the radius. This radial

variation is known as the coning, which is defined by the difference in the film thickness between the inner and outer radius of the seal face. The coning is “positive” when the film thickness converges in the direction of fluid flow through the face gap, and it is “negative” when film thickness convergence opposes fluid flow. Coning is typically defined as an angle describing the seal face’s departure from perfect flatness. These angles are very small, usually on the order of micro-radians. An example of positive coning is shown in Figure 2.3.

The sealed pressure distribution in the face gap of a hydrostatic seal with a known coning and film thickness can be found from the solution of the Reynolds equation where r is the radial coordinate, θ is the circumferential coordinate, h is the film thickness, μ is the viscosity, and U is the relative tangential velocity between the two seal faces.

$$\frac{\partial}{\partial r} \left(\frac{rh^3}{12\mu} \frac{\partial p}{\partial r} \right) + \frac{1}{r} \frac{\partial}{\partial \theta} \left(\frac{h^3}{12\mu} \frac{\partial p}{\partial \theta} \right) = \frac{U}{2} \frac{\partial h}{\partial \theta} \quad (2.6)$$

For a hydrostatic seal, neither the pressure nor the film thickness vary in θ , so the second term on the left side and the term on the right side of equation 2.6 become zero, leaving

$$\frac{\partial}{\partial r} \left(\frac{rh^3}{12\mu} \frac{\partial p}{\partial r} \right) = 0 \quad (2.7)$$

Thus, the pressure distribution in the seal face depends on the film thickness, which is influenced by the coning. Figure 2.4 illustrates the sealed pressure distribution’s dependence on the coning. The coning, δ , is represented here as a ratio relative to the average film thickness, h_{avg} . A seal with perfectly parallel faces will have zero coning, creating a nearly linear sealed pressure distribution. As positive coning increases, the sealed pressure distribution becomes more convex, and since the opening force is the area underneath the sealed pressure curve, the opening force consequently

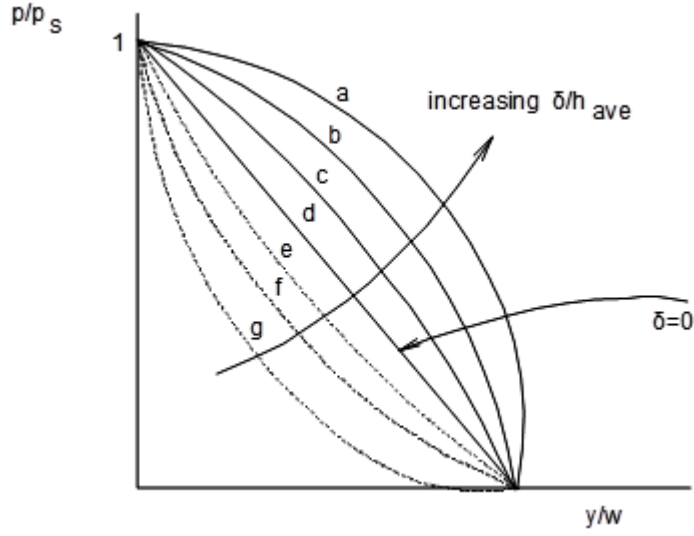


Figure 2.4: Sealed Pressure Distribution with Varied Coning [5]

increases with the coning. Also, if the average film thickness decreases and the coning remains constant, the opening force will increase. This mimics the “stiffness” phenomenon in hydrostatic bearings, by which a decrease in film thickness yields an increase in load support. This effect contributes to the stability of the hydrostatic seal if the coning is positive by naturally preventing the seal faces from contacting.

2.1.4.1 Full Film Hydrostatic Seals

For a hydrostatic seal operating in full-film lubrication, Equation 2.5 can be simplified by neglecting the contact force term. Also, at higher sealed pressures, the spring force is negligible compared to the forces generated by the sealed pressure. These two simplifications yield

$$p_s N_B A_f \approx \int_{A_f} p dA \quad (2.8)$$

Rearranging with respect to the balance ratio gives

$$N_B = \int \frac{p}{p_s} d\frac{A}{A_f} \quad (2.9)$$

If the value of $\frac{\delta}{h_{avg}}$ is given, the integral in Equation 2.9 is the area under the matching curve in Figure 2.4. Therefore, each curve in that figure represents a seal with a specific balance ratio if $\frac{\delta}{h_{avg}}$ is held constant. Curves for positive conings correspond to balance ratios larger than 0.5. Likewise, a seal with a known balance ratio will have a constant value of $\frac{\delta}{h_{avg}}$. The average film thickness, then, is proportional to the coning. A larger coning yields a thicker film. The leakage rate, Q , is directly proportional to the pressure drop across the seal, proportional to the average film thickness cubed, and inversely proportional to the fluid viscosity.

$$Q \propto \frac{\Delta p (h_{avg})^3}{\mu} \quad (2.10)$$

Since the film thickness has a strong effect on the leakage rate and the coning and film thickness influence one another, hydrostatic seal designs must specify carefully the amount of desired coning both during manufacturing (known as “pre-coning”) and during operation from thermal and mechanical deformation. Generally, the geometry and balance ratio of a seal design are fixed or variable with small windows, so manipulation of the coning provides the best opportunity for a designer to arrive at the desired leakage rate.

2.1.4.2 *Contacting Hydrostatic Seals*

In applications where the leakage rate must be extremely low, a full film hydrostatic seal may be impractical. In this case, a reduced film thickness is used such that the asperities on the seal faces are in contact. The face gap is closed by reducing the coning of the seal faces, thus reducing the sealed pressure distribution and the resultant opening force. In addition, if the sealed pressure is relatively low, a hydrostatic seal cannot evolve enough pressure in the face gap to generate a satisfactory opening force to maintain full film lubrication. The result of these effects is that the contact term in the force balance of Equation 2.5 can no longer be neglected. Thus the relationship

between film thickness and coning and the coning's effect on seal stability are not always valid for contacting seals.

2.1.5 Production of Coning

Most mechanical seal faces are manufactured to be as flat as possible during unpressurized conditions. Initially flat, parallel faces develop coning during operation by mechanical deformation induced by the sealed pressure and thermal deformation induced by heat generation in the face gap. For stable operation with a full fluid film, a positive coning (converging gap) is desired. Mechanical deformation can produce either a converging or diverging gap from the outer diameter to the inner diameter. Thermal deformation usually produces a converging gap from the outer to inner diameters. Thus, most commercial seals are designed such that they are pressurized from the outside, so the mechanical and thermal deformations work in concert to generate a converging gap in the direction of fluid flow.

Some mechanical seals, especially for high pressure applications, have a converging gap machined into the faces during manufacturing. This process is known as pre-coning, and works to give further assurance that a converging gap will be maintained during operating conditions. The seal faces are still subject to thermal and mechanical deformation, so the actual coning during operation will vary from the specified pre-coning given at unpressurized conditions.

2.1.6 Hydrodynamic Seals

Hydrodynamic seals evolve a pressure distribution in the face gap through the relative motion between the seal faces. This pressure generated by motion is caused by some circumferential variation in the film thickness, in contrast with the axisymmetric film thickness of hydrodynamic seals. This circumferential variation in film thickness is caused by one or more instances of irregular geometry which create a converging gap

along the circumference of the seal face. This converging gap generates elevated pressure when the seal faces slide relative to one another, as in a slider bearing. Typically, hydrodynamic seals operate with full-film lubrication, and the film thickness tends to be proportional to the speed of rotation.

Some hydrodynamic seals contain hydropads, which are grooves or slots machined into the seal face. These hydropads create an asymmetric seal face that deforms differently under mechanical and thermal loads; this irregular deformation creates circumferential waviness with height on the same order as the film thickness, usually in the microns.

All hydrodynamic seals also have a hydrostatic component of pressure generation. The influence of the hydrostatic component depends on the design and operating conditions of the seal; sometimes, it may be significant compared to the hydrodynamic behavior of the seal. Other times, the hydrodynamic action is the main driver of the sealed pressure distribution and the hydrostatic behavior is relatively insignificant. In some designs, a hydrostatic seal generates an inadequate opening force to maintain full-film lubrication, and hydropads will be added to the seal face to generate some hydrodynamic behavior, increasing the opening force. Occasionally, a nominally hydrostatic seal will acquire some circumferential waviness and will exhibit hydrodynamic behavior. This often happens if the seal geometry deforms non-uniformly under mechanical or thermal load, or in the event of solid contaminants on the seal face.

2.2 The Nuclear Reactor Coolant Pump Seals

The mechanical seal examined in this thesis is the first-stage seal in the Westinghouse family of reactor coolant pumps for pressurized water reactors. This seal is the first of three stages in the sealing package that contains reactor coolant system water in the cooling loop. In industry, this seal is commonly called the Westinghouse #1 seal. Some schematics of the Westinghouse reactor coolant pump and the sealing assembly

are shown in Appendix A. This seal is usually maintained as a cartridge system, in which the entire seal assembly can be replaced as a single unit. This complicates maintenance on individual parts, but allows greater quality control and simplicity of installation, reducing potential problems encountered during seal replacement. The #1 seal operates normally as a hydrostatic, full-film lubrication seal with a nominal leakage rate of 11.36 L/min (3.0 gpm). The rotating face (rotor) is axially fixed, and the non-rotating face (stator) is allowed to travel axially. The #1 seal contains the vast majority of the pressure drop in the sealing system, since it is pressurized at the full RCS pressure of 15.51 MPa (2250 psi) at the outer diameter and at 0.4826 MPa (70 psi) at the inner diameter. The faces of the #1 seal were originally coated with aluminum oxide, but recent designs have employed silicon nitride. Both materials are hard ceramics which are very resistant to wear during normal operation, but may be vulnerable to fracture and sliding wear if face contact occurs for long periods. The seals have a manufactured pre-coning that contains a dual taper, meaning that there are two different levels of pre-coning across the seal face. This dual taper is the result of fine-tuning the pre-coning to manage the nominal leakage rate.

The nominal water temperature in the RCS is around 288 °C (550 °F). If the seal is exposed to this high temperature in the face gap, some of the water would flash to steam as the pressure drops across the seal face, causing undesirable two-phase effects and potentially serious seal instability. To combat this, under normal operation, the water entering the seal face is cooled by a system that injects cooler water from the reactor volume control tank. This system reduces the seal intake temperature to around 66 °C (150 °F), which prevents steam flashing even at ambient pressures. It is important to note that during station blackout conditions (when the nuclear power plant has lost all external power and no backup generators are running), seal injection is lost, and the still-operating seals can be exposed to full RCS temperature. Westinghouse has developed an upgraded #1 seal package that can withstand the

much harsher conditions encountered during station blackout for a number of hours until normal operation can be restored.

The second and third seal stages in the RCP are important because they restrict coolant leakage to the environment and maintain the back pressure of 0.4826 MPa (70 psi) on the #1 seal. The #2 and #3 seals operate as partially-contacting hydrostatic seals with a much smaller pressure drop across their seal faces. Together, all three seal stages form the sealing package for a single reactor coolant pump. Typically, each reactor in a nuclear power plant has multiple reactor coolant pumps for redundancy, and many nuclear power plants employ multiple reactors, so most power stations must maintain several sealing packages simultaneously.

The #1 seal sometimes exhibits abnormal behavior in which the leakage rate departs significantly from the nominal value. Excessively high leakage rates can result in significant loss of coolant volume, and low leakage rates can result in loss of full-film lubrication, leading to seal wear and damage. Consequently, power plant operators are required to maintain the leakage rate within an acceptable range. The inability to do so requires special permission from regulatory bodies to continue operation with out-of-spec leakage rates or shutting down the reactor until the problem can be corrected. Seal failure and subsequent reactor shutdown is expensive to utility companies, so an effort has been made to determine and mitigate the causes of abnormal seal leakage.

2.3 Causes of Abnormal Seal Leakoff

The reactor coolant pump seal system is a complex environment, with many interacting conditions that influence seal behavior. The pressure, temperature, water chemistry, and the operation of other mechanical components of the system can all affect the leakage rate. As such, the root causes of abnormal seal leakage are not always well-understood by plant operators. A greater understanding of the phenomena behind the seal behavior can lead to more effective strategies to restore normal seal

leakage. Of primary concern for this document are conditions that cause otherwise normally-operating seals to exhibit abnormal leakage. Seal system design inadequacies or failures resulting from improper installation or maintenance are not covered.

2.3.1 Electrophoresis

For RCP seals that are running normally, the leakage rate can gradually change to approach unacceptable levels. Frequently, this gradual, ongoing departure from normal leakage rates is caused by chemical deposition on the seal faces. This chemical deposition, also called electrophoresis, represents one of the most common issues affecting seal operation encountered by power plant operators. Typically, adverse temperature and water chemistry in the reactor coolant system are the primary causes of electrophoresis. The deposition of solids on the seal faces affects their geometry, causing circumferential irregularity and affecting the radial coning. This both generates a hydrodynamic component of pressure and changes the hydrostatic pressure distribution in the face gap. These effects can generate abnormal leakage on their own or reduce the ability of the #1 seal to self-adjust to other changing reactor conditions. Frequently, electrophoresis causes excessive leakage due to the creation of a hydrodynamic response, which increases the opening force, moving the face gap farther open. However, electrophoresis can occasionally cause insufficient leakage as well [4]. In 2006, PSE&G's Salem Unit 2 experienced a manual reactor trip during a planned coast-down due to excessive #1 seal leakage. The root cause of this high leakage was determined to be corrosion products deposited on the seal faces [1]. These products precipitated out of solution from the RCS due to low boron concentration and lithium in the water, which created a higher-than-normal pH and sensitivity to chemical composition changes.

The two major conditions which are believed to cause electrophoresis are water chemistry and temperature. The water chemistry in the reactor coolant system is

believed to be the primary cause. Chemical deposition on seal faces seems to be driven by increased pH in the RCS. This pH increase is driven by a reduction in boron concentration in the RCS as a fuel cycle proceeds. At the beginning of a nuclear fuel cycle, the boron concentration in coolant water is relatively high, but towards the end of a cycle, as reactor make-up water dilutions (the adding of water volume from a volume control tank) are more frequent, the boron concentration becomes almost nonexistent. In addition, at the end of a fuel cycle, the lithium concentration in the RCS is increased, which further increases the water pH. This gradual rise in pH over the duration of a fuel cycle permits an increased amount of chemical scale to deposit on seal faces, altering the geometry of the face gap and affecting the seal's ability to maintain appropriate leakage. Also, the presence of carbon steel in RCS components may contribute to an increase in dissolved iron in the coolant water, which can be deposited as hematite on the seal faces, causing similar alterations of face geometry [4]. Utilities have experienced high leakage during the days or weeks leading up to a planned refueling outage. Then, it becomes important to maintain the leakage rate within acceptable ranges so that the reactor is not forced into a premature shutdown to avoid catastrophic seal failure rather than being shut down in accordance with the refueling outage schedule.

The second condition which appears to drive electrophoresis is the temperature at the seal inlet. Since cooling water injection buffers the seal inlet from the full temperature of the reactor coolant system, the inlet temperature remains relatively constant. However, slight temperature rises can lower the concentration of dissolved oxygen at the seal inlet, leading to a further rise in pH and contributing to chemical deposition. Conversely, seal injection temperature decreases can create a flushing effect by lowering the pH and stripping some deposited material from the seal faces, as well as lowering leakage through affecting the response of the floating seal face, as discussed below.

2.3.2 Particulate Contamination

A somewhat rarer cause of abnormal leakage for seals currently in stable operation is particulate contamination. This encompasses a group of problems related to the presence foreign components in the face gap. Foreign material can cause damage to the seal faces or become lodged in the face gap, affecting both the fluid flow in the face gap and the seal's ability to move freely to adjust. In addition, some types of seal failures result in fracture of the seal faces, so a seal failure can produce particulates of its own, potentially causing contamination of a different seal stage. Also, occasionally particulates from outside the RCS can enter the seal face if they are introduced to the RCS during operation. Some utilities have experienced failure of one or more seal stages due to particulates introduced from a volume control tank or seal injection water. In 2008, Duke Energy's Oconee Unit 1 experienced a cascading seal stage failure partly due to particulate contamination [2]. During coast-down before an outage, the #3 seal of an RCP exhibited failure due to heat checking caused by thermal excursions during the fuel cycle (see Section 2.3.3 below). The failure of the #3 seal caused heavy debris contamination in the RCS, which later traveled to the #1 and 2 seals, causing damage and excessive leakage. This failure shows that particulate contamination can arise from many sources, including damage to other seal stages. Therefore, adverse conditions that otherwise do not include particulate intrusion into the RCS may lead to seal failure if they promote fracture of a seal face.

2.3.3 Reactor Coolant Pump Transients

Transient behavior in the operation of the reactor coolant pump, up to and including trip (sudden shutdown), places stress on the sealing system by forcing it to respond to changing temperature and pressure conditions in the coolant system. A seal previously operating with a stable face gap and leakage rate must adjust to the new conditions, which may lead to undesirable performance or even failure of a seal stage.

The 2008 seal failure at Oconee Unit 1, also described above, occurred during coast down, or the process of slowly shutting down the reactor and its support systems for refueling. During shutdown and then subsequent restart, the reactor coolant pump undergoes large changes in fluid pressure, as well as changes to flow characteristics that may affect seal operation. In addition, before sufficient sealed pressure or leakage is established during startup, seal faces may operate in partial face contact, causing significant thermal buildup in the faces and surrounding components. This may create mechanical wear and damage to the seal faces [2]. It is likely that high vibration during operation, which is another form of pump transient, and additional stress from shutdown and startup accelerated the failure of the #3 seal stage, which then caused particulate contamination and the cascading failures in the #1 and #2 seals.

2.3.4 Temperature and Pressure Excursions

The seals in an RCP operate best when coolant system conditions are stable and the seals have reached a satisfactory, stable leakage rate. Although mechanical seals are designed to be self-adjusting, changes in coolant system temperature or pressure force the seal to adapt to the new set of operating conditions, creating a potential for failure or undesirable performance. Excursions are often caused by sudden, unwanted changes in cooling injection temperature or pump operation. Some excursions cause a sudden change in leakage rate, while the seal later stabilizes at a different leakage rate.

In 2009, Duke Energy's Catawba Unit 1 was forced to shut down due to high #2 seal leakage. The cause of the high leakage was determined to be elevated operating temperature in the cooling system [3]. The higher-than-normal operating temperature resulted in thermal expansion of several components and caused advanced wear on the softer carbon graphite sealing face. The carbon face expanded and came into face contact with the harder seal ring on its outer diameter, causing wear at the outer

diameter of the carbon face. The elevated temperature excursion was determined to have lasted about 36 hours, during which time the carbon face received enough wear to adversely affect its operation. Even relatively short-lived excursions during a fuel cycle can cause mechanical wear or chemical problems such as increased deposition rate of particulates. During a post-shutdown inspection, hematite corrosion was present on the sealing faces; higher operating temperature was also found to increase the rate of conversion of iron oxide to hematite in the RCS.

2.4 Abnormal Seal Leakoff Mitigation Strategies

Utilities have employed a variety of strategies to restore abnormal leakage to acceptable levels. In most cases, these mitigation strategies involve changing water conditions to alleviate issues caused by electrophoresis. If seal faces are physically damaged through fracture, excessive wear, or solid particulate intake, it is unlikely that the following strategies will correct leakage long-term; typically, a reactor shutdown and replacement of the damaged parts are required. Note that physical damage to seal faces can occur after periods of abnormal leakage, so employing mitigation strategies early can prevent a catastrophic failure in the future, in addition to restoring desired leakage rates in the short term. As such, well-documented and implemented mitigation strategies can be valuable for continued operation of a reactor, which is extremely financially beneficial to operating utilities. The following two strategies involve deliberately altering reactor coolant system conditions by changing parameters which are under the control of plant operators during normal operation. As such, they are excellent first steps for troubleshooting and correcting abnormal leakage without resorting to more intensive measures, up to and including shutting down an RCP for maintenance.

2.4.1 Changing Seal Injection Water Temperature

A previous EPRI maintenance guide states that reducing seal injection water temperature increases the viscosity of the water flowing through the seal, resulting in a decreased leakage rate [4]. The guide recommends this action as a reliable first step to reduce excessive leakage. It also states that raising the seal injection temperature can increase the leakage rate by reducing the water viscosity. This recommendation is based on experience by utilities and is based on the temperature dependence of the viscosity of water. The viscosity has an inverse relationship with water temperature. Equation 2.10 shows the inverse relationship of leakage rate and viscosity, which explains the temperature/leakage relationship. Previous guides for seal maintenance [4] suggest that leakage rate can decrease about 1.9 L/min (0.5 gpm) for a 5 °F change in seal injection temperature. This large change in leakage cannot be explained through changing water viscosity alone. For an initial injection temperature of 38 °C (100 °F), a decrease of 3 °C (5 °F) increases the viscosity by approximately 3.3%. If the initial leakage rate were 11.36 L/min (3.0 gpm), this change would account for a decrease of about 0.4 L/min (0.1 gpm) in leakage.

Therefore, it is concluded that the direct effect of viscosity change is one of multiple effects that cause a leakage rate change when altering seal injection temperature. The cubic dependence of leakage rate on film thickness is also noted in Equation 2.10, so a small change in average film thickness will lead to a significant change in the leakage rate. As noted, the film thickness is proportional to the coning of the seal faces, so the leakage rate is thus very sensitive to the total coning.

Another effect that can change the leakage rate is thermal deformation. In most mechanical seals, thermal deformation generates positive coning, increasing the leakage rate. Thermal deformation is generated by viscous dissipation in the interface between the seal faces. This dissipation is proportional to the fluid viscosity. Thus, an increase in viscosity indirectly increases the heat generation and the coning, thus

increasing the leakage rate. It is also noted in [4] that changing the seal injection water temperature has a short and long term transient response. A short term transient of increased leakage occurs after reducing the seal injection temperature, and after 30-60 minutes, the long term transient effect results in a new lower leakage rate.

Since cooling the seal injection water results in a near-instant change in viscosity, the direct effect of viscosity on leakage rate cannot cause the transient change described above. An increased viscosity would reduce the leakage rate, but plant operator experience suggests that the short term transient is an increased leakage rate. An explanation for the short term transient is the thermal deformation described above. The change in viscous dissipation will result in a changing temperature distribution in the seal assembly, and the time required for the new temperature distribution to reach a steady state and change the thermal deformation of the assembly causes the short term transient response.

Finally, changing seal injection water temperature can be helpful if electrophoresis is the cause of abnormal leakage rates. As described above, electrophoresis is sensitive to the pH of the environment, which can be changed by altering the injection water temperature. A decrease in temperature will reduce deposition on the faces by creating a more acidic environment, while an increase in temperature will increase deposition. For all the above reasons, changing seal injection water temperature is effective in mitigating abnormal leakage rates from a variety of causes, including face wear, unusual operating conditions, or electrophoresis.

2.4.2 Seal Injection Filter Replacement to Alter Reactor Coolant System Chemistry

In some cases, unintentional changes in reactor coolant water chemical composition lead to electrophoresis, where some chemical components become deposited on the seal faces, altering their geometry. If the coning is changed, the leakage rate can become too high or too low. If the deposition is nonuniform around the circumference,

a hydrodynamic behavior can develop, increasing the film thickness and the leakage rate. However, intentional changes in water chemistry to reverse the conditions that cause electrophoresis can prevent or eliminate deposition, thus restoring optimal leakage rates.

One simple method of altering water chemistry near the seal inlet is replacing or swapping the seal injection filters, as discussed in [4]. Some utilities have experienced a reduction in particulates by swapping to a smaller filter media. Replacement filters are typically maintained in a filter pit which is cooler than the seal injection temperature and has a dissolved boron and oxygen concentration from the last time it was removed from the RCS. When this filter is introduced into the system, it provides a flush of cool, oxidized water with a higher boron concentration into the seal intake. These conditions combine to reduce the local pH and create a more oxidizing environment, chemically stripping some deposits and restoring normal seal geometry. The guide states that in one case, a 9.0 L/min (2.4 gpm) leakage rate reduction was observed, and that normal cases can expect a roughly 3.8 L/min (1.0 gpm) reduction in leakage rate, depending on the level of abnormal leakage experienced. These effects are attributed to both the chemical and temperature effects. Cooler water holds more dissolved oxygen and has a lower pH, and the dissolved boron contributes to the acidic effect.

Swapping the seal injection filter to one maintained at cooler, more acidic conditions can mitigate abnormal leakage by treating the root cause. This may be a method for restoring long-term stability to seal if operators expect that abnormal leakage is due to electrophoresis, especially near the end of a fuel cycle. However, it is noted that changing filters will likely not be effective if electrophoresis is not the cause of the abnormal leakage.

2.5 Previous Controllable Seals

Previous approaches to controllable seals have generally utilized two methods of control. The first is to control the closing force on the floating seal face [7], [18]. This is easily accomplished through linear actuators and controls the leakage rate by directly altering the average film thickness, through either closing or opening the face gap. However, a distinct disadvantage of this method is that when the controlled seal operates only hydrostatically, if the coning becomes negative, the seal will become unstable and difficult to control.

The second method is to control the opening force on the floating seal face by controlling the face geometry [14], [15]. One approach is to vary the coning. This method utilizes the dependence of the sealed pressure distribution (and thus the opening force) on the coning. The film thickness is proportional to the coning, so the leakage rate can be controlled by varying the coning. Generally, the coning is varied by deformation caused by an actuator within the seal face. The produced deformation counters the thermal and mechanical deformations in the seal face caused by operating conditions, and can generate the required coning for desired operation. If the film thickness is too large, causing a high leakage rate, the coning is decreased, which decreases the film thickness and thus the leakage rate. Likewise, if the film thickness is too small and the leakage rate is insufficient, the coning is increased to increase the leakage rate. By this operation, the opening force, which separates the seal faces and prevents face contact, is regulated by changing the coning. In addition, this approach is appropriate for both hydrostatic and hydrodynamic seals, since hydrodynamic seals have a hydrostatic component of operation.

Previously developed controllable seals include two attempts based on variation of the coning. The first is a controllable seal for a boiler feedwater pump [14] and the second is for a liquid oxygen turbopump [15], [16]. A schematic of the boiler feedwater pump seal is shown in Figure 2.5.

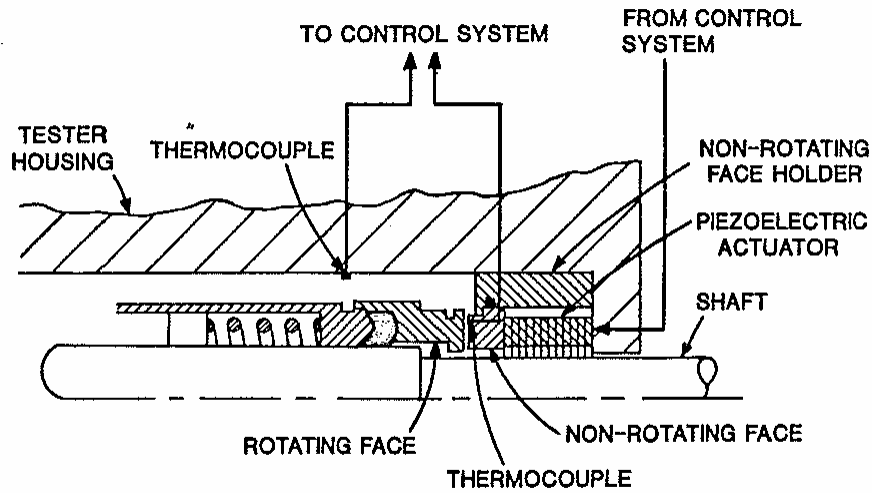


Figure 2.5: Controllable Seal Schematic for Boiler Feedwater Pump [14]

In the above assembly, the rotating face is spring loaded and floats axially, and is composed of stellite. The non-rotating face is composed of carbon graphite. The sealed fluid is water. The assembly resembles that of a conventional mechanical seal, but the holder for the non-rotating face is configured to allow an actuator to be located behind the back of the face. The actuator is an annular ring of stacked piezoelectric layers with brass electrodes between layers. A positive voltage is applied to the electrode stack from an external power supply, causing the piezoelectric elements to expand and exert a force on the carbon graphite face. The outer diameter of the carbon graphite face is constrained by the seal holder, so the inner diameter of the face deforms downward, contributing to the positive coning of the face gap. As the applied voltage increases, the coning increases, causing a thicker fluid film. Likewise, a negative voltage causes the piezoelectric elements to contract, reducing the coning and decreasing the film thickness. A preload is included in the non-rotating face and actuator assembly, so contracting the piezoelectric elements allows the coning to reduce.

The above seal assembly uses an adaptive control system with the seal face temperature and chamber temperature input from thermocouples. The system controls the coning to avoid excessive face contact and minimize the film thickness. Face contact is detected as large spikes in seal face temperature caused by frictional heating. In Figure 2.6 below, the performance of the seal is examined with the control system disabled. A duty cycle with several transients is performed and the temperature monitored. The temperature spikes shown in the figure indicate frequent face contact. In contrast, when the control system is enabled and the same duty cycle is performed again, face contact is significantly reduced, as shown in Figure 2.7. This figure shows that the control system effectively avoids face contact in situations where an uncontrolled seal cannot.

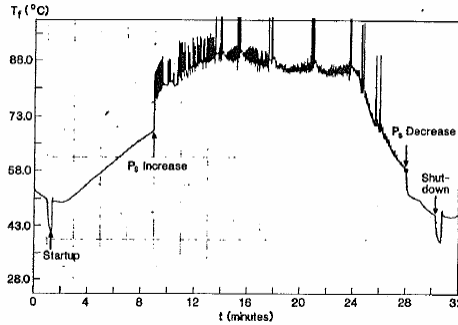


Figure 2.6: Transient Performance in Uncontrolled Seal [14]

The second controllable seal, the liquid oxygen turbopump, is shown in figure 2.8. This arrangement is a double mechanical seal system, in which helium serves as a buffer gas to separate liquid oxygen from hot combustion gases in the turbopump. For the experimental design, helium is replaced with air.

The two non-rotating face assemblies are spring loaded and allowed to float axially. They are composed of a piezoelectric element with a thin face of carbon graphite. There is a single rotating face, which is tungsten carbide. The electrodes which polarize the piezoelectric elements are located on the axial surfaces of each element.

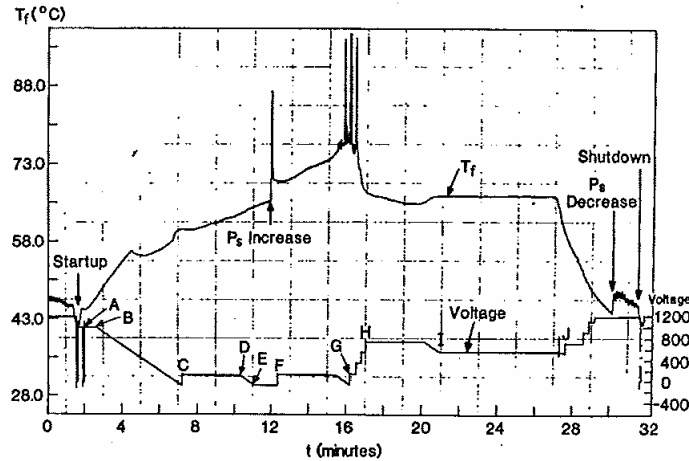


Figure 2.7: Transient Performance in Controlled Seal [14]

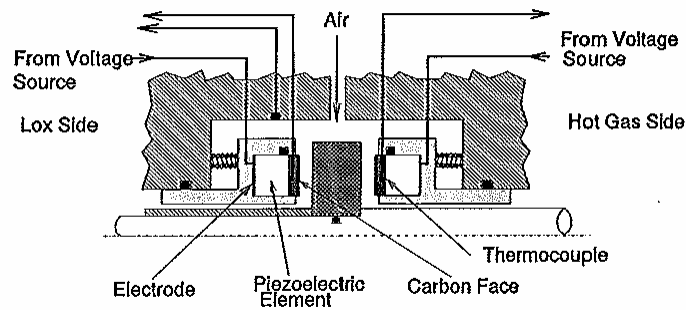


Figure 2.8: Controllable Seal for LOX Turbopump [15]

The carbon face is the ground electrode while the charged electrode is on the opposite face. The poling axis of the piezoelectric element is oriented radially, so an applied voltage in the axial direction induces a shear deformation within the element. The attached carbon face is deformed by this shear to produce coning. The larger the applied voltage, the larger the coning and the film thickness. A negative voltage produces negative coning. In hydrostatic seals with liquids, negative coning tends to produce unstable operation and is highly undesirable. Due to the more complex nature of a gas seal, negative coning does not necessarily cause instability.

A closed-loop proportional-integral-derivative control system receives either the air leakage rate from a flow meter or the face temperature from a thermocouple to

control the seal for either a fixed leakage rate or a fixed face temperature. Figure 2.9 shows an experimental duty cycle which includes temperature and pressure transients. Figures 2.10 and 2.11 show the seal response during the experimental duty cycle while controlling for a fixed leakage rate and fixed face temperature, respectively.

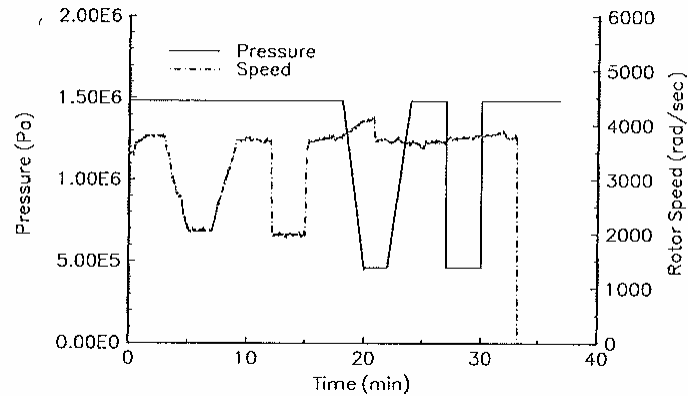


Figure 2.9: Duty Cycle for LOX Turbopump Seal [16]

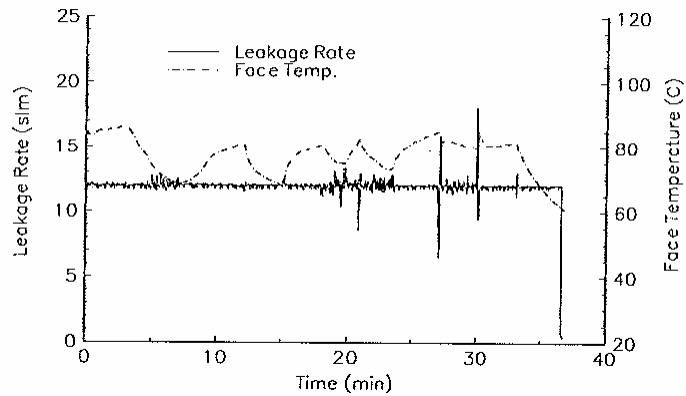


Figure 2.10: Controllable Seal Performance for Fixed Leakage Rate [16]

The above results for the seals in both a boiler feedwater pump and a liquid oxygen turbopump show that controlling the seal face geometry, specifically the coning, is an appropriate method for controlling seal face behavior. Both controllable seals are able to respond to large transients in a variety of operating conditions, such as sealed pressure and temperature, by generating a deformation that alters the seal face

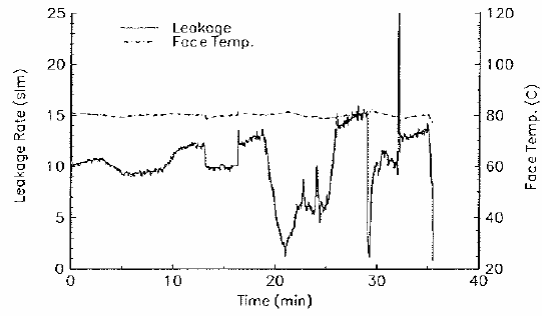


Figure 2.11: Controllable Seal Performance for Fixed Face Temperature [16]

geometry to produce favorable conditions in the face gap.

CHAPTER III

PROPOSED CONTROLLABLE SEALS AND SEAL MODELING

3.1 Proposed Controllable Seals

3.1.1 Motivation

Because utilities often encounter abnormal leakage rates from current Westinghouse #1 seals and have limited tools to mitigate these abnormal leakage rates, it is desired to modify the existing seal to provide leakage rate control. This modification's goal is to improve reliability and prevent some scenarios in which plant operators may be forced to shut down an operating reactor because of unsatisfactory leakage rates from the #1 seal. Previous work has indicated that face contact can be avoided and leakage rates can be moderated through deformation induced by an actuator in a controllable seal. A greater ability to moderate abnormal leakage rates in nuclear reactor coolant pumps is beneficial to utilities in many areas, including significant cost savings when a shutdown is avoided. As such, possible controllable seals are introduced below and their performance modeled to determine the greatest obtainable controllability.

3.1.2 Proposal

The controllable mechanical seals proposed for replacement of existing Westinghouse #1 seals operate by providing an actuation to adjust the coning of one seal face. Controlling the coning is the preferred method of control because it can ensure positive coning, and thus stable operation. Two forms of actuation are proposed. The first works by pressurizing cavities filled with a hydraulic fluid inside the seal face to induce a deformation and modify the coning. The second employs a seal face

composed of a piezoelectric crystal. Inducing a voltage across this crystal induces a deformation to modify the coning. Both proposed controllable seals are intended as drop-in replacements for existing #1 seals, so their design is chosen to match the dimensions of existing seals. The exact dimensions of the proposed controllable seals are illustrated in Sections 3.3.3 and 3.3.4 below.

3.2 Modeling

3.2.1 Purpose

The numerical model detailed below is intended to approximate the behavior of the proposed controllable mechanical seal face. The model's goal is to investigate whether the seal's leakage rate can be controlled satisfactorily by varying the coning of the seal face, and thus the shape of the face gap. In addition, the model is employed to determine the controllability of each proposed seal design. This controllability is determined by the uncontrolled leakage rate that the seal is able to correct to the nominal leakage rate. Using data output by the model, the most controllable seal design can be selected.

3.2.2 Methods

The model will use an iterative approach to solve both the lubrication problem and the deformation analysis in order to reach a converged solution in which the calculated pressure distribution is in agreement with the seal face deformation. The controlling parameters will be either hydraulic pressures in "voids" inside the seal face or a voltage across a piezoelectric element, both of which will be used to induce deformation. For the fluid mechanics solution, important parameters are the pressures at the boundaries of the face gap and the overall height of the face gap at discrete points along the face. Because the solver only considers the relative positions of the two seal faces, it is convenient to assume that the rotor is rigid and flat. It is thus assumed that the stator, which is the face being modeled, exhibits all of the coning and the deformation

experienced by the seal.

The model consists of two analyses: a fluid mechanics solver utilizing a finite-difference solution of the Reynolds Equation and a deformation analysis solved in ABAQUS, a commercial finite element program. The fluid mechanics solver is used to find the sealed pressure distribution in the face gap as a function of the radius and the height of the face gap, or the film thickness. This pressure distribution is then input to ABAQUS to find the deformation of the seal face. Then, the model uses an iterative process in which the computed deformation is used to determine the next iteration of the pressure distribution, followed by finding a new deformation profile. This process is continued until a converged deformation is reached.

When the deformation is converged, the sealed pressure and film thickness distributions are also known, as well as the initial minimum film thickness (at the seal's inner diameter), which is guessed at the beginning of the analysis. Thus, the lubrication problem in the face gap is fully characterized. The pressure field can be integrated along the seal radius and over the circumference of the seal to find the opening force exerted on the seal face. The closing force is a constant for this analysis. The computed opening force is compared to the closing force to check for equilibrium. If equilibrium is not reached, a new minimum film thickness is chosen and the fluid mechanics/deformation iteration process begins again. This nested iteration process continues until the solved opening force balances the closing force, at which point the system is fully converged and the leakage rate can be calculated and output. Thus, the four features of the numerical model, which will be detailed below, are the fluid mechanics solver, the deformation analysis, the force balance calculation, and the iteration process.

3.2.3 Language and Scripting

The model is constructed using the coding language Python. This language is chosen because ABAQUS uses Python for its native scripting commands, meaning that the numerical model for the fluid mechanics can be integrated with the deformation analysis in a single script which can be run within ABAQUS, requiring no separate pre- or post-processing, which can be cumbersome. In addition, Python is a modular and easy-to-understand language, and several Python add on packages can be used for simple numerical analysis. For this model, Numpy and SciPy are used within the script by installing them for the Python package included with ABAQUS.

3.3 Geometry and Materials

3.3.1 Dimension Approximation

Table 3.1: Seal Face Dimensions

Feature	Seal Face Dimensions		
	Inches	mm (absolute)	mm (nominal)
Inner Diameter	8.5	215.9	216
Sealing Face Width	1.8	45.72	46
Outer Diameter	12.1	307.34	308
Seal Face Thickness	0.5	12.7	13

The geometry of the seal model is designed to approximate closely the dimensions of the first stage of the mechanical sealing system in a Westinghouse RCP used in many active PWRs. This seal stage is referred to in industry as the Westinghouse #1 seal. The scope of this research project is confined to these existing #1 seal packages, so the proposed solutions are designed as drop-in replacements for them. Dimensions are gathered in inches and converted to millimeters for analysis in SI units, then rounded to convenient values. The inner diameter used for the seal ring is 8.5”, which is converted to 215.9 mm and rounded to 216 “nominal” mm. Table 3.1 shows

the dimensions used in the construction of the seal model. The nominal millimeter dimensions are used to build the seal face in ABAQUS. Note that dimensions are not always rounded to the nearest integer, but sometimes to the nearest even integer. This method creates evenly divisible dimensions while still providing a close approximation of the real #1 seal. The model simulates only the non-rotating face of the seal assembly. The non-modeled rotor is assumed to be perfectly flat and rigid, so that the stator accounts for all coning and deformation experienced in the seal face pair.

The seal face is modeled as a cross-sectional slice of the seal ring, which in reality is a thick ring shape that fits around the large central shaft of an RCP. Modeling a cross-section creates an axisymmetric analysis in the r and z dimensions. An axisymmetric analysis is both convenient and applicable, since the total number of finite elements, and thus the computation time, is significantly reduced versus a full three-dimensional model and the geometry of the seal varies only with r and is independent of θ . The seal's operation ideally is completely hydrostatic, meaning that all of the opening force is generated from the sealed pressure distribution within the seal face gap and no pressure is generated dynamically from the relative motion between the rotor and the stator. This means that the form of the Reynolds equation used to describe the pressure distribution contains no circumferential terms. This method describes the performance of a new seal uncontaminated by chemical deposition and unmarred by wear, but as a real seal operates, it may gradually obtain some circumferential waviness due to these effects. This waviness can introduce some hydrodynamic effects and change seal operation. In fact, previous research suggests that water chemistry and electrophoresis (the mechanism behind chemical deposition on the seal faces) are major contributors to adverse seal leakage rates during operation. As such, this is a concern, but this model seeks only to prove that adjusting the coning can adjust the leakage rate, so it is reasoned that if a seal exhibits undesirable behavior possibly attributed to hydrodynamic effects, that the change of coning through actuation could

change the hydrostatic response to neutralize the undesirable behavior and moderate the leakage rate, thus extending the operation of the seal and preventing a shutdown scenario.

3.3.2 Materials

Existing Westinghouse #1 seals have seal ring holders manufactured from 410 stainless steel, a hard material chosen because of its corrosion resistance and low carbon content. For this analysis, the entire seal face is modeled as 410 stainless steel with an elastic modulus of 200 GPa and a Poisson ratio of 0.3 [11]. In actual seals, the face is coated with a thin layer of a ceramic such as silicon carbide or nitride, but since the coating is thin and most deformation would occur in the bulk material behind the coating, it is considered to have a negligible effect on the overall deformation and is neglected from the model's geometry. This particular arrangement simulates a hard/hard seal ring and runner pair, since the rotating face is assumed to be rigid and flat.

It is noted that the use of a hard material will restrict intentional deformation by a control system, so the use of a softer material could increase the ability of a control system to affect the leakage rates. It is also possible that the elastic modulus could be chosen deliberately to obtain a seal face that is more or less responsive to both control attempts by applied deformation and passive deformation from RCP pressure and thermal stresses.

Many seals in industry also use a hard/soft pairing, where one seal face is a hard ceramic material designed to resist wear and the other is a softer material, often carbon graphite, designed as a sacrificial face in the event of face contact and wear. The softer material rubs away without marring the harder face, so that maintenance requires only replacing the softer face under normal circumstances. In addition to this desirable wear behavior, a controllable carbon graphite seal face is more responsive to

active control by virtue of its reduced modulus compared to steel. As such, a carbon graphite seal face composed of SGL Carbon Group’s EK-2200 resin-bonded graphite typically used in mechanical seals with an elastic modulus of 26.9 GPa and a Poisson ratio of 0.3 will also be modeled [8].

Table 3.2: Elastic Properties of Modeled Materials

Material	Modulus (GPa)	Poisson Ratio
410 Stainless Steel	200	0.3
EK-2200 Carbon Graphite	26.9	0.3
PZT-4	64.5	0.31

$$d = \begin{bmatrix} 0 & 0 & 0 & 0 & 496 & 0 \\ 0 & 0 & 0 & 496 & 0 & 0 \\ -123 & -123 & 289 & 0 & 0 & 0 \end{bmatrix} \times 10^{-12} \frac{C}{N} \quad (3.1)$$

Table 3.3: Relative Dielectric Constants of Modeled PZT-4

Property	Value
ϵ_{11}	1475
ϵ_{22}	1475
ϵ_{33}	1300

Finally, a seal ring composed of a piezoelectric crystal is modeled for the method of piezoelectric actuation. The piezoelectric material used is PZT-4 (lead zirconate titanate), which is modeled as a ceramic with an isotropic elastic modulus of 64.5 GPa and a Poisson ratio of 0.31 [6]. The piezoelectric strain-charge relations of the material are shown in Equation 3.1, the orthotropic relative dielectric constants of the piezoelectric material are shown in Table 3.3 and the elastic properties of all materials are compared in Table 3.2. Two types of piezoelectric seal are modeled: A seal in which the entire face is composed of piezoelectric material and a seal in which

the piezoelectric element is coated with a 2 millimeter thick layer of carbon graphite along the sealing face, resulting in a seal construction similar to that used by Wolff in the liquid oxygen turbopump controllable seal [17].

3.3.3 Hydraulic Actuation Geometry

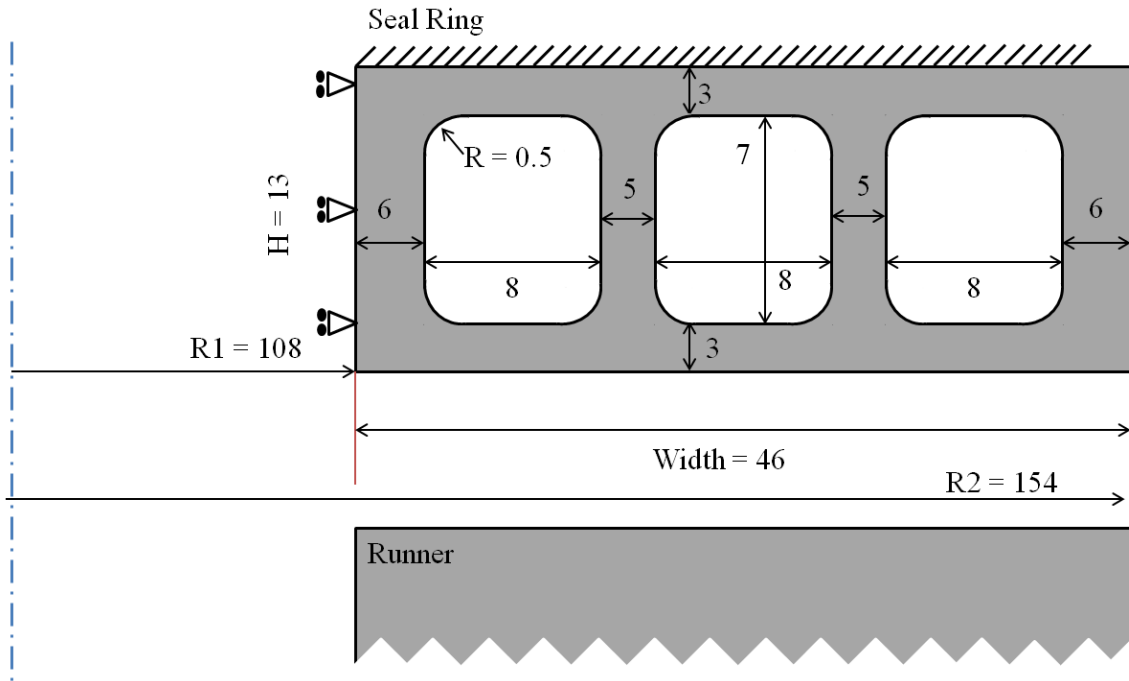


Figure 3.1: Hydraulic Actuation Seal Model (dimensions in mm)

The proposed method of hydraulic actuation uses hydraulic pressure either obtained from the discharge of the RCP (and thus limiting the maximum pressure to the full RCS pressure) or from another existing pump in the RCS system. Alternatively, an additional pumping system could be implemented to pressurize the hydraulic system for control. Three cavities are introduced into the seal face cross-section. These cavities are each 7 mm tall and 8 mm wide and are evenly spaced within the seal face. All corners of the cavities are filleted with a radius of 0.5 mm to reduce stress concentrations in the corners. Within these cavities, which will be filled with hydraulic fluid, a control pressure can be applied which will induce a downward

deflection of the seal face to counteract the deflection caused by the sealed pressure. The applied (or control) pressure attempts to adjust the coning of the seal face, which will alter the leakage rate. Figure 3.1 shows both the overall dimensions of the seal face and the dimensions of the cavities used in the hydraulic control system.

Note that the bottom edge of the seal face is not modeled as perfectly flat. Rather, a dual-taper pre-coning is included in the geometry. This pre-coning is created using three parameters: the two coning angles, α_1 and α_2 , and the radius at which the coning angles change, r_{coning} . The point along the bottom at the inner radius has nominally zero height, and the height of the point at the radius of coning change is found by

$$h_1 = (r_{coning} - r_i) \tan(\alpha_1) \quad (3.2)$$

The height of the point at the outer radius is found by

$$h_2 = h_1 + (r_o - r_{coning}) \tan(\alpha_2) \quad (3.3)$$

The bottom edge is then specified by drawing straight lines between the three points.

3.3.4 Piezoelectric Actuation Geometry

One proposed method of piezoelectric actuation uses a seal face of the same outer dimensions as above, but the entire seal face is modeled as a piezoelectric crystal. No voids are present in the seal cross-section, and a dual-taper pre-coning is included in the geometry. In reality, a coating would be bonded or deposited onto the seal face to provide improved wear and durability properties, but this coating is neglected in one model geometry. A second model which includes a 2 millimeter carbon graphite layer along the bottom edge of the seal face is analyzed. Figure 3.2 shows a schematic of the full piezoelectric seal model, and Figure 3.3 shows a schematic of the piezoelectric

seal with a carbon graphite coating. Note that in Figure 3.3, the carbon graphite face serves as the ground electrode. To simulate the seal ring holder, the top edge of the seal face is given a fixed boundary condition. The piezoelectric crystal is oriented such that it is polarized in the transverse mode, so a voltage applied across the height of the seal, as indicated by the electrodes in the schematic, produces a shear-mode deformation, which will directly influence the coning.

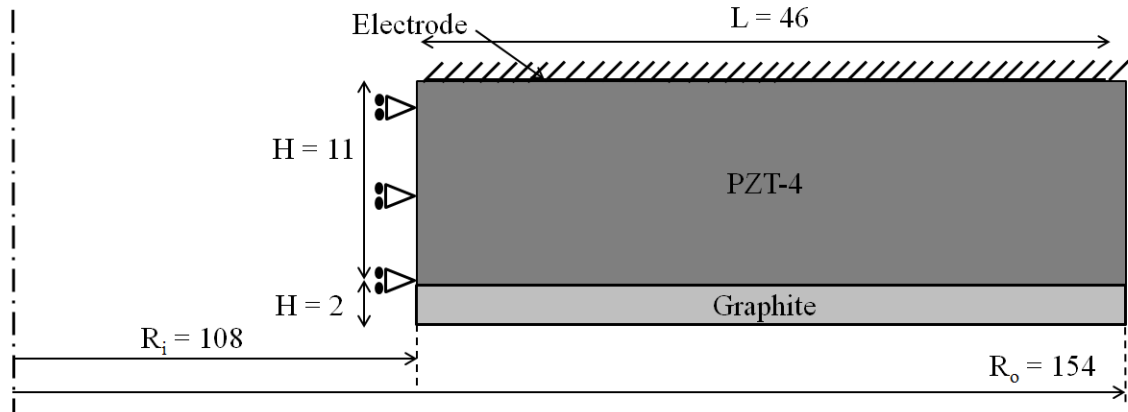


Figure 3.2: Piezoelectric Actuation Seal Model (dimensions in mm)

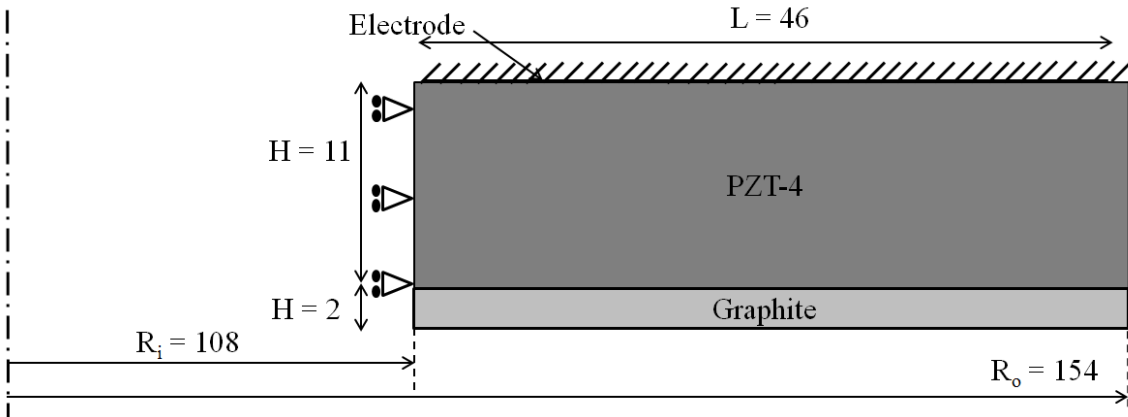


Figure 3.3: Piezoelectric Actuation Seal Model with Carbon Graphite Coating (dimensions in mm)

3.4 Fluid Mechanics Analysis

The fluid mechanics portion of the model is comprised of a numerical solution for the pressure distribution in the fluid film between the seal faces. This represents a lubrication problem because the film thickness is very small compared to the radius and circumference of the seal faces, the fluid film is pressurized, and there is relative motion between the seal faces. These characteristics allow for the general Navier-Stokes equations, which govern fluid mechanics, to be reduced to the less complex Reynolds equation, which is appropriate for the solution of a lubrication problem.

The general form of the Reynolds equation in cylindrical coordinates is [9]

$$\frac{\partial}{\partial r} \left(rh^3 \frac{\partial p}{\partial r} \right) + \frac{1}{r} \frac{\partial}{\partial \theta} \left(h^3 \frac{\partial p}{\partial \theta} \right) = 12\mu_0 \left(v_r \frac{\partial}{\partial r} (rh) + v_\theta \frac{\partial h}{\partial \theta} \right) \quad (3.4)$$

For this analysis, the relative seal face velocity is in the circumferential direction only and the film thickness and pressure field are axisymmetric. Using these assumptions, the cylindrical Reynolds equation is reduced to

$$\frac{\partial}{\partial r} \left(rh^3 \frac{\partial p}{\partial r} \right) = 0 \quad (3.5)$$

Equation 3.5 is discretized using uniform finite volumes across the domain from 1 to N, placing a node every 0.1 mm, such that 461 total nodes are used. The simplified differential equation resembles a one-dimensional heat conduction equation, with rh^3 replacing k , the thermal conductivity, and the pressure replacing the temperature as the desired solution. Patankar describes the discretization and solution of the one-dimensional heat conduction equation using the Tri-Diagonal Matrix Algorithm, so called because the assembled matrix of coefficients for the equations has all the non-zero terms aligned along three diagonals [12]. This TDMA method of solution, adapted from Patankar, is expressed below for the solution of the reduced Reynolds equation. The discretized equation is written as

$$a_i P_i = b_i P_{i+1} + c_i P_{i-1} + d_i \quad (3.6)$$

where P_i represents the sealed pressure at the i^{th} node. b_i represents the coefficient value at the ‘forward’ surface of a finite volume surrounding the i^{th} node. Since the nodal spacing is uniform, it is convenient to place the surface exactly halfway between node i and node $i + 1$. This leads to an expression for b_i that is the harmonic mean of the rh^3 term at nodes i and $i + 1$. In the heat equation, this is expressed in terms of conductivity, k ,

$$b_i = \frac{k_{i+1/2}}{\Delta r} \quad (3.7)$$

where $k_{i+1/2}$ is the harmonic mean of k_i and k_{i+1}

$$k_{i+1/2} = \frac{2k_i k_{i+1}}{k_i + k_{i+1}} \quad (3.8)$$

Replacing k with rh^3 for the reduced Reynolds equation and expressing the film thickness, h , as a function of the radius gives

$$b_i = \frac{\frac{2r_i r_{i+1} h^3(r_i) h^3(r_{i+1})}{r_i h^3(r_i) + r_{i+1} h^3(r_{i+1})}}{\Delta r} \quad (3.9)$$

Likewise, c_i is formulated the same way, except that it represents the finite volume’s left surface, exactly halfway between nodes $i - 1$ and i , as follows

$$c_i = \frac{\frac{2r_i r_{i-1} h^3(r_i) h^3(r_{i-1})}{r_i h^3(r_i) + r_{i-1} h^3(r_{i-1})}}{\Delta r} \quad (3.10)$$

a_i is defined as

$$a_i = b_i + c_i \quad (3.11)$$

Finally, d_i represents a ‘source term’ that will equal zero for any non-boundary node (that is, $d_i = 0$ if $i \neq 1$ or N).

The pressure at each node, P_i , is related to the pressure at the neighboring nodes, P_{i+1} and P_{i-1} . At the left boundary ($i = 1$), $c_1 = 0$. Likewise, when $i = N$, $b_N = 0$. If P_1 is given as a boundary condition, then $a_1 = 1$, $b_1 = 0$, $c_1 = 0$, and $d_1 = P_1$.

This leads to an expression for P_1 in terms of P_2 . When $i = 2$, equation 3.6 is an expression in terms of P_1 , P_2 , and P_3 . Since P_1 can be expressed in terms of P_2 , then the equation becomes a relation between P_2 and P_3 . This process of forward-substitution continues until T_N is expressed in terms of T_{N+1} . At this point, the numerical solution of T_N is found, and the reverse process begins, such that T_{N-1} is found using the numerical value of T_N , and so on.

For the forward substitution, it is desired to have an arrangement such that the current pressure is defined in terms of the next pressure and a coefficient term.

$$P_i = X_i P_{i+1} + Y_i \quad (3.12)$$

The relationship of the previous node is of the same form

$$P_{i-1} = X_{i-1} P_i + Y_{i-1} \quad (3.13)$$

Substituting Equation 3.13 into Equation 3.6 gives

$$a_i P_i = b_i P_{i+1} + c_i X_{i-1} P_i + Y_{i-1} + d_i \quad (3.14)$$

which can be rearranged to have a similar form to Equation 3.12. After rearrangement, the coefficients X_i and Y_i are

$$X_i = \frac{b_i}{a_i - c_i X_{i-1}} \quad (3.15)$$

$$Y_i = \frac{d_i + c_i Y_{i-1}}{a_i - c_i X_{i-1}} \quad (3.16)$$

Patankar refers to these coefficients as the 'recurrence relations,' because they express X_i and Y_i in terms of X_{i-1} and Y_{i-1} . To begin the recurrence process, plug in the values given above for $i = 1$. These values simplify to

$$X_1 = \frac{b_1}{a_1} \quad (3.17)$$

$$Y_1 = \frac{d_1}{a_1} \quad (3.18)$$

Continuing the forward-substitution eventually reaches $i = N$, where $b_N = 0$, which implies $X_N = 0$. Hence $Y_N = P_N$, the known pressure at the right boundary.

In summary, the solution can be described as follows:

1. Find X_1 and Y_1 using Equations 3.17 and 3.18 (For this case, $X_1 = 0$ and $Y_1 = P_1$ from the known boundary pressure).
2. Use the recurrence relations to formulate an X_i and Y_i for $i = 2, 3, \dots, N$.
3. Set $Y_N = P_N$ using the other known boundary pressure.
4. Backsolve for P_i using Equation 3.12, the known values of X_i and Y_i , and the solved value of P_{i+1} .

The boundary conditions for the numerical method are the fluid pressures at the inner and outer diameters of the seal face. For a Westinghouse #1 seal, the operating pressures are 15.51 MPa (2250 psi) at the outer diameter and 0.4826 MPa (70 psi) at the inner diameter. These conditions bound the pressure distribution inside the seal face and serve as the basis for the matrix of coefficients developed during the numerical solution. Also, the film thickness distribution, $h(r)$, must be specified; it is obtained

from the deformation analysis, force balance, and iterative procedure described below. Figure 3.4 shows a typical pressure distribution computed by the numerical model compared to a linear pressure drop across the seal face. Once the nodal pressure distribution is obtained, it is approximated by a fourth-order polynomial curve fit to input into ABAQUS for the deformation analysis. The polynomial form is a more convenient input method, and a warning is included when the curve-fitted pressure differs by more than 1 percent from the computed pressure at a nodal point.

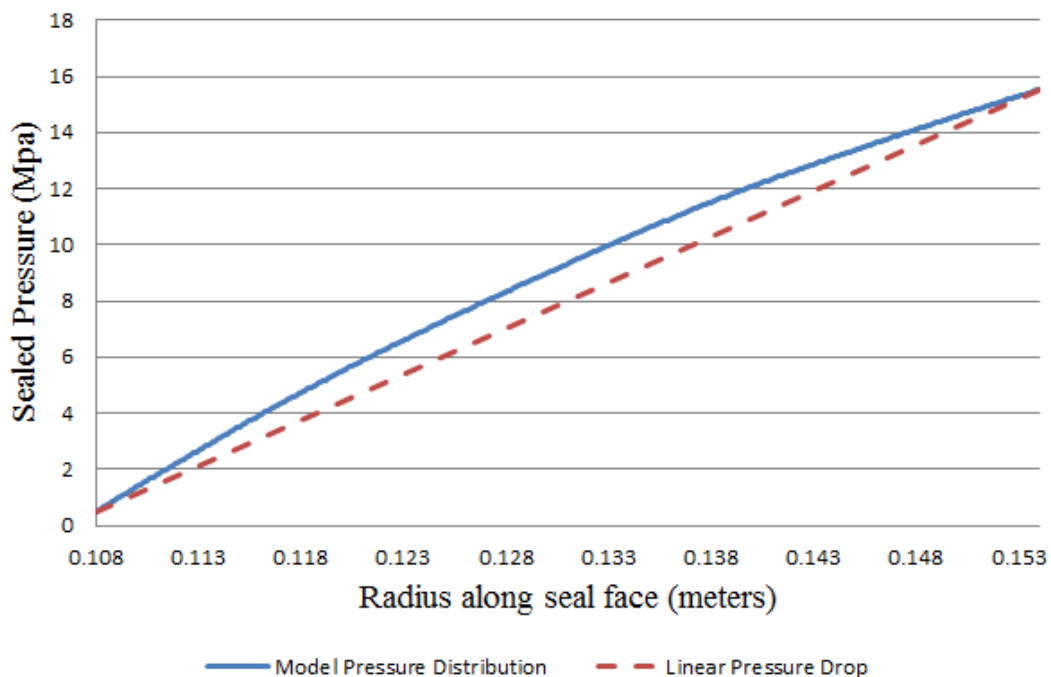


Figure 3.4: Typical Sealed Pressure Distribution

3.5 Deformation Analysis

The deformation analysis component of the model is performed in the commercial finite-element software ABAQUS. Figures 3.5 and 3.6 show typical deformation overlay plots from ABAQUS. The deformation is displayed in millimeters. Figure 3.5 shows the vertical deformation in a stainless steel hydraulic seal with cavity pressures

of 4, 6, and 8 MPa from left to right. Figure 3.6 shows the vertical deformation in a piezoelectric seal with an applied voltage of -4000 V. A portion of the model script is devoted to generating the seal face geometry and creating a finite-element mesh over the axisymmetric cross-section. For the stainless steel hydraulic seal model with base coning angles, a mesh with 26,956 CAX4R 4-node axisymmetric quadrilateral elements is used. The carbon graphite hydraulic seal model with its base coning angles uses a mesh with 27,062 CAX4R elements. The piezoelectric seal model with default coning uses a mesh with 30,695 CAX4E 4-node axisymmetric quadrilateral piezoelectric elements. When the coning is changed, the geometry of the model changes slightly, resulting in small variations in the overall number of elements for other modeled cases. Along the bottom edge of the seal face, at the interface with the fluid film, the mesh is constrained to match that used for the Reynolds equation solver, with 461 equally-spaced nodes. These nodes are not affected by changes in the coning, since their number and spacing are specified manually.

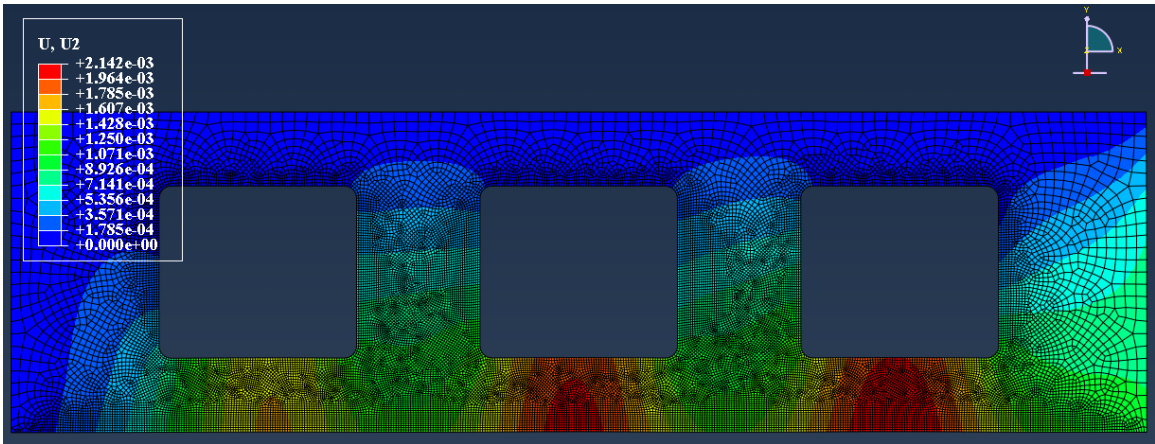


Figure 3.5: Typical ABAQUS Hydraulic Deformation Output (mm)

The pressure field, obtained from the fluid mechanics analysis, is applied and the deformation is computed. To extract the seal face deformation, a nodal path is created in the script by selecting all of the nodes along the bottom edge of the seal face and reading the z displacement of those nodes. Three components dictate

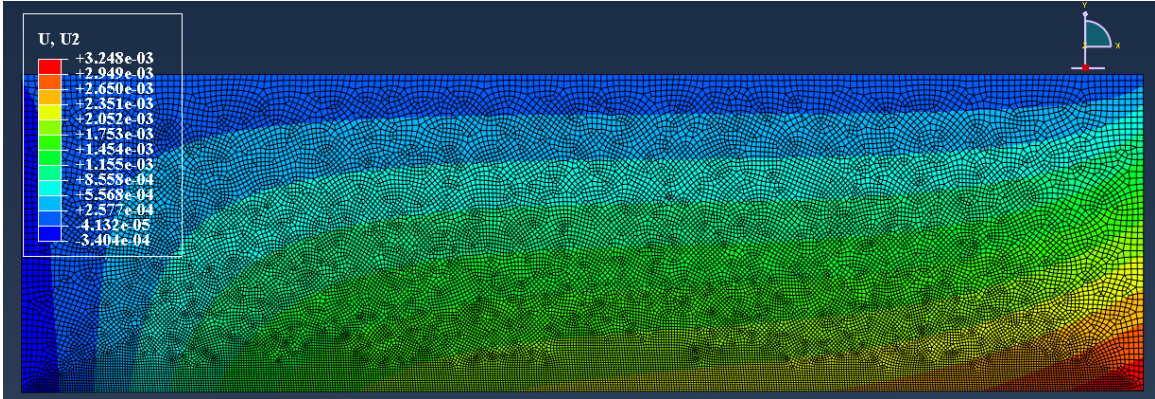


Figure 3.6: Typical ABAQUS Piezoelectric Deformation Output (mm)

the overall film thickness: the minimum film thickness (the narrowest point of the face gap at the inner diameter), the pre-coning (the coning manufactured into the seal face), and the deformation. The sum of these three components yields the film thickness at each node. Figure 3.7 shows a typical film thickness distribution after convergence of the deformation analysis for a stainless steel hydraulic seal with cavity pressures of 4, 6, and 8 MPa from left to right, corresponding with the deformation case shown in Figure 3.5. Note that the vertical axis is shown in microns, while the horizontal axis is shown in millimeters, so the apparent waviness is magnified.

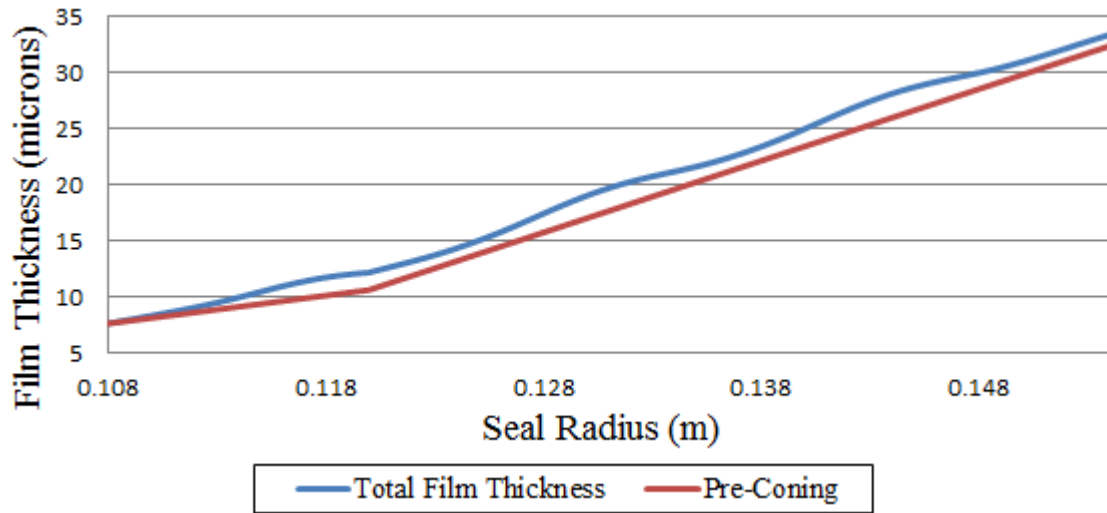


Figure 3.7: Typical Film Thickness Distribution

3.6 Force Balance

After the fluid mechanics and deformation analyses are converged, a component of the results is a vector of pressures at each radial node. These values represent the radial sealed pressure distribution, which is integrated over the area of the seal face to obtain the opening force. Since the pressures are represented as discrete numerical values, Simpson's rule is used to integrate along the radial coordinate. Because the pressure varies only with the radius, the circumferential coordinate is included through multiplication by 2π .

$$F_{opening} = 2\pi \int_{r_i}^{r_o} p(r) dr \quad (3.19)$$

A mechanical seal operating in axial equilibrium has an opening and closing force that oppose and balance one another. The closing force is produced by the sealed pressure acting on the back surface of the floating face and forces exerted by other components of the seal assembly (e.g. the spring force and friction from the secondary seals). For this analysis, the closing force is specified to be constant and the model proceeds iteratively until the opening force balances the closing force within a convergence criterion. The nominal closing force for the seal is estimated by running the model with base coning and without including deformation for varied values of the closing force until the leakage rate equals the nominal leakage rate for the Westinghouse #1 seal.

3.7 Iteration Process

The structure of the numerical model is its iterative computational procedure by which an equilibrium configuration is found. The model is constructed using specified parameters of the seal, including operating conditions, geometry, and fluid properties, and the numerical procedure is initialized with guesses of the minimum film thickness and the film thickness and pressure distributions. Then, the model adjusts the guessed

parameters until a convergence criterion is reached and the seal operation satisfies the equilibrium condition. This framework reflects the self-adjusting nature of mechanical seals and their ability to modify the face gap with changing system conditions to achieve stable operation. For the hydraulic control model, the critical parameters are the pressures applied within the control cavities, because these pressure dictate the deformation of the seal face and thus control the coning and the seal response. For the piezoelectric control model, the critical parameter is the applied voltage across the piezoelectric element, because it likewise dictates the deformation and coning of the seal face.

The iteration procedure is illustrated in Figure 3.8. The procedure contains two nested loops. The internal loop is responsible for the convergence of the seal deformation, the resulting film thickness distribution, and the pressure distribution. The external loop checks for force balance and guesses a new minimum film thickness until force balance is obtained. For the steel model, an initial minimum film thickness guess of 5 microns is used. For the carbon graphite model, the reduced coning leads to a reduced film thickness on average, so to speed convergence an initial minimum film thickness guess of 3 microns is used. The piezoelectric model uses an initial guess of 5 microns. If the internal loop converges but the forces are not balanced, a new minimum film thickness guess of 80 percent of the first guess is used. When the internal loop converges again, if the forces are still not balanced, the external loop continues to guess a new minimum film thickness using the following scheme [13]

$$h_m^{i+1} = \exp \left[\frac{\Delta f^{i-1} \ln h_m^i - \Delta f^i \ln h_m^{i-1}}{\Delta f^{i-1} - \Delta f^i} \right] \quad (3.20)$$

where $i+1$ represents the guessed value for the next iteration, i is the current iteration, and $i-1$ is the previous iteration. Δf is the difference between the closing force and the opening force, and h_m is the minimum film thickness. This scheme provides a somewhat directed method of guessing, where the past values of the minimum film

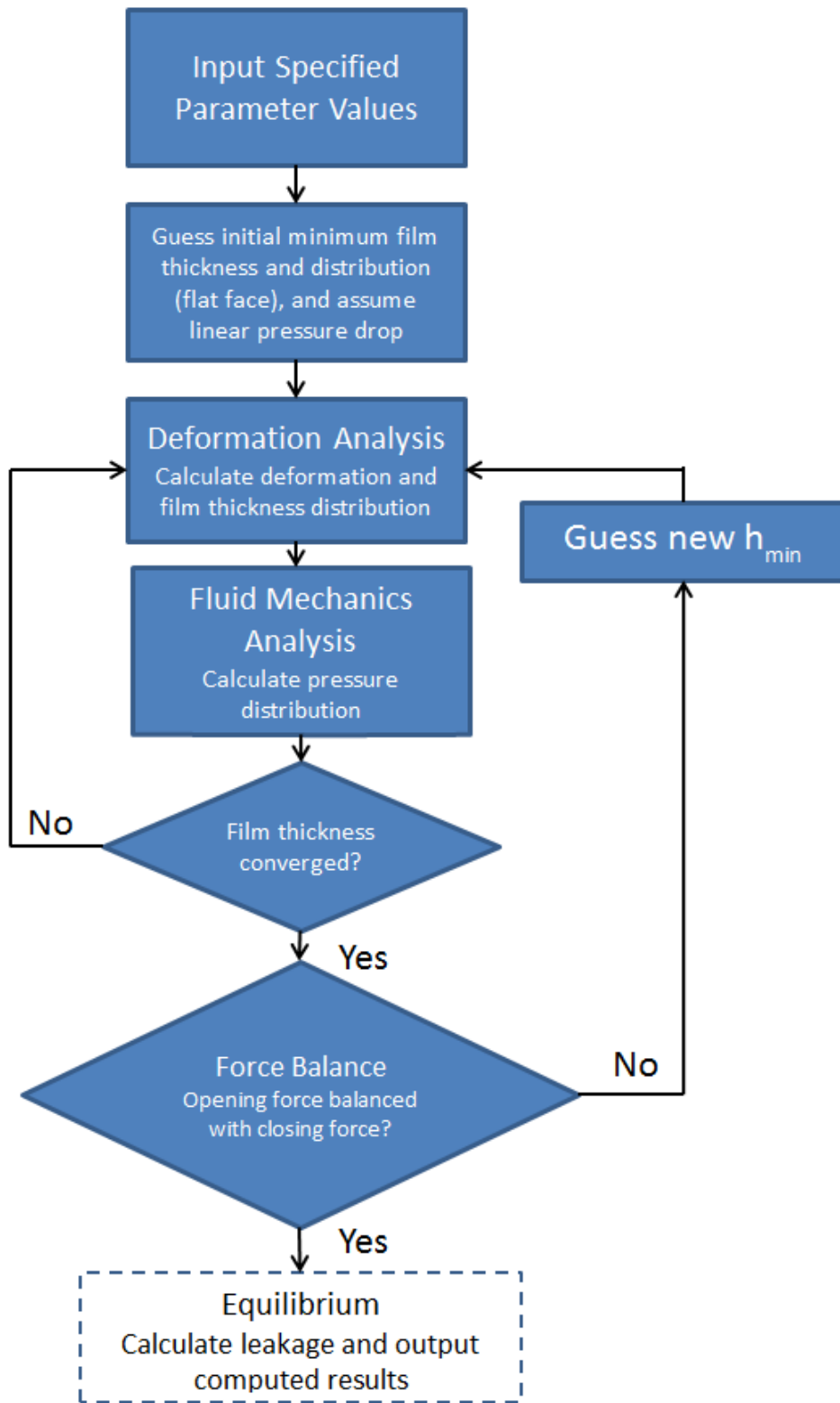


Figure 3.8: Computational Procedure

thickness and the opening forces they produced are used to influence the next guess to be input. This is much more efficient than simply guessing from a prescribed range of values and allows the algorithm to achieve the correct value in fewer iterations, greatly speeding convergence of the force balance. A convergence criterion of 0.5 kN is used for the force balance; the closing force is on the order of 500 kN.

For the internal loop, a convergence criterion of 0.03 microns is used to check the local convergence of deformation at each node along the bottom edge of the seal face. An under-relaxation factor of 0.2 is used on the film thickness to avoid numerical instability after five iterations of the internal loop. The first five iterations of every cycle of the internal loop are not relaxed, because they generally contain large changes in film thickness as the model rapidly approaches convergence before relaxation is implemented.

When the iteration process is completed, a converged deformation profile has been found. The most recent minimum film thickness guess and the converged deformation profile produce a total film thickness distribution that is used to calculate a sealed pressure distribution. The sealed pressure distribution is then integrated to give an opening force, and for a fully converged analysis, the opening force balances the closing force. Thus, an equilibrium state has been achieved and the leakage rate can be calculated using

$$Q = \frac{-\pi}{6\mu} \left[h^3 r \frac{\partial p}{\partial r} \right]_{r=r_i} \quad (3.21)$$

3.8 Potential Control Systems

The control system used to moderate the hydraulic control pressures or piezoelectric voltage to control seal operation is an important component of the proposed controllable seal. While a fully developed control system is considered beyond the scope of this thesis, some preliminary options for the general structure of the control system

are considered below. These include a schematic of a potential control system and some comments for its basic components and operation.

3.8.1 Hydraulic Control System

Two possibilities are considered for a hydraulic control system: a method that uses a single point of electronic control and hardware to create three separate control pressures and a method that uses three independent electronically-controlled valves to provide the control pressures. The first method is illustrated in Figure 3.9. A microcontroller is connected to a single pressure control valve which moderates the full sealed RCS pressure. Then, the controlled pressure is fed by three lines into three independent hydraulic intensifiers, which are devices that amplify hydraulic pressure by using a ratio of areas exposed to fluid on either side of the device. The RCS side of each intensifier would be exposed to RCS water at the electronically controlled pressure, and the seal face side of each intensifier would act on a sealed line of hydraulic oil which would independently pressurize a single control cavity. By carefully choosing the area ratio of each intensifier, three different control pressures which are proportional to one another could be achieved. In this control method, the relationships between the three control pressures would be fixed by the selected hardware.

The second control system approach is shown in Figure 3.10. In this approach, a single hydraulic intensifier is exposed to RCS water at the full sealed pressure on one side and hydraulic oil on the other side. A microcontroller is connected to three independent pressure control valves which moderate the pressure in the hydraulic oil from the intensifier. This method can employ software-based control of the cavity pressures and can provide for any desired relationship (or none at all) between them. In addition, the intensifier isolates the entire control system from possible contaminants in RCS water.

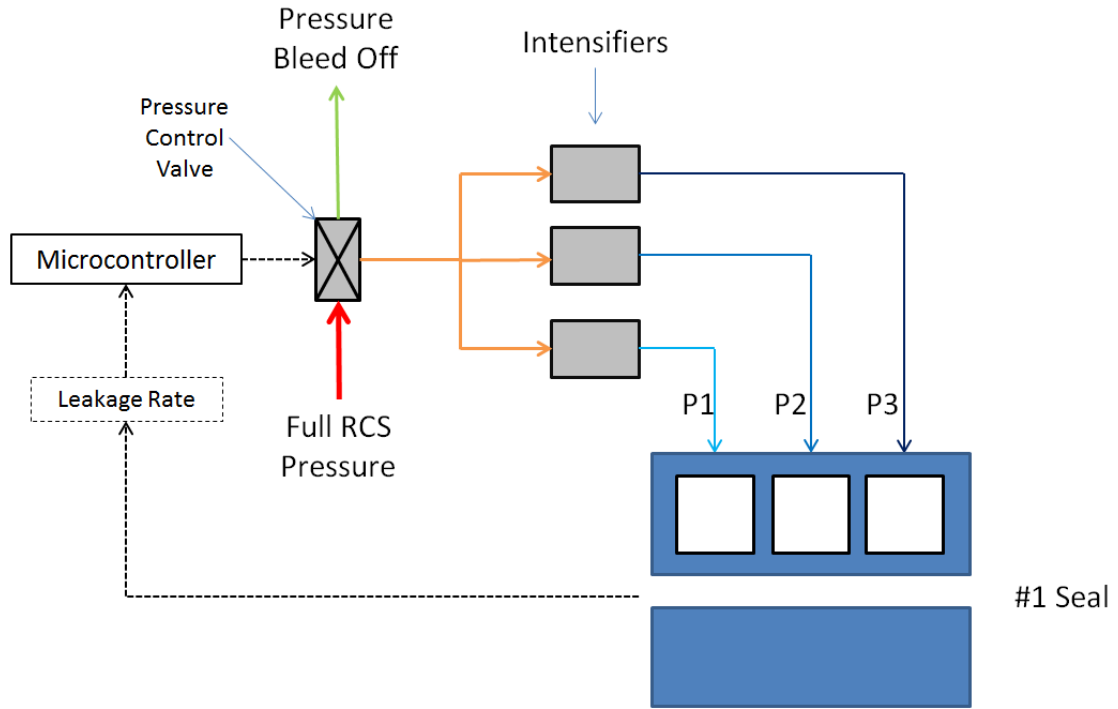


Figure 3.9: Proposed Hardware-Based Hydraulic Control System

3.8.2 Piezoelectric Control System

The proposed control system for the piezoelectric seal is shown in Figure 3.11. This system is extremely simple compared to the hydraulic control systems, requiring only a microcontroller to regulate the voltage applied to the top electrode. The bottom electrode serves as the ground. The main concern for this system would be isolation of the electrodes from the RCS water to avoid corrosion or other unintended interactions with the cooling system.

Note that all three figures for the control systems exhibit closed-loop control, in which the leakage rate is fed from a sensor into the microcontroller, which then adjusts the control parameters to obtain the desired leakage rate. Any of the above systems could also be operated in open-loop mode, in which a plant operator manually adjusts one or multiple control pressures or the applied voltage, depending on the scenario.

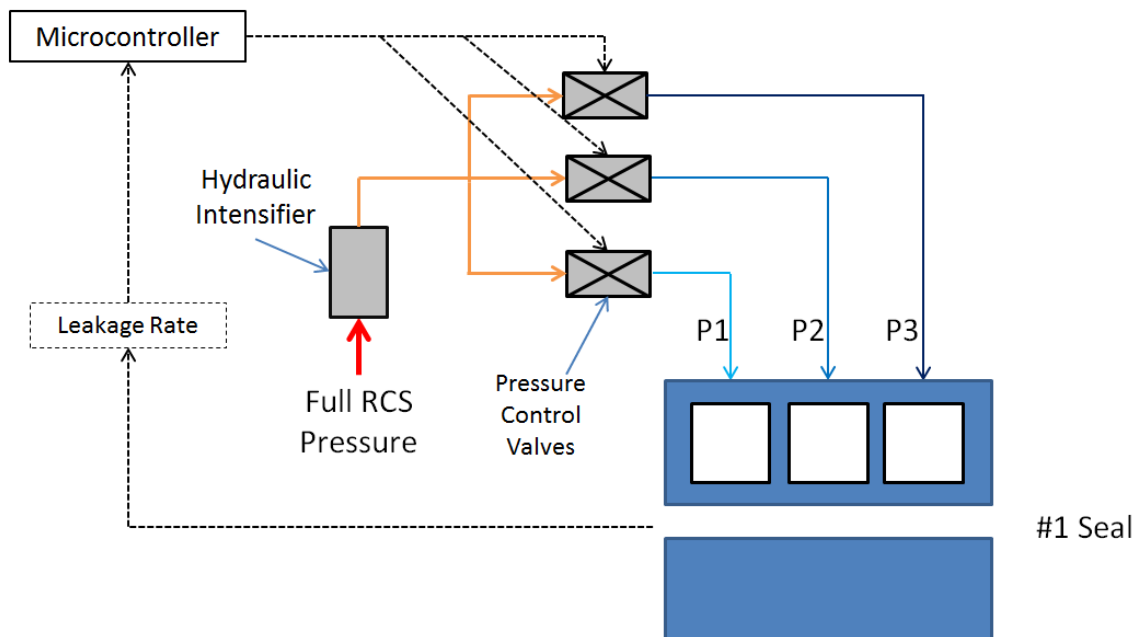


Figure 3.10: Proposed Software-Based Hydraulic Control System

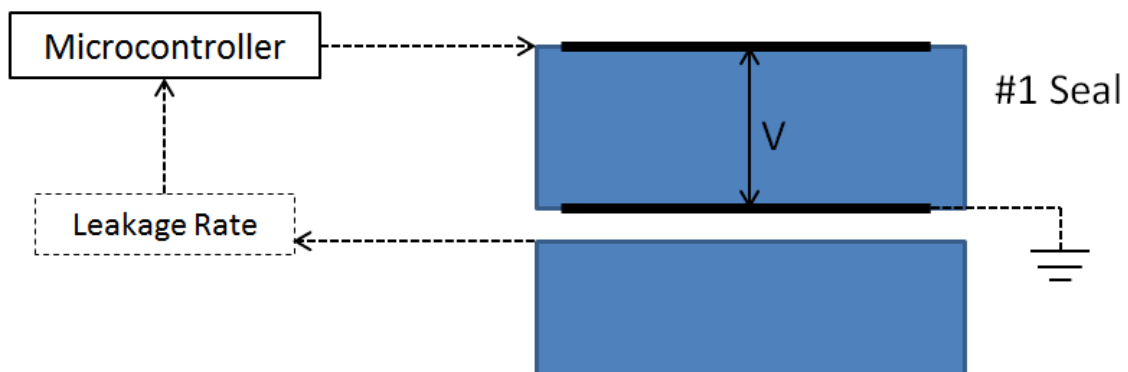


Figure 3.11: Proposed Piezoelectric Control System

CHAPTER IV

RESULTS

The numerical model described above finds a state of equilibrium seal operation for a given set of operating conditions. The parameter of interest for utilities is the leakage rate of the seal, and the desired result of the numerical model is to demonstrate that active control of the seal can alter the leakage rate. Several cases of seal operation are considered, with varied values of pre-coning and closing force and different seal materials. To demonstrate the controllability of the seal in each case, the active control parameter (either the hydraulic pressure in the cavities or the voltage across the piezoelectric element) is varied for several trials per case and the leakage rate is recorded for each trial. The sections below detail the leakage rate versus the control parameter for each case and comment on the controllability of the various proposed seal materials and control methods.

4.1 Hydraulic Actuation Results - Varying Leakage Rates

The proposed method of hydraulic actuation uses maximum control pressures on the order of the nominal reactor coolant system pressure. Since the sealed pressure does not vary linearly with the seal radius due to pre-coning and additional coning caused by seal face deformation, using high pressures in all three control cavities can highly restrict the leakage. It is reasoned that using a control pressure in each cavity that roughly corresponds with the sealed pressure at the radius directly beneath the cavity can achieve satisfactory control of the leakage. A variety of control schemes could be used, but in the present study, it is reasoned that a method which moderates the control pressures such that the control pressures decrease from outer diameter to inner diameter, much like the sealed pressure, while allowing each control pressure

to be expressed in terms of a single value will give the desired positive coning with a simple control scheme. The leakage rate studies are performed by choosing a pressure for the innermost cavity (P_1) and setting the center cavity and outer cavity pressures (P_2 and P_3 , respectively) with respect to P_1 as follows

$$\begin{aligned} P_2 &= P_1 + 2 \text{ MPa} \\ P_3 &= P_1 + 4 \text{ MPa} \end{aligned} \tag{4.1}$$

This arrangement yields concise results in which the calculated leakage rate can be compared to a single control value. In addition, results are recorded for cases in which all cavity pressures are set to 0.01 MPa, which simulates a total loss of control pressure, as might happen during station blackout conditions. This conveniently also represents the maximum leakage rate achieved by each configuration of the controllable seal. Finally, results are recorded for a nominal maximum pressure in all three cavities of 14 MPa, which is approximately the same as the nominal reactor coolant system pressure of 15.51 MPa (2250 psi). The slightly lower pressure is used both as a small factor of safety and to factor in some head loss in any potential control system. Also, a maximum pressure of 14 MPa ensures that the yield stress of the seal material is not reached, even under maximum pressurization in all three cavities.

4.1.1 Stainless Steel Face

A typical film thickness distribution for the steel seal face is illustrated in figure 4.1. The Deformed Face Gap shown is the converged film thickness distribution, composed of the minimum film thickness at the inner radius, the pre-coning (also plotted separately), and the mechanical deformation caused by the sealed pressure distribution. This film thickness distribution was computed with base values for pre-coning and closing force, the nominal sealed pressure of 15.51 MPa (2250 psi), and control pressures of 4, 6, and 8 MPa from inner to outer cavities.

Note that the apparent waviness in the deformed face gap is due to the steel ‘ribs’

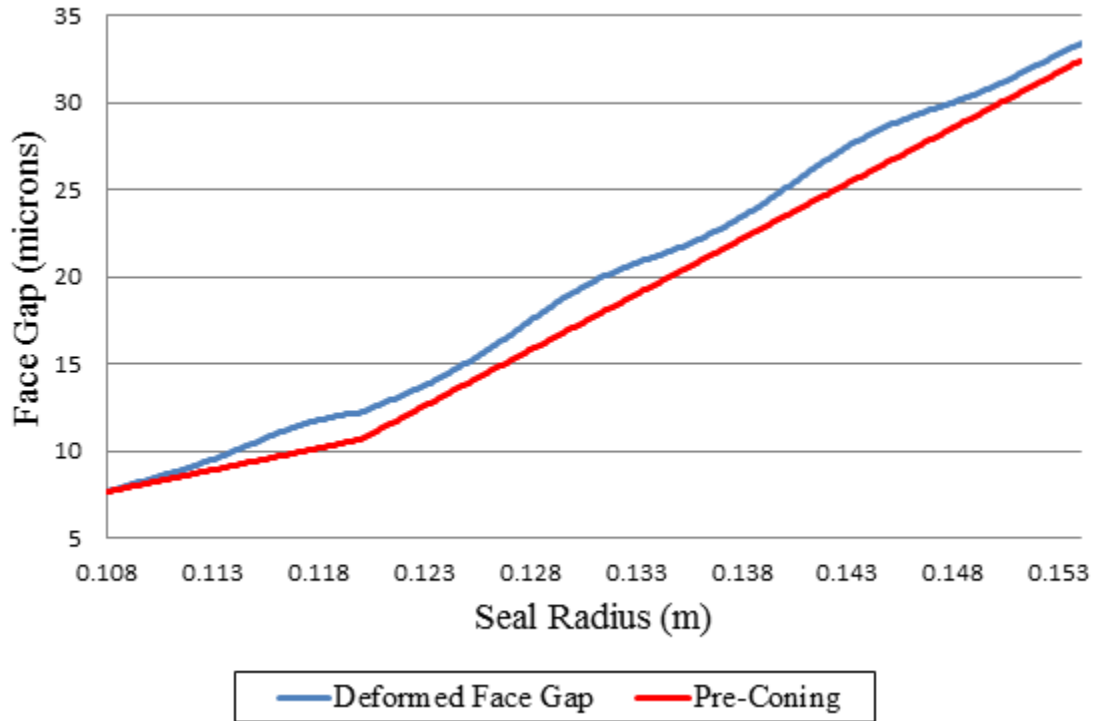


Figure 4.1: Typical Film Thickness and Pre-Coning for Steel Face

between the control pressure cavities. These ribs, being solid material, resist deformation more effectively than the pressurized cavities, resulting in a slight concavity across the radial extent of each internal void. Because the sealed pressure in the face gap is relatively high, the possible presence of a slight diverging gap does not result in below-ambient pressure or cavitation. Also, the appearance of waviness is exaggerated in the figure, since the vertical axis is shown in microns while the radius is shown in meters. Figure 4.2 shows the sealed pressure distribution computed for the same configuration as described above. Note that the sealed pressure distribution shows the expected curved shape for a mechanical seal with positive coning. This sealed pressure distribution is typical in appearance for all trials with the steel seal face, with variations based on the amount of coning change by the active control method.

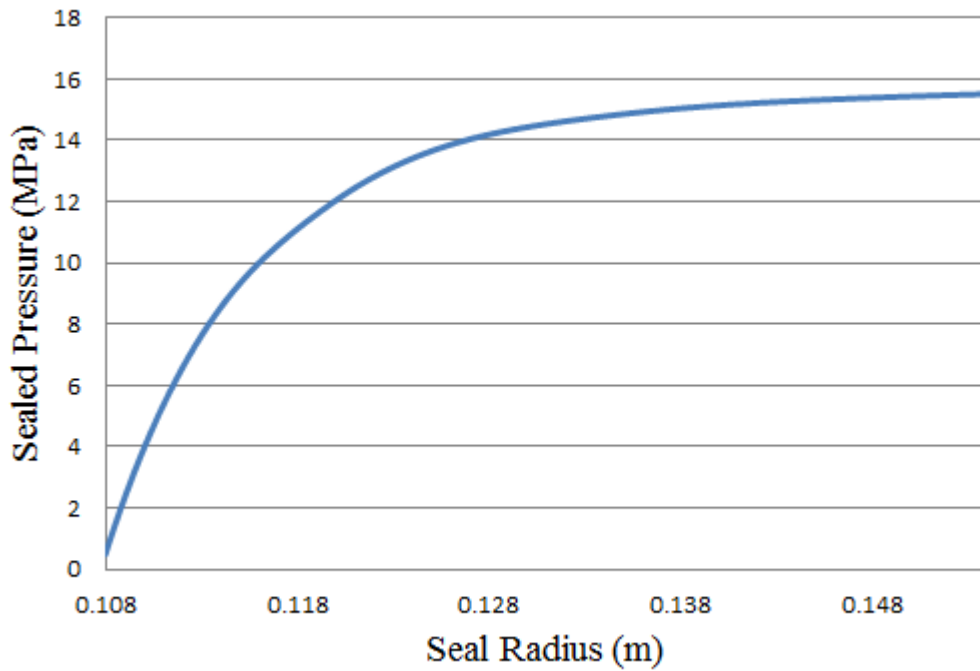


Figure 4.2: Typical Sealed Pressure Distribution for Steel Face

4.1.1.1 *Default Pre-Coning and Closing Force*

The calculated leakage rate as a function of cavity pressure P_1 (Note that P_2 and P_3 are functions of P_1) is shown in Table 4.1 for the base values of closing force and pre-coning. Also shown are leakage rates for complete loss of control pressure (control pressures equal to 0.01 MPa) and maximum control pressure (14 MPa). The leakage rate in L/min is plotted versus P_1 in Figure 4.3. Note that the base closing force magnitude of 0.495 MN was chosen with the Reynolds equation solver without including deformation. Therefore, when the full model is run and deformation is included, the calculated leakage rate will be higher than the nominal leakage rate. This is illustrated as expected in the table below.

Table 4.1: Stainless Steel, Base Coning Leakage Study

F_{close}	0.495 MN			
P_1 (MPa)	P_2 (MPa)	P_3 (MPa)	Q (L/min)	Q (gpm)
1	3	5	17.59	4.65
2	4	6	17.16	4.53
4	6	8	16.19	4.28
6	8	10	15.22	4.02
8	10	12	14.40	3.80
10	12	14	13.51	3.57
0.01	0.01	0.01	18.91	5.00
14	14	14	12.44	3.29

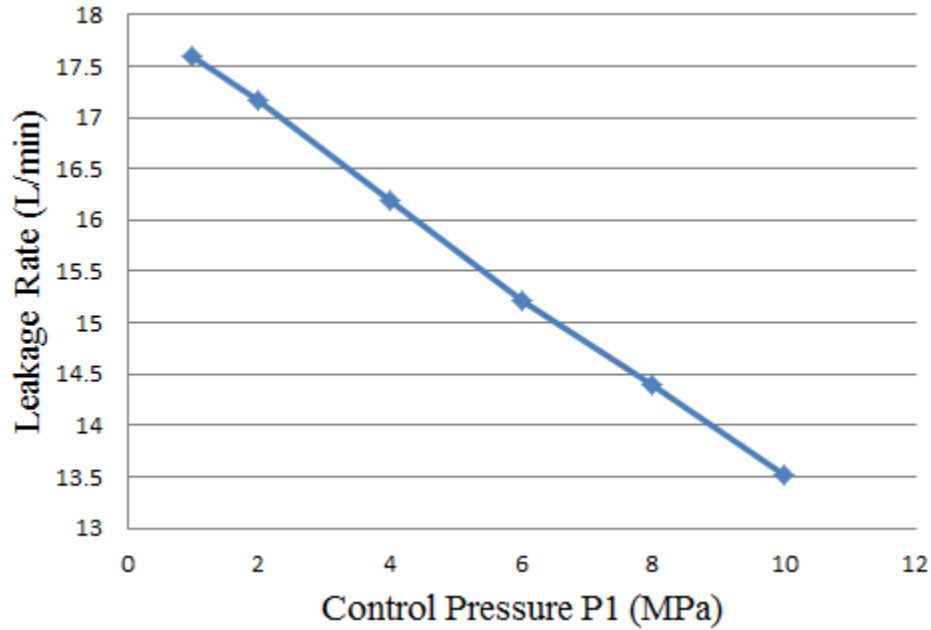


Figure 4.3: Leakage Rate vs. Cavity 1 Pressure, Steel, Base Case

4.1.1.2 Default Pre-Coning, Increased Closing Force

One method of obtaining the nominal leakage rate after deformation is included in the analysis is to increase the closing force on the seal. This has the effect of reducing the minimum film thickness, closing the face gap and reducing the leakage rate. To obtain the leakage study detailed below, the closing force is increased such that a P_1

value of 5 MPa gives roughly the nominal leakage rate of 11.36 L/min (3.00 gpm). This value of P_1 represents the center of the control range between 0 and 10 MPa. 10 MPa is the nominal maximum value of P_1 because it gives a P_3 value of 14 MPa, the desired maximum value of control pressure. This effectively ‘centers’ the range of controllability around the nominal leakage rate, ensuring that the seal can respond to leakage rate deviations in either direction. The closing force that gives the desired behavior described above is found to be 0.5025 MN, and the results of the increased closing force configuration are shown in Table 4.2 and Figure 4.4.

Table 4.2: Stainless Steel, Increased Closing Force Leakage Study

F_{close}	0.5025 MN				
P_1 (MPa)	P_2 (MPa)	P_3 (MPa)	Q (L/min)	Q (gpm)	
1	3	5	13.01	3.44	
2	4	6	12.66	3.34	
4	6	8	11.89	3.14	
6	8	10	11.15	2.95	
8	10	12	10.42	2.75	
10	12	14	9.71	2.56	
0.01	0.01	0.01	14.05	3.71	
14	14	14	8.72	2.30	

While increasing the closing force centers the seal’s range of control around the nominal leakage rate, it does not have a significant effect on the size of the range. Note that the steel seal can vary the leakage rate between 9.71 and 13.01 L/min (2.56 and 3.44 gpm) when P_1 is varied between 1 and 10 MPa and P_2 and P_3 are set according to P_1 using the control scheme discussed above, discounting the loss of pressure and maximum pressure cases in all three cavities. This range of control during normal operation can address some abnormal leakage rates encountered by utilities, but may not be sufficient in extreme cases of abnormal leakage, since it can vary the leakage rate only around 2 L/min in each direction from the nominal leakage rate of 11.36

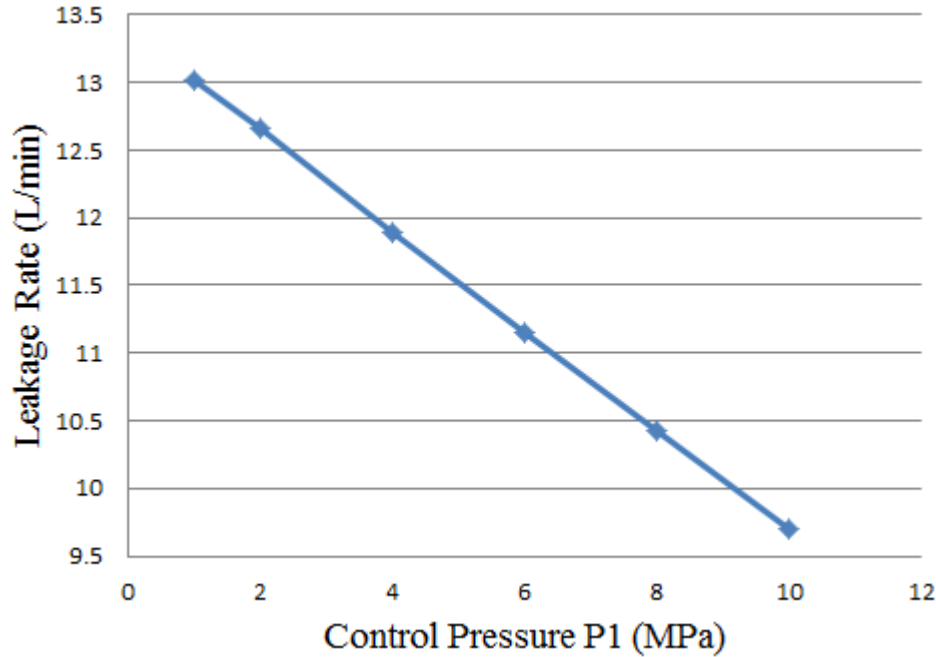


Figure 4.4: Leakage Rate vs. Cavity 1 Pressure, Steel, Increased Closing Force

L/min.

4.1.1.3 Reduced Pre-Coning, Default Closing Force

Another method of obtaining the nominal leakage rate when deformation is included is to reduce the pre-coning of the seal face. As described in Section 2.1.4.1, the coning and the average film thickness are proportional to one another. A reduction in pre-coning results in less coning overall, so the minimum film thickness is reduced as well, which in turn reduces the leakage rate. Again, a pre-coning configuration is chosen so that a P_1 of 5 MPa gives approximately the nominal leakage rate. The results of the reduced pre-coning configuration are shown in Table 4.3 and Figure 4.5.

Adjusting the pre-coning is a preferable method of adjusting the seal's performance so that roughly the nominal leakage rate is given when P_1 is 5 MPa. Again, this adjustment moves the range of leakage rates so that the nominal leakage rate is in the center of the range, but the steel seal with reduced pre-coning can vary the

Table 4.3: Stainless Steel, Reduced Pre-Coning Leakage Study

F_{close}	0.495 MN			
P_1 (MPa)	P_2 (MPa)	P_3 (MPa)	Q (L/min)	Q (gpm)
1	3	5	13.15	3.47
2	4	6	12.73	3.36
4	6	8	11.96	3.16
6	8	10	11.24	2.97
8	10	12	10.55	2.79
10	12	14	9.79	2.59
0.01	0.01	0.01	14.21	3.75
14	14	14	8.94	2.36

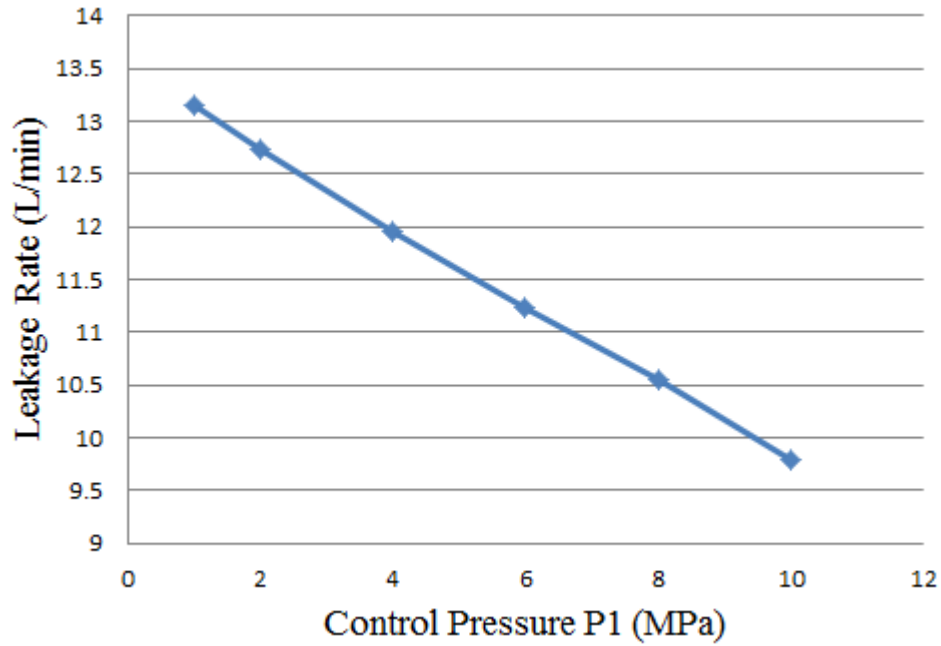


Figure 4.5: Leakage Rate vs. Cavity 1 Pressure, Steel, Reduced Pre-Coning

leakage rate only between 9.79 and 13.15 L/min (2.59 and 3.47 gpm). This is a range of 3.36 L/min. The results for the steel seal show that the hydraulic control system is effective at changing the leakage rate, but the magnitude of the change may be insufficient due to steel's resistance to deformation. In the next section, the carbon graphite seal's response is shown. This softer material is expected to yield a larger

range of leakage rate variation.

4.1.2 Carbon Graphite Face

It is noted that the mechanical deformations caused by both the sealed pressure and the control pressures strongly affect the leakage rate by changing the coning. Therefore, it is reasoned that seal controllability could be increased by decreasing the elastic modulus of the seal face material, thus making it more sensitive to deformation by similar loads. A softer material that is commonly used in general mechanical seal applications and even nuclear reactor coolant pump seals is carbon graphite. Because the carbon graphite face deforms more under the same loads as the steel face, it should exhibit a greater range of leakage rate control. The results described below are of similar form to the steel results above, so that the controllability of a seal composed of each material can be directly compared.

First, a typical film thickness distribution is shown for the carbon graphite seal in Figure 4.6. Note that the carbon graphite seal appears much more wavy in the radial direction than the steel seal. This is indeed due to the softer material, as expected. This film thickness distribution was calculated using the base closing force, a sealed pressure of 15.51 MPa (2250 psi), and control pressures of 4, 6, and 8 MPa. The pre-coning is also shown.

Again, the exaggeration of the apparent waviness in the figure is due to a vertical scale of microns versus a horizontal scale of meters. The waviness is caused by the carbon graphite ribs between the control pressure cavities. These ribs, identical to the ribs in the steel seal, resist deformation more than the cavities, and the softness of the carbon graphite causes more pronounced waviness. When Figure 4.6 is compared to Figure 4.1, it is clear that the carbon graphite face experiences much more deformation under identical pressures than the steel face. The pressure distribution found for the carbon graphite seal is shown in Figure 4.7.

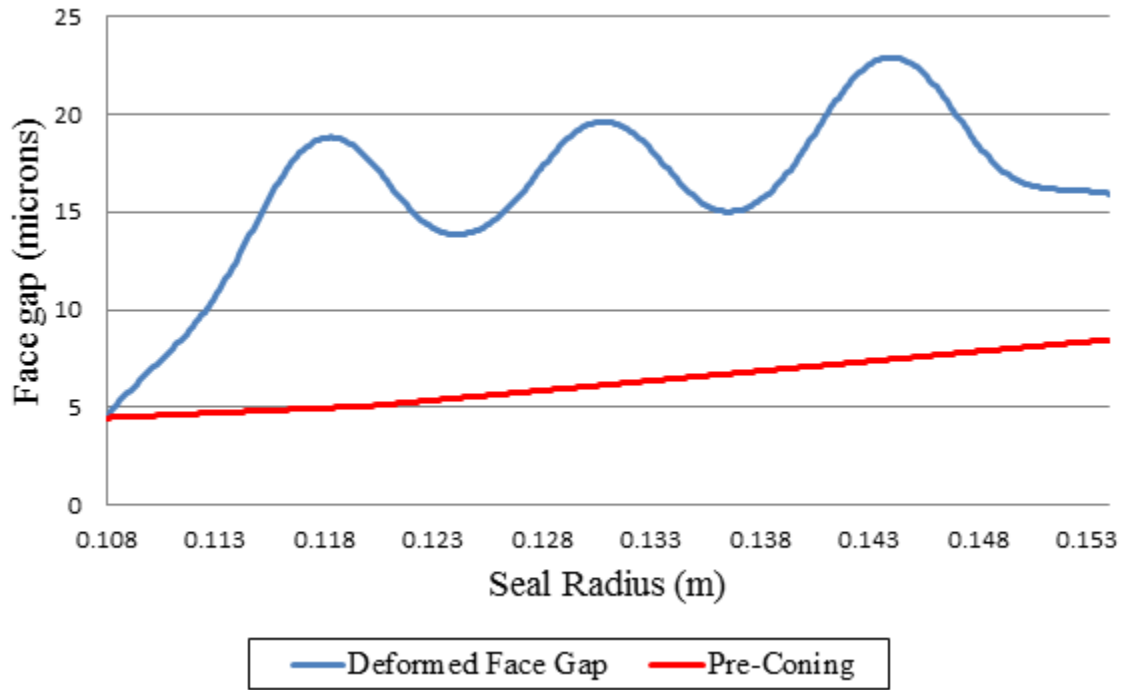


Figure 4.6: Typical Film Thickness Distribution for Carbon Graphite Seal Face

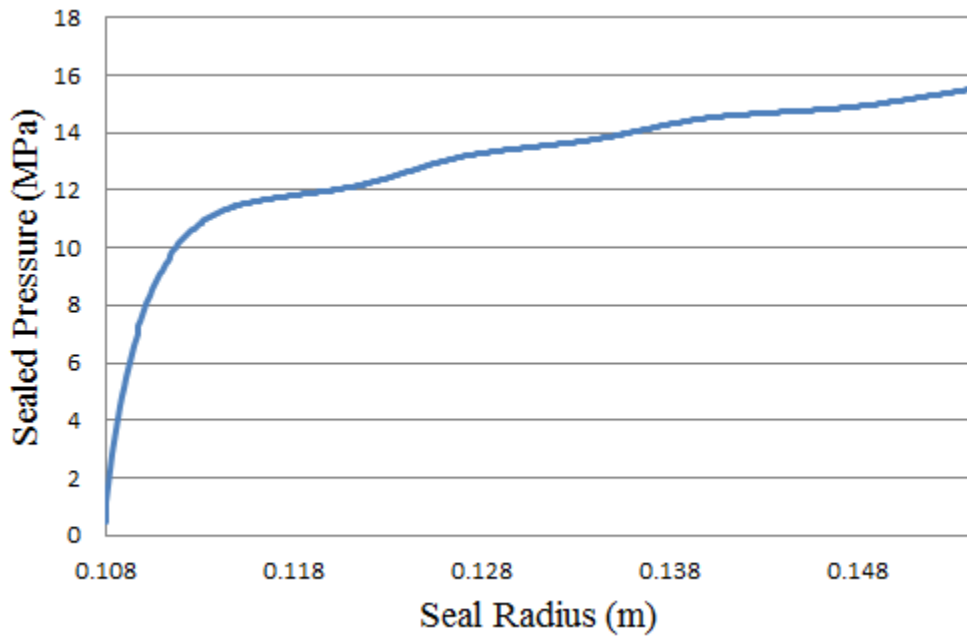


Figure 4.7: Typical Sealed Pressure Distribution for Carbon Graphite Seal Face

4.1.2.1 Carbon Graphite Base Case

As described above, the softer carbon graphite material deforms more than the steel seal face, so in order to obtain the nominal leakage rate for a base case, the pre-coning must be reduced compared to the base value. Thus, the base case for carbon graphite has the nominal closing force of 0.495 MN and a reduced pre-coning. Note that the same value for the reduced pre-coning is used in all three carbon graphite studies described in this section. The results for the base carbon graphite case are shown below in Table 4.4 and Figure 4.8.

Table 4.4: Carbon Graphite Base Case

F_{close}	0.495 MN				
P_1 (MPa)	P_2 (MPa)	P_3 (MPa)	Q (L/min)	Q (gpm)	
1	3	5	17.91	4.73	
2	4	6	16.27	4.30	
4	6	8	12.72	3.36	
6	8	10	9.74	2.57	
8	10	12	7.49	1.98	
10	12	14	4.79	1.27	
0.01	0.01	0.01	25.09	6.63	
14	14	14	3.72	0.98	

It is apparent that the carbon graphite face experiences more deformation than the steel face, so it is expected that the carbon graphite face should respond more easily to the control pressures and give a wider variation of leakage rates. This behavior is readily shown in Figure 4.8. The carbon graphite face can vary the leakage rate between 4.79 and 17.91 L/min (1.27 and 4.73 gpm). This range of 13.12 L/min is nearly four times as large as the 3.36 L/min range of the steel seal face with reduced pre-coning. Thus, the carbon graphite controllable seal is shown to be far more capable than the steel controllable seal at varying the leakage rate under the same operating conditions.

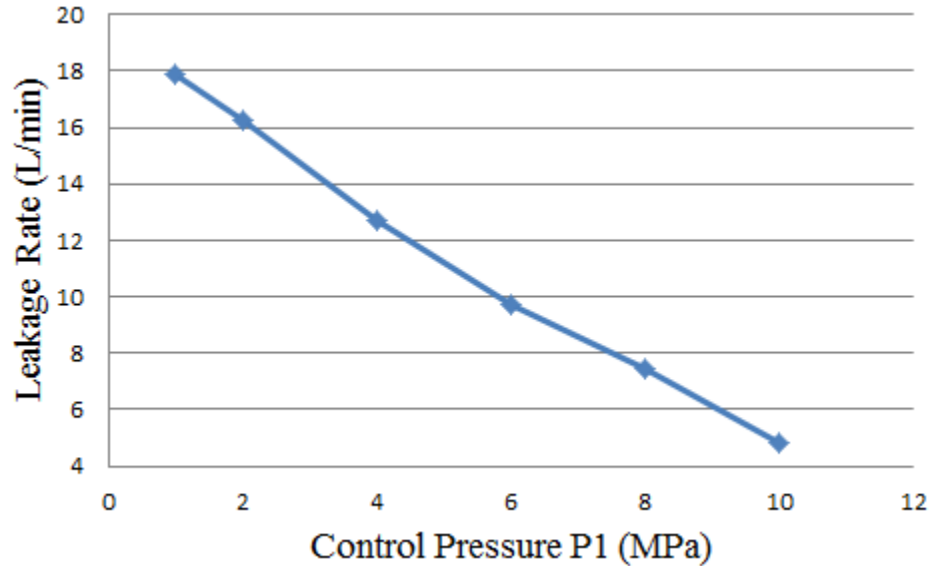


Figure 4.8: Leakage Rate vs. Cavity 1 Pressure, Carbon Graphite, Base Case

4.1.2.2 Carbon Graphite Reduced Closing Force

To examine the effect of the closing force on the leakage rate, the pre-coning is left the same as the base case and the closing force is reduced to 0.49 MN (a reduction of 0.005 MN or 5,000 N). This reduction in closing force causes an increased leakage rate because the face gap opens as the seal adjusts to a new equilibrium position. The results of the reduced closing force leakage study are shown below in Table 4.5 and Figure 4.9.

Reducing the closing force increases the leakage rate for the same set of control pressures, giving a range of leakage rates between 5.68 and 19.83 L/min (1.50 and 5.24 gpm). This range of 14.15 L/min is comparable to the range of the base carbon graphite case. Changing the closing force can shift the values of the leakage rates but does not change the basic response of the seal to the control pressures. A changed closing force in a seal design could be useful to bias the range of leakage rate variation higher or lower than the nominal leakage rate, depending on which type of abnormal leakage rate is anticipated to be most frequent or severe.

Table 4.5: Carbon Graphite, Reduced Closing Force Leakage Study

F_{close}	0.490 MN			
P_1 (MPa)	P_2 (MPa)	P_3 (MPa)	Q (L/min)	Q (gpm)
1	3	5	19.83	5.24
2	4	6	17.87	4.72
4	6	8	14.37	3.80
6	8	10	11.34	3.00
8	10	12	8.06	2.13
10	12	14	5.68	1.50
0.01	0.01	0.01	28.79	7.60
14	14	14	4.46	1.18

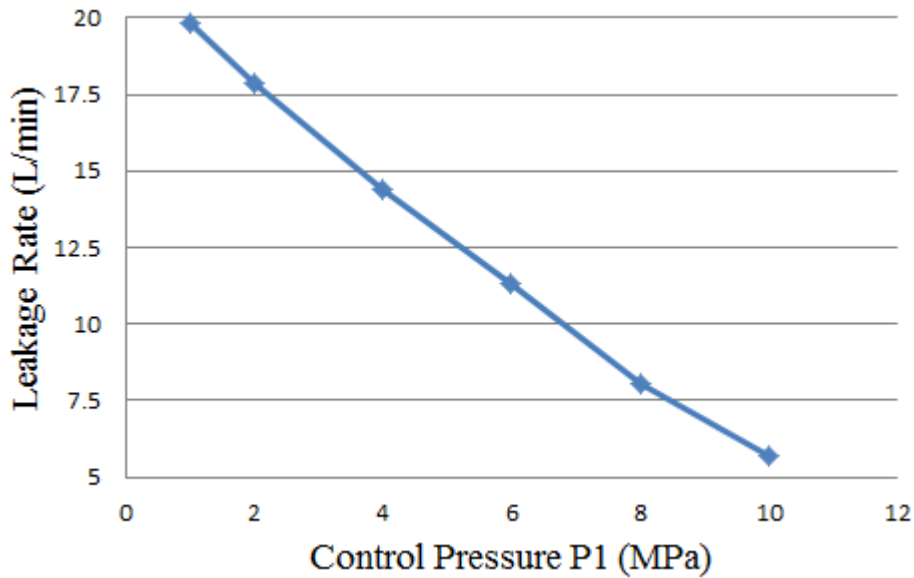


Figure 4.9: Leakage Rate vs. Cavity 1 Pressure, Carbon Graphite, Reduced Closing Force

4.1.2.3 Carbon Graphite Increased Closing Force

In addition, the effect of increasing the closing force is studied. An increased closing force reduces the minimum film thickness, closing the face gap and reducing the leakage rate. Note also that the difference between 0.01 MPa of control pressure and 14 MPa of control pressure in all cavities is the maximum range of control. As the

closing force increases, this range shrinks. This mimics the positive stiffness effect in hydrostatic bearings, in which a smaller film thickness yields a greater load support. For a seal, this means that as the film thickness decreases, the next subsequent decrease yields more opening force than the previous. Therefore, as the average film thickness shrinks, the range of control shrinks as well. For the increased closing force leakage study, the closing force is increased 5,000 N from the nominal value, resulting in a closing force of 0.500 MN. The results of this study are displayed below in Table 4.6 and Figure 4.10.

Table 4.6: Carbon Graphite, Increased Closing Force Leakage Study

F_{close}	0.500 MN				
P_1 (MPa)	P_2 (MPa)	P_3 (MPa)	Q (L/min)	Q (gpm)	
1	3	5	15.84	4.18	
2	4	6	14.61	3.86	
4	6	8	11.82	3.12	
6	8	10	8.95	2.36	
8	10	12	6.38	1.68	
10	12	14	4.50	1.19	
0.01	0.01	0.01	23.55	6.22	
14	14	14	3.19	0.84	

The increased closing force case shows the opposite effect from the reduced closing force case. The leakage rate is biased lower, with variation between 4.50 and 15.84 L/min (1.19 and 4.18 gpm). This is an overall range of variation of 11.34 L/min. This range is smaller than the range found for the reduced or base closing force cases because of an effect analogous to the positive stiffness effect in hydrostatic thrust bearings. The positive stiffness effect is exhibited in a bearing when each incremental decrease in the film thickness yields an growing incremental increase in the load support. The load support in a hydrostatic thrust bearing is generated similarly to

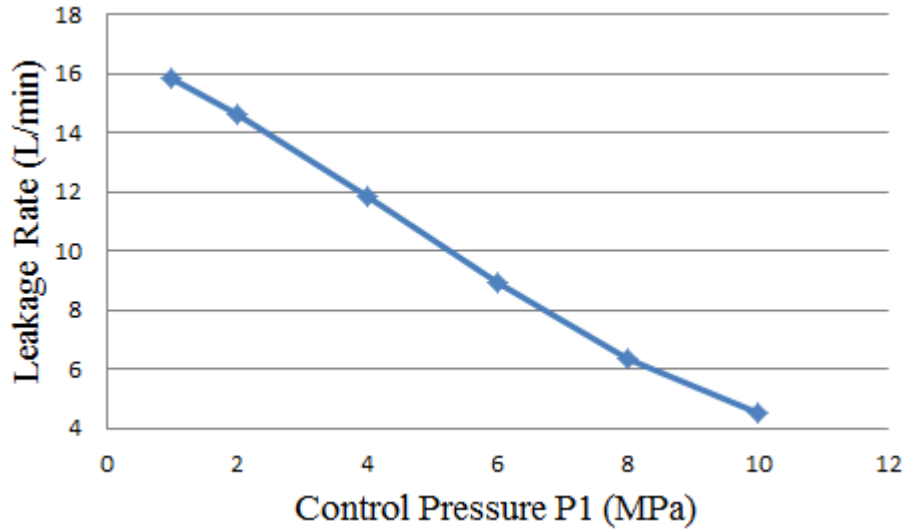


Figure 4.10: Leakage Rate vs. Cavity 1 Pressure, Carbon Graphite, Increased Closing Force

the opening force in a mechanical face seal. Likewise, as the minimum film thickness increases incrementally, each incremental increase in the opening force is larger. Thus, a control system becomes less effective as the minimum film thickness decreases. Therefore, since higher closing forces give smaller minimum film thicknesses, it is expected that as the closing force increases, the overall range of control should decrease. However, the carbon graphite seal with an increased closing force still has a range of control much larger than the steel seal, so increasing the closing force could be useful to bias the range of leakage rate variation lower.

4.2 Piezoelectric Actuation Results - Varying Leakage Rates

The piezoelectric seal is controlled by inducing a voltage across the height of the seal face. This method of control has only one active parameter, simplifying the control system. For this seal, the pre-coning is again varied so that the nominal leakage is obtained when the applied voltage is at 0 V. The voltage range tested is -5000 V to 5000 V. First, a film thickness profile is shown in Figure 4.11 for the base closing force of 0.495 MN and an applied voltage of -4000 V using the full piezoelectric seal model. This voltage is chosen for the film thickness plot because it provides a clear difference between the pre-coning and the deformed face gap.

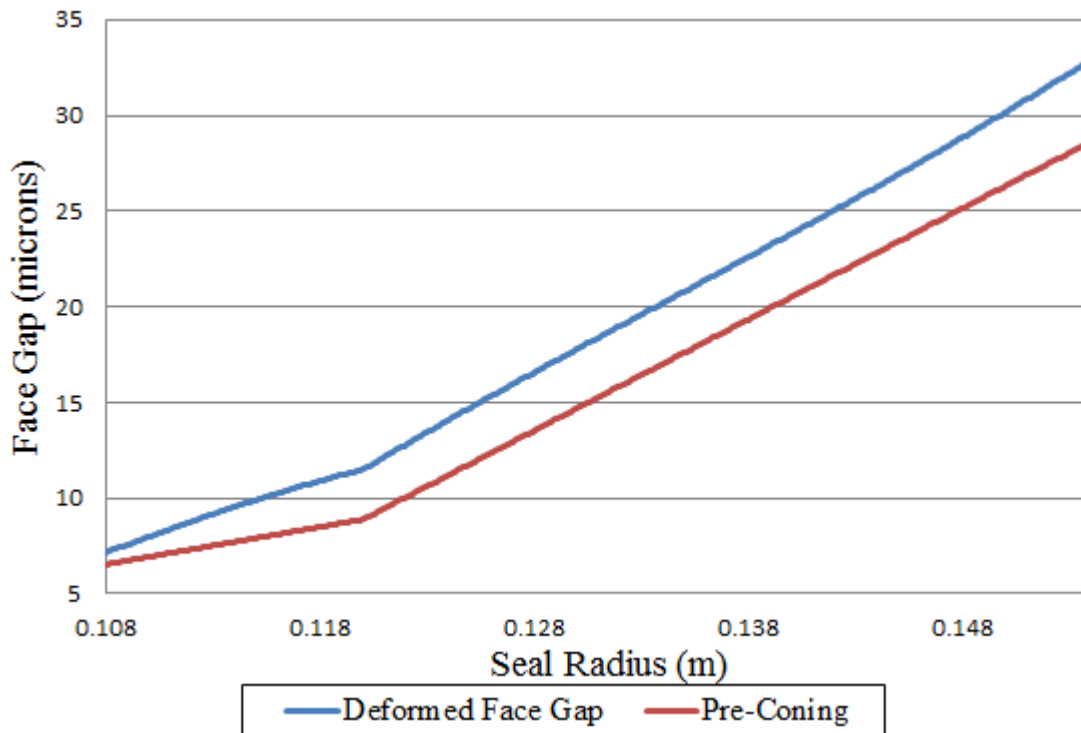


Figure 4.11: Typical Film Thickness Distribution for Piezoelectric Seal Face

Note that the piezoelectric seal lacks the waviness in the film thickness present in both the steel and carbon graphite seals, shown in Figures 4.1 and 4.6, respectively. The piezoelectric seal has no voids in its interior geometry, so the entire structure

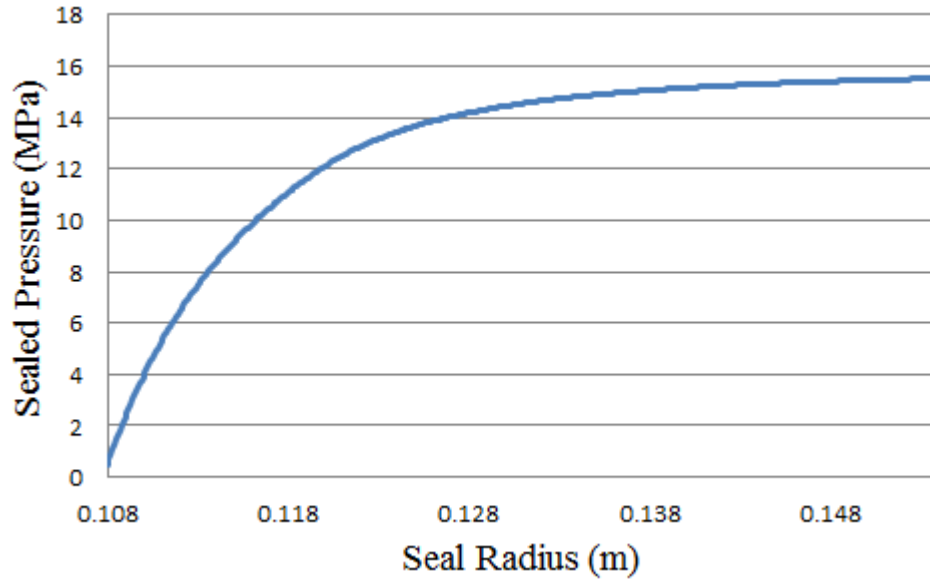


Figure 4.12: Typical Sealed Pressure Distribution for Piezoelectric Seal Face

experiences more uniform deformation at the sealing face. The sealed pressure distribution which corresponds to the above film thickness profile is shown in Figure 4.12. Again, the curved pressure distribution consistent with a positive coning is observed.

4.2.1 Full Piezoelectric Seal Face

The leakage study performed using the full piezoelectric seal face for voltages between -5000 V and 5000 V is shown below in Table 4.7 and Figure 4.13. The total range of leakage rate variation is slightly larger than the range shown by the steel hydraulic seal face. The piezoelectric seal can vary the leakage rate between 8.93 and 15.04 L/min (2.36 and 3.97 gpm), or a range of 6.11 L/min. Both the piezoelectric and steel seal faces exhibit significantly less control range than the graphite seal face.

4.2.2 Piezoelectric Seal Face with Carbon Graphite Layer

The leakage study performed between -5000 V and 5000 V for the piezoelectric seal face with a carbon graphite layer is shown in Table 4.8 and Figure 4.14. The pre-coning is altered from the full piezoelectric seal face so that the leakage rate at zero

Table 4.7: Full Piezoelectric Seal Leakage Study

F_{close}	0.495 MN	
Voltage (V)	Q (L/min)	Q (gpm)
-5000	15.04	3.97
-4000	13.97	3.69
-3000	13.49	3.56
-2000	12.63	3.34
-1000	12.05	3.18
0	11.43	3.02
1000	10.81	2.85
2000	10.47	2.77
3000	9.83	2.60
4000	9.38	2.48
5000	8.93	2.36

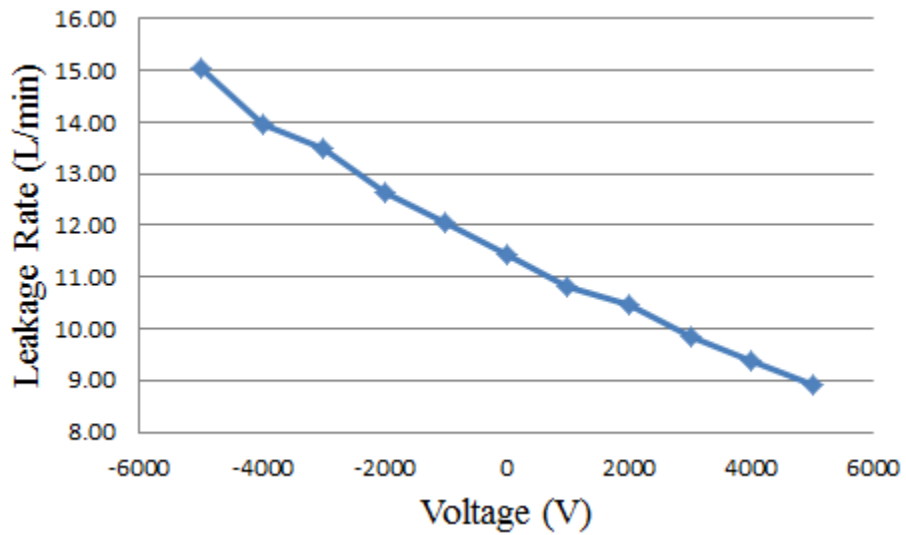


Figure 4.13: Leakage Rate vs. Voltage, Full Piezoelectric Seal Face

Table 4.8: Piezoelectric Seal with Carbon Graphite Layer Leakage Study

F_{close}	0.495 MN	
Voltage (V)	Q (L/min)	Q (gpm)
-5000	14.94	3.95
-4000	14.23	3.76
-3000	13.18	3.48
-2000	12.84	3.39
-1000	12.13	3.20
0	11.36	3.00
1000	10.86	2.87
2000	10.25	2.71
3000	9.76	2.58
4000	9.19	2.43
5000	8.60	2.27

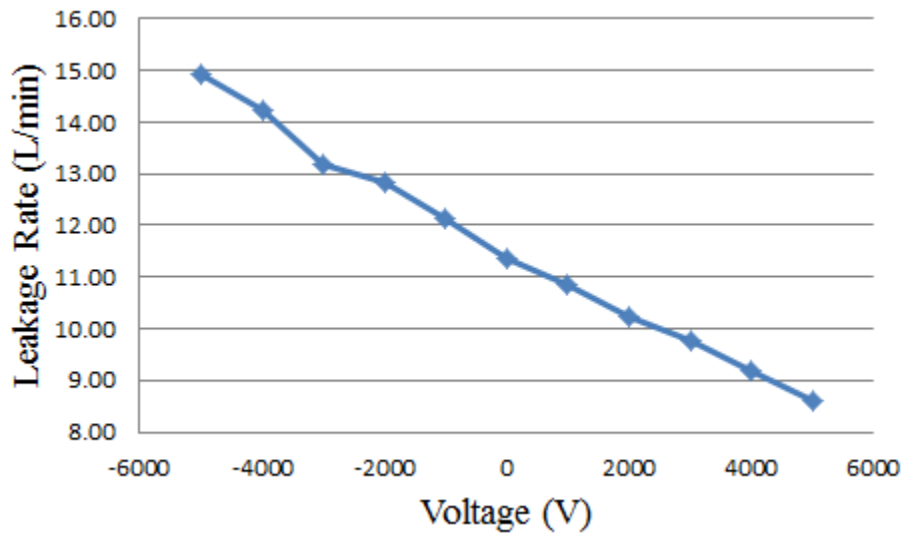


Figure 4.14: Leakage Rate vs. Voltage, Piezoelectric Seal Face with Carbon Graphite Layer

applied voltage is roughly the nominal leakage rate. It is expected that because the size of the piezoelectric element is reduced, that the maximum induced deformation for a given voltage should be less than that for the full piezoelectric seal. However, the compliance of the carbon graphite layer compared to the piezoelectric material means that the sealed pressure causes a higher deformation along the sealing face. It appears from the results below that these two effects approximately cancel one another. Note that for a given voltage, the leakage rates in Tables 4.7 and 4.8 are comparable.

The range of leakage rate variation for the piezoelectric seal with a carbon graphite layer is 8.60 to 14.94 L/min (2.27 to 3.95 gpm). This range of 6.34 L/min is very similar to the range shown by the full piezoelectric seal. Thus, the addition of the carbon graphite layer does not significantly impact the ability of the piezoelectric element to vary the leakage rate. The piezoelectric seal with a carbon graphite layer can vary the leakage rate about 3 L/min below the nominal leakage rate and about 3.5 L/min above the nominal leakage rate. This performance is about 50% better than the steel hydraulic seal's performance, but still significantly less than the carbon graphite hydraulic seal's performance.

4.3 Hydraulic and Piezoelectric Results - Restoring Nominal Leakage Rates

While the above results for the seal models illustrate how well the control parameter can vary the leakage rate under fixed operating conditions, in a real system the object of controlling the seal is to maintain the nominal leakage rate through a range of changing operating conditions. To simulate the process of adjustment to restore the nominal leakage rate, each seal is modeled with a range of closing forces, and the control parameter is allowed to vary. The specified closing force represents the interaction of the seal face with all other components of the seal assembly, and the seal's ability to respond to an altered closing force represents the seal's ability to

respond to changes in conditions during operation. The varying control parameter changes the coning, which alters the sealed pressure distribution and the opening force to match the specified closing force, thus illustrating how the control parameter can be used to adjust the coning and maintain the nominal leakage rate. For comparison between the seal models, the wider the range of closing forces and uncontrolled leakage rates accommodated, the more controllable the seal.

4.3.1 Steel Hydraulic Seal

First, the hydraulically-controlled steel seal is examined. In Table 4.9 below, the specified closing force for each trial is shown in the first column. Then, the control pressure in the first cavity is shown. Note that the same control scheme is employed as in the leakage studies: the value of P_1 is chosen, P_2 equals P_1 plus 2 MPa, and P_3 equals P_1 plus 4 MPa. Next, the corrected leakage rate using the specified control pressures is shown in both L/min and gpm. This leakage rate is constrained to be 11.36 ± 0.11 L/min (3.0 ± 0.03 gpm) to allow for a small acceptable variation. Finally, the uncontrolled leakage rate is shown in both L/min and gpm. The uncontrolled leakage rate is the leakage rate obtained using the specified closing force if the control pressure P_1 is set at its ‘base’ value of 5 MPa and the other control pressures are set consistent with the above control scheme. This represents the leakage rate that would occur if no active control of the seal were attempted and serves to illustrate the seal’s ability to adjust from that uncontrolled rate to the nominal leakage rate using the control pressure shown in the table.

In Figure 4.15 below, the control pressure used to restore the nominal leakage rate is plotted versus the specified closing force for the steel seal. This figure shows the range of closing forces that can be accommodated by the controllable seal, and is a good indirect method of estimating how effectively the seal can maintain the nominal leakage rate.

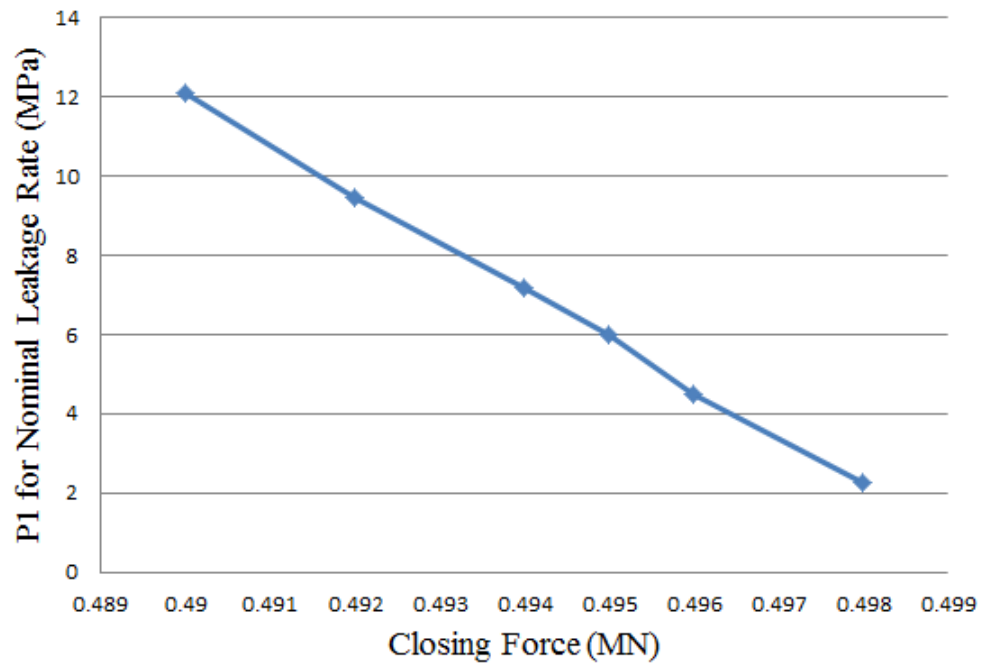


Figure 4.15: Steel, Control Pressure to Restore Nominal Leakage Rate vs. Closing Force

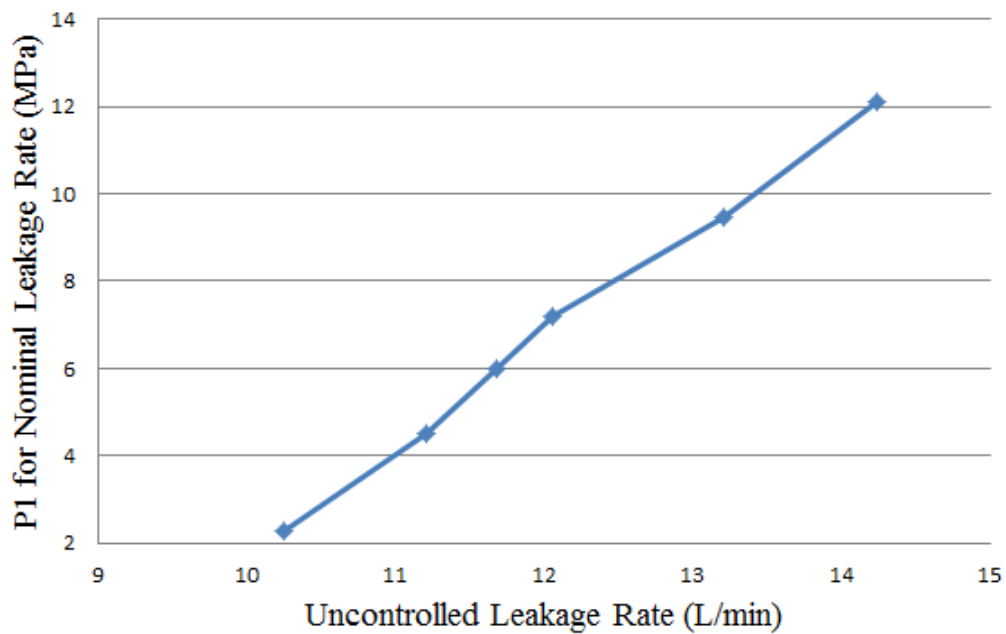


Figure 4.16: Steel, Control Pressure to Restore Nominal Leakage Rate vs. Uncontrolled Leakage Rate

Table 4.9: Stainless Steel, Restoring Nominal Leakage Rate

F_{close} (MN)	P_1 (MPa)	Corrected Leakage		Uncorrected Leakage	
		Q (L/min)	Q (gpm)	Control $P_1 = 5$ MPa	Q (gpm)
0.49	12.11	11.39	3.01	14.24	3.76
0.492	9.46	11.43	3.02	13.22	3.49
0.494	7.20	11.28	2.98	12.05	3.18
0.495	6.00	11.24	2.97	11.69	3.09
0.496	4.51	11.32	2.99	11.21	2.96
0.498	2.26	11.26	2.97	10.25	2.71

Figure 4.16 below shows the control pressure in the first cavity (P_1) used to restore the nominal leakage rate versus the uncorrected leakage rate for the same operating conditions. This represents a direct assessment of the seal’s leakage rate adjustment ability. If the seal is confronted with an uncorrected leakage rate of the displayed magnitude, it can correct that leakage rate and restore it to the nominal leakage rate using the displayed control pressure. As shown in the figure and in Table 4.9, the steel seal can correct a range of abnormal leakage rates between 10.24 and 14.24 L/min (2.71 to 3.76 gpm), with the nominal leakage rate being 11.36 L/min (3.00 gpm).

4.3.2 Carbon Graphite Hydraulic Seal

Because the carbon graphite seal model exhibits a far greater range of leakage rates in the leakage study performed above, it is reasoned that it will be able to correct for a wider range of abnormal leakage rates than the steel seal. The carbon graphite seal’s performance in restoring the nominal leakage rate is examined below in Table 4.10. The same display format is used as in the steel seal’s study.

Figure 4.17 below shows the control pressure P_1 necessary to restore the nominal leakage rate versus the closing force. As expected, the carbon graphite seal handles a wider range of closing forces within its acceptable control pressure P_1 range of 0 to

Table 4.10: Carbon Graphite, Restoring Nominal Leakage Rate

F_{close} (MN)	P_1 (MPa)	Corrected Leakage		Uncorrected Leakage	
		Q (L/min)	Q (gpm)	Control $P_1 = 5$ MPa Q (L/min)	Q (gpm)
0.46	11.67	11.36	3.00	25.61	6.76
0.465	10.02	11.46	3.03	22.25	5.88
0.475	8.31	11.26	2.97	18.08	4.78
0.48	7.45	11.35	3.00	15.77	4.17
0.488	6.01	11.46	3.03	13.11	3.46
0.49	5.60	11.41	3.01	12.47	3.29
0.492	5.40	11.27	2.98	11.98	3.16
0.494	5.23	11.37	3.00	11.59	3.06
0.495	5.00	11.38	3.01	11.38	3.01
0.50	4.13	11.27	2.98	10.28	2.72
0.515	0.97	11.28	2.98	7.44	1.97

10 MPa.

Figure 4.18 shows the control pressure P_1 necessary to restore the nominal leakage rate versus the uncontrolled leakage rate for the same operating conditions. Again, the carbon graphite seal exhibits a far wider range of control due to the compliance of the material versus the steel seal. The carbon graphite seal can correct a range of abnormal leakage rates from 7.44 to 25.61 L/min (1.97 to 6.76 gpm) and restore them to the nominal leakage rate of 11.36 L/min (3.00 gpm). This represents a significant range of control which is appropriate to address many of the abnormal leakage rate events encountered in existing #1 seals in operation. Note also that the range of control is not perfectly centered around the nominal leakage rate. The seal is able to correct for a wider range of high leakage rates than low leakage rates. This behavior is desirable because utilities more commonly experience abnormal high leakage rates than low leakage rates. However, the performance of any of the proposed controllable seals can be tuned such that the range of leakage control available is biased higher or lower by adjusting the pre-coning or the closing force. This tuning can bias the

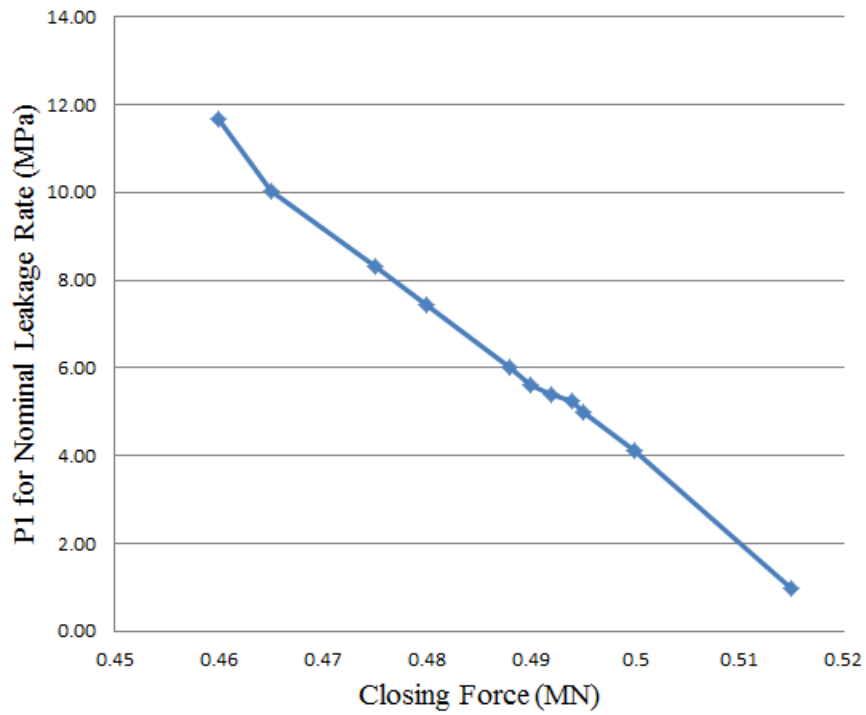


Figure 4.17: Carbon Graphite, Control Pressure to Restore Nominal Leakage Rate vs. Closing Force

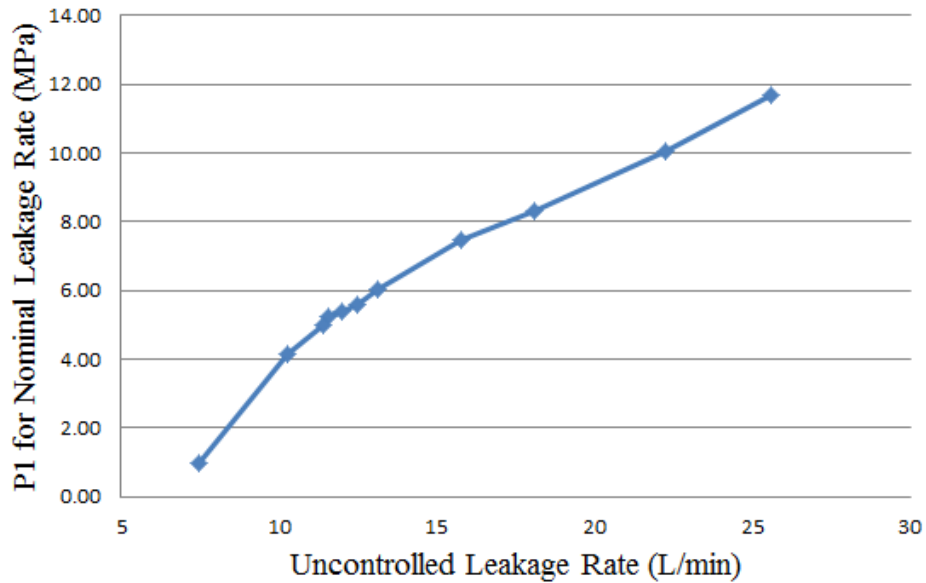


Figure 4.18: Carbon Graphite, Control Pressure to Restore Nominal Leakage Rate vs. Uncontrolled Leakage Rate

range of control to address the most common instances of abnormal leakage rates, and could be used in other applications where abnormal high leakage rates are not the most common form of undesirable behavior.

4.3.3 Piezoelectric Seal

The piezoelectric controllable seal uses the induced voltage across the seal face as its control parameter. This simplifies the control system greatly. The general structure of the trials for restoring the nominal leakage is the same as for the hydraulically controlled seals, but instead of a set of three linked control parameters, the single voltage parameter is used. Thus, in Table 4.11 below, the closing force is shown in the first column, the control voltage is shown in the second column, the corrected leakage rates in SI and standard units are shown in the third and fourth columns, and finally the uncorrected leakage rates in SI and standard units are shown in the fifth and sixth columns.

Table 4.11: Full Piezoelectric Seal, Restoring Nominal Leakage Rate

F_{close} (MN)	Voltage (V)	Corrected Leakage		Uncorrected Leakage	
		Q (L/min)	Q (gpm)	Control Voltage = 0 V	Q (gpm)
0.49	4800	11.41	3.01	14.74	3.89
0.491	3800	11.38	3.01	13.88	3.67
0.492	2900	11.41	3.01	13.25	3.50
0.493	1850	11.46	3.03	12.84	3.39
0.494	900	11.38	3.01	12.09	3.19
0.495	0	11.43	3.02	11.43	3.02
0.496	-675	11.36	3.00	11.03	2.91
0.497	-1400	11.35	3.00	10.48	2.77
0.498	-2300	11.41	3.01	10.09	2.67
0.499	-3200	11.39	3.01	9.62	2.54
0.50	-4040	11.27	2.98	9.18	2.42

In Figure 4.19, the control voltage necessary to restore the nominal leakage is

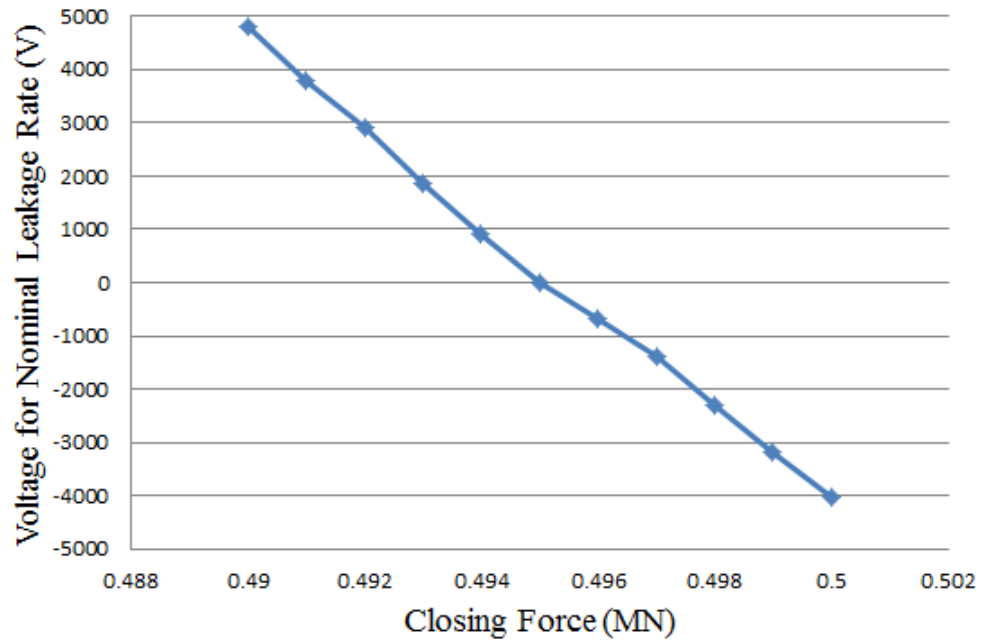


Figure 4.19: Piezoelectric Voltage to Restore Nominal Leakage Rate vs. Closing Force, Full Piezoelectric Seal

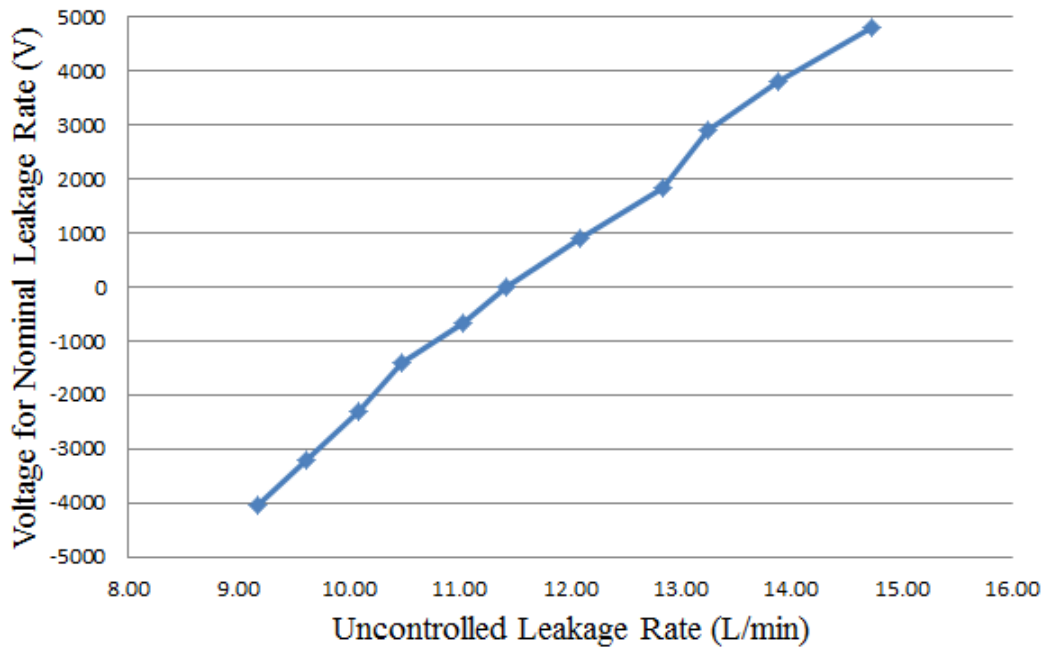


Figure 4.20: Piezoelectric Voltage to Restore Nominal Leakage Rate vs. Uncorrected Leakage Rate, Full Piezoelectric Seal

shown versus the closing force for each trial. Again, this plot shows an indirect association between the control parameter and the seal controllability.

The direct assessment of the piezoelectric seal’s controllability is shown in Figure 4.20. The seal can adjust for abnormal leakage rates between 9.18 and 14.74 L/min (2.42 to 3.89 gpm) and restore them to the nominal leakage rate of 11.36 L/min (3.00 gpm). This range is slightly larger than the range for the steel hydraulic seal, but significantly smaller than the range for the carbon graphite hydraulic seal.

4.3.4 Piezoelectric Seal with Graphite Layer

Because the leakage study results for the piezoelectric seal with a carbon graphite layer are comparable to the results for the full piezoelectric seal, it is expected that the addition of the carbon graphite layer will not significantly affect the seal’s ability to restore nominal leakage rates. Table 4.12 below shows the ability of the piezoelectric seal with carbon graphite to restore the nominal leakage rate.

Table 4.12: Piezoelectric Seal with Carbon Graphite Layer, Restoring Nominal Leakage Rate

F_{close} (MN)	Voltage (V)	Corrected Leakage		Uncorrected Leakage	
		Q (L/min)	Q (gpm)	Control Voltage = 0 V Q (L/min)	Q (gpm)
0.49	4300	11.41	3.01	14.02	3.70
0.491	3300	11.38	3.01	13.51	3.57
0.492	2350	11.45	3.02	13.00	3.43
0.493	1625	11.38	3.01	12.37	3.27
0.494	800	11.36	3.00	12.02	3.18
0.495	0	11.36	3.00	11.36	3.00
0.496	-800	11.37	3.00	11.10	2.93
0.497	-1500	11.32	2.99	10.55	2.79
0.498	-2350	11.31	2.99	10.11	2.67
0.499	-3125	11.27	2.98	9.59	2.53
0.50	-4020	11.46	3.03	9.10	2.40

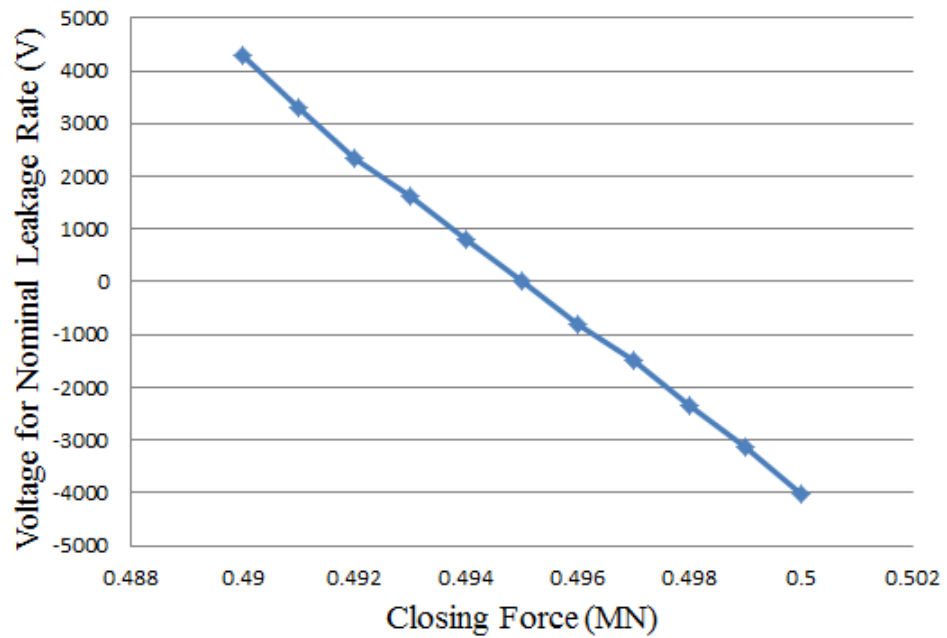


Figure 4.21: Piezoelectric Voltage to Restore Nominal Leakage Rate vs. Closing Force, Piezoelectric Seal with Carbon Graphite Layer

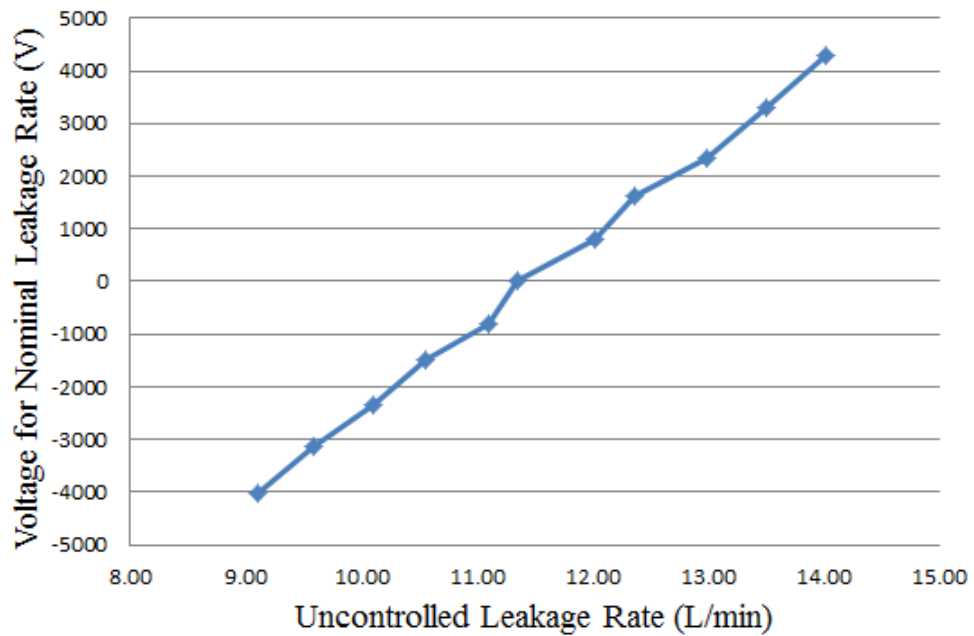


Figure 4.22: Piezoelectric Voltage to Restore Nominal Leakage Rate vs. Uncorrected Leakage Rate, Piezoelectric Seal with Carbon Graphite Layer

Figure 4.21 illustrates the control voltage required to restore the nominal leakage rate versus the closing force. The piezoelectric seal with carbon graphite shows very similar results to the full piezoelectric seal which is shown in Figure 4.19.

Figure 4.22 shows the voltage required to restore the nominal leakage rate versus the uncontrolled leakage rate for the piezoelectric seal with a carbon graphite layer. This seal is able to correct for abnormal leakage rates between 9.10 and 14.02 L/min (2.40 and 3.70 gpm). This performance is very similar to that of the full piezoelectric seal.

The presence of the carbon graphite layer on the sealing face does not appear to have a significant effect on the controllability of the piezoelectric seal. However, neither piezoelectric seal model examined exhibits a range of control approaching that of the carbon graphite hydraulic controllable seal.

4.4 Stress Results

Because the controllable seal faces are exposed to considerable sealed pressure, and in the case of the hydraulic controllable seals, hydraulic pressure from within the faces, stress information is gathered for the maximum control parameter values to determine if the seal face experiences stress above its material's yield strength or fracture strength. In addition, the face geometry has several areas which may encounter stress concentration, especially in the corners of the cavities within the hydraulic faces. While a full study of fatigue cycle limits and detailed stress information is beyond the scope of this thesis, the stress information gathered ensures that the seals are at least theoretically capable of handling the loads experienced during potential operation.

The stress results for the steel hydraulic seal are shown below in Figure 4.23. These results are obtained using the maximum control pressure of 14 MPa in each cavity within the seal face for the base value of coning and closing force. The maximum

Von Mises stress experienced by the seal is 63.75 MPa, well below the yield strength of 1225 MPa [11]. Note that the maximum stress is experienced only in extremely small areas in the upper corners of some control pressure cavities. The vast majority of the seal face experiences much lower internal stresses.

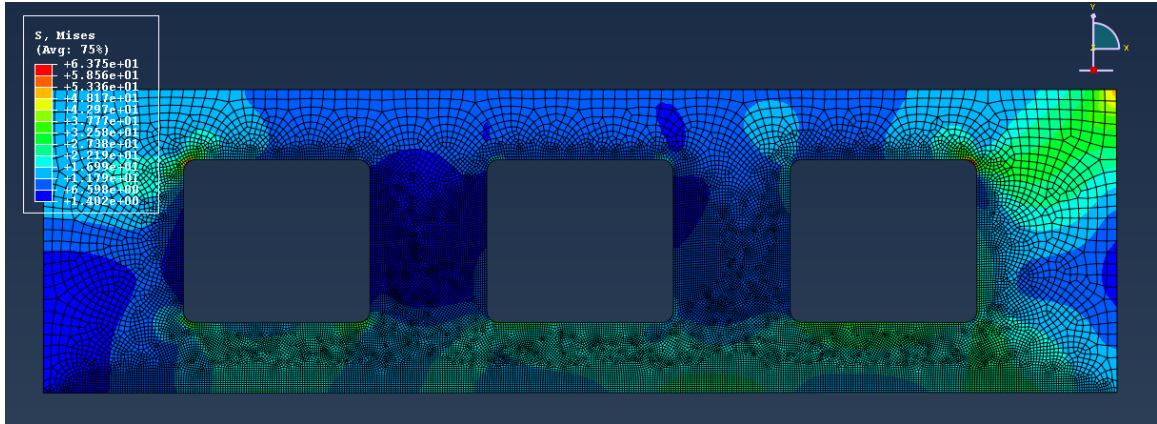


Figure 4.23: Von Mises Effective Stress at Maximum Control Pressures, Steel Hydraulic Seal

The stress results for the carbon graphite hydraulic seal are shown in Figure 4.24. Again, the maximum control pressure of 14 MPa is applied to each cavity and base values of coning and closing force are used to generate the results. The maximum Von Mises stress experienced by the carbon graphite seal is 63.37 MPa, which is below the flexural strength of 75.8 MPa and well below the compressive strength of 200 MPa for the material [8]. Note again that the highest stresses are experienced only in extremely small regions in the corners of the control pressure cavities. The control pressures cause compressive stresses in those areas.

Because the piezoelectric seal face lacks internal voids, which expose the remaining structure to higher stresses, and because the internal stress due to the applied voltage is relatively small, fracture is unlikely to be a concern during normal operation of a piezoelectric controllable seal. However, potential stress concentrations exist where the carbon graphite layer is bonded to the piezoelectric crystal and potentially in the

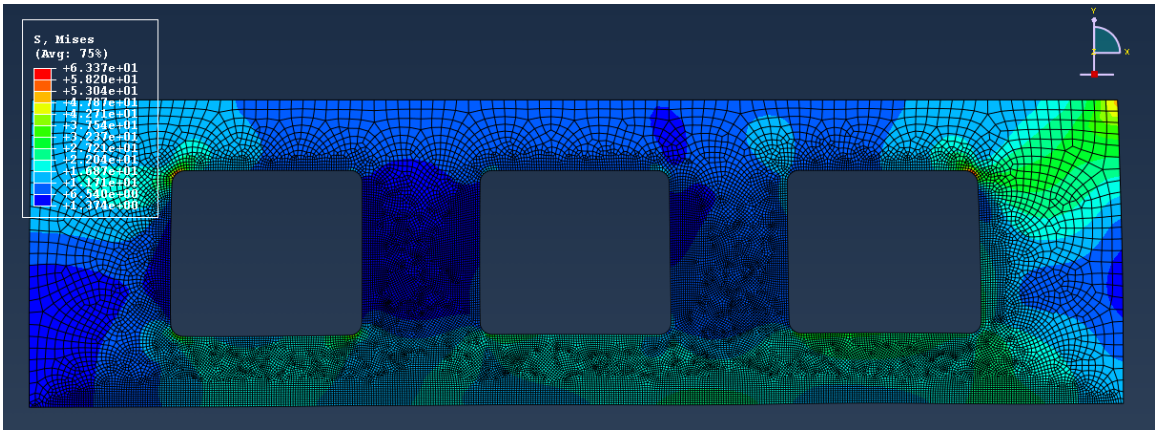


Figure 4.24: Von Mises Effective Stress at Maximum Control Pressures, Carbon Graphite Hydraulic Seal

corners of regions where the crystal abuts the holder material (modeled as boundary condition locations). The stress results for the piezoelectric seal with a carbon graphite layer are shown in Figure 4.25 and are obtained by applying a voltage of 5000 V, the maximum control voltage used. Note that the highest stress of 41.4 MPa is experienced only in very small areas in the upper corners of the seal.

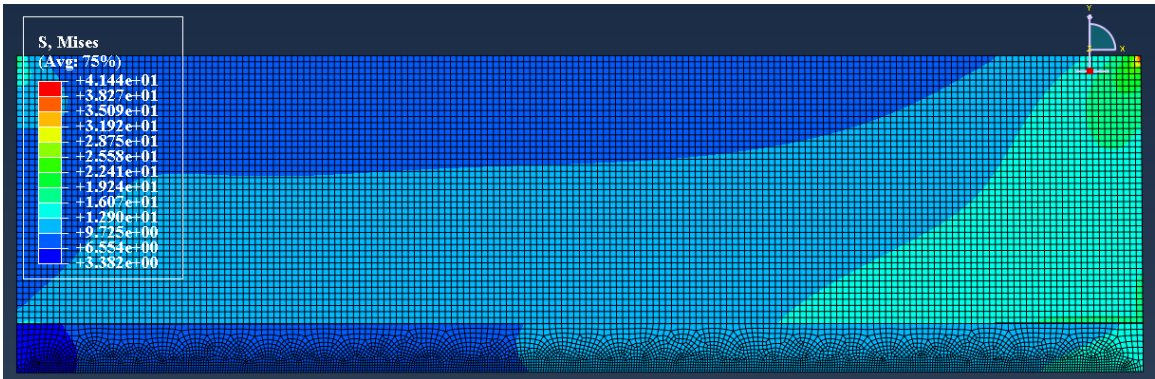


Figure 4.25: Von Mises Effective Stress at 5000 V, Piezoelectric Seal with Carbon Graphite Layer

CHAPTER V

CONCLUSION

Abnormal Westinghouse #1 seal leakage rates are commonly encountered by nuclear power plant operators, especially towards the end of nuclear fuel cycles [4]. Operators currently have limited tools at their disposal to mitigate abnormal leakage rates, and usually these tools, such as lowering seal injection water temperature and changing seal injection filters, rely on secondary effects to restore nominal leakage rates or are only effective against a limited number of causes of these abnormal leakage rates. In addition, some scenarios can occur where deviations from the nominal leakage rate are too large for these mitigation tools to address adequately. As such, it is desired to introduce a method to give plant operators the ability to control actively the leakage rate of the #1 seal. In addition, this method of active control should be appropriate to counteract a variety of causes of abnormal leakage rates, so it should control the basic operation of the seal.

The basic operation of mechanical face seals is covered in Section 2.1, where the coning of the seal face is introduced as a critical parameter of seal operation. In addition, previous controllable mechanical seals discussed in Section 2.5 have shown that varying the coning is a reliable method of controlling seal performance while maintaining a positive coning for stable operation. As such, proposed controllable seals that operate by varying the coning of the non-rotating seal face and a model for their performance are introduced in Chapter III. One proposed method of control is the application of hydraulic pressure to cavities inside the seal face. This method is explored for seals composed of 410 stainless steel with a ceramic coating and high-strength carbon graphite. The other proposed method of control is the application

of a voltage across a piezoelectric element. Piezoelectric actuation is explored for an idealized seal composed entirely of a piezoelectric element and for a seal that utilizes a piezoelectric element behind a layer of carbon graphite.

The results shown in Chapter IV detail the capabilities of each controllable seal design. In each case, the use of an active control system to vary the coning of the seal face is effective in restoring the nominal leakage rate from abnormal uncontrolled leakage rates. However, each tested case presents different results. The steel hydraulic seal face is able to restore the nominal leakage rate of 11.36 L/min (3.00 gpm) from uncontrolled leakage rates of 10.25 to 14.24 L/min (2.71 to 3.76 gpm), as shown in Section 4.3.1. Both varieties of piezoelectric seal are tested to determine their ability to restore the nominal leakage rate in Section 4.3.3. The seal composed fully of piezoelectric material is able to restore the nominal leakage rate from uncontrolled leakage rates of 9.18 to 14.74 L/min (2.42 to 3.89 gpm). The piezoelectric seal with a carbon graphite layer is able to restore the nominal leakage rate from uncontrolled leakage rates of 9.10 to 14.02 L/min (2.40 to 3.70 gpm). These performances are strikingly similar and show that the addition of a small carbon graphite layer to improve wear and durability performance on the sealing surface does not impact the ability of the piezoelectric seal to control the leakage rate.

While the above cases showed that the proposed methods of control are capable of moderating some abnormal leakage rates, the ranges of control are not sufficient to address a wide range of abnormal #1 seal leakage rates that may be experienced by plant operators. The ability of the carbon graphite hydraulic seal to restore the nominal leakage rate, as shown in Section 4.3.2, is much improved due to the deformation response of the softer carbon graphite material. The carbon graphite seal tested is able to provide correction for a range of uncontrolled leakage rates between 7.44 and 25.61 L/min (1.97 and 6.76 gpm). This range of control is significantly larger than those provided by the steel or piezoelectric proposed seals, and the stress

results shown in Section 4.4 confirm that the carbon graphite seal face is capable of withstanding the loads applied by the maximum allowed control pressure of 14 MPa in all control cavities. If a large factor of safety is preferred, the maximum allowable control pressure could be reduced somewhat and the design tuned to accommodate the desired range of abnormal leakage rates while still providing superior performance to the steel or piezoelectric seal faces. In addition, the bias towards correcting high abnormal leakage rates is desired because high abnormal leakage rates are more commonly encountered by plant operators, but tuning of the design could be performed to shift the range of control so that the ability to correct for any desired abnormal leakage rate can be accomplished.

5.1 Future Work

Future work on the proposed controllable seal designs would likely include the development of a full electronic control system, development of a prototype for experimental testing, selection of specific materials for the controllable seal, and collaboration with a manufacturer such as Westinghouse and utilities to specify aspects of the design to create a controllable seal compatible with existing reactor coolant pumps. The development of a control system would include selection of specific components and their location in the reactor coolant pump assembly, as well as developing a control profile to specify the control pressures or control voltage for the desired leakage rate. The design of the control system would depend on the desire for open- or closed-loop control, or compatibility for both methods of operation as desired by plant operators.

Because of the large scale and significant cost of a full-size reactor coolant pump and its support system, direct laboratory testing of a full-scale controllable seal model is impractical except for pump and seal manufacturers. A scale model could be developed to confirm the viability of hydraulic actuation to control the coning and to gather more data about the appropriateness of stainless steel or carbon graphite as

materials for a hydraulic controllable seal. Previous work has validated experimentally the use of piezoelectric crystals to vary the coning [17], but the high sealed pressures and large scale of a reactor coolant pump present challenges that may necessitate further experimental testing.

Collaboration with utilities and a pump and seal manufacturer is expected to be vital if a commercially-viable controllable seal for a reactor coolant pump is desired. Compliance with industry standards, specific dimensions, and demands of existing equipment is expected to present significant challenges without the involvement of industry partners. Due to the even more rigorous demands for safety and reliability in the nuclear power industry, extensive testing and validation of a full-scale controllable seal design is necessary before it could be implemented in an operating nuclear power station.

APPENDIX A

WESTINGHOUSE REACTOR COOLANT PUMP AND SEAL ASSEMBLY DIAGRAMS

The following images are from EPRI Technical Report 1022315, *Nuclear Maintenance Applications Center: Westinghouse Reactor Coolant Pump Seal Maintenance Guide* [4], and are originally courtesy of Westinghouse Electric. They illustrate the reactor coolant pump assembly, the #1 seal assembly within the RCP, and the flow of sealed fluid throughout the entire sealing mechanism.

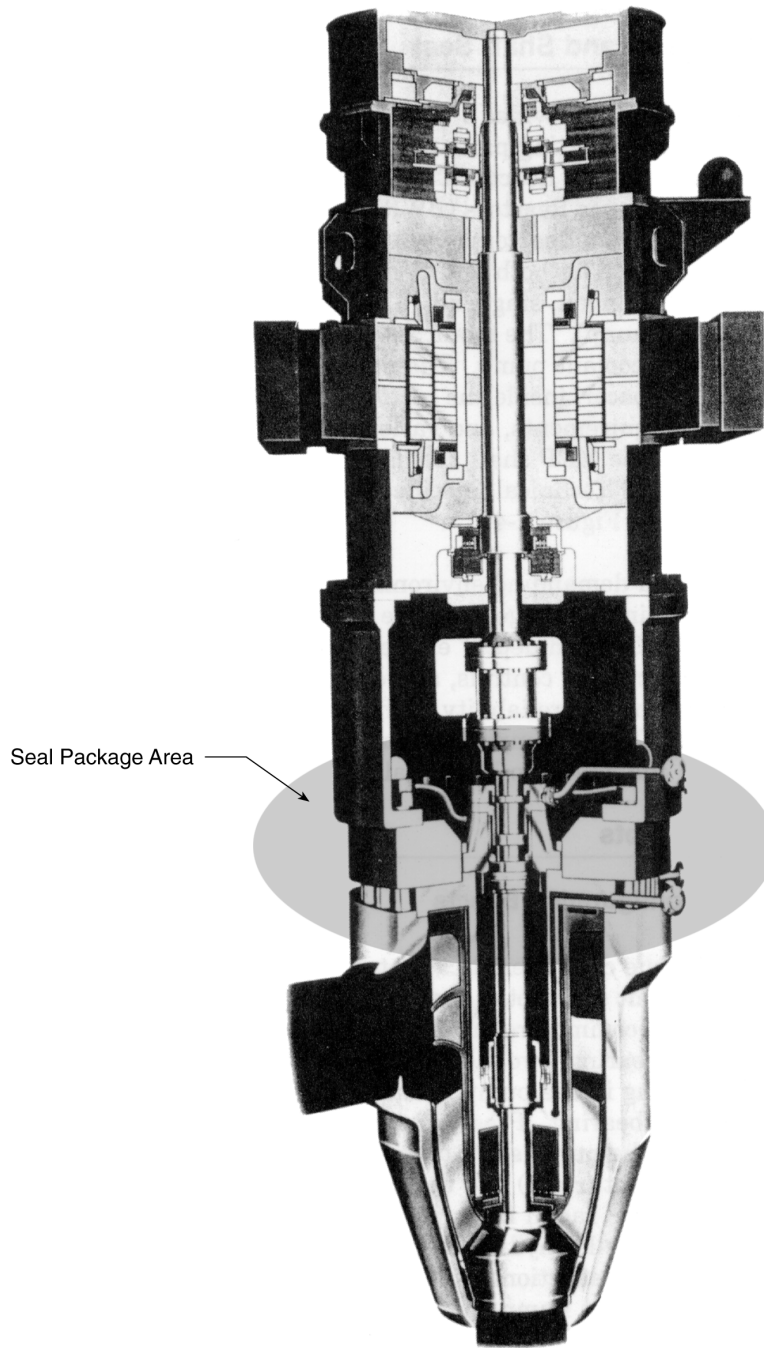


Figure A.1: Westinghouse Reactor Coolant Pump and Motor Assembly [4]

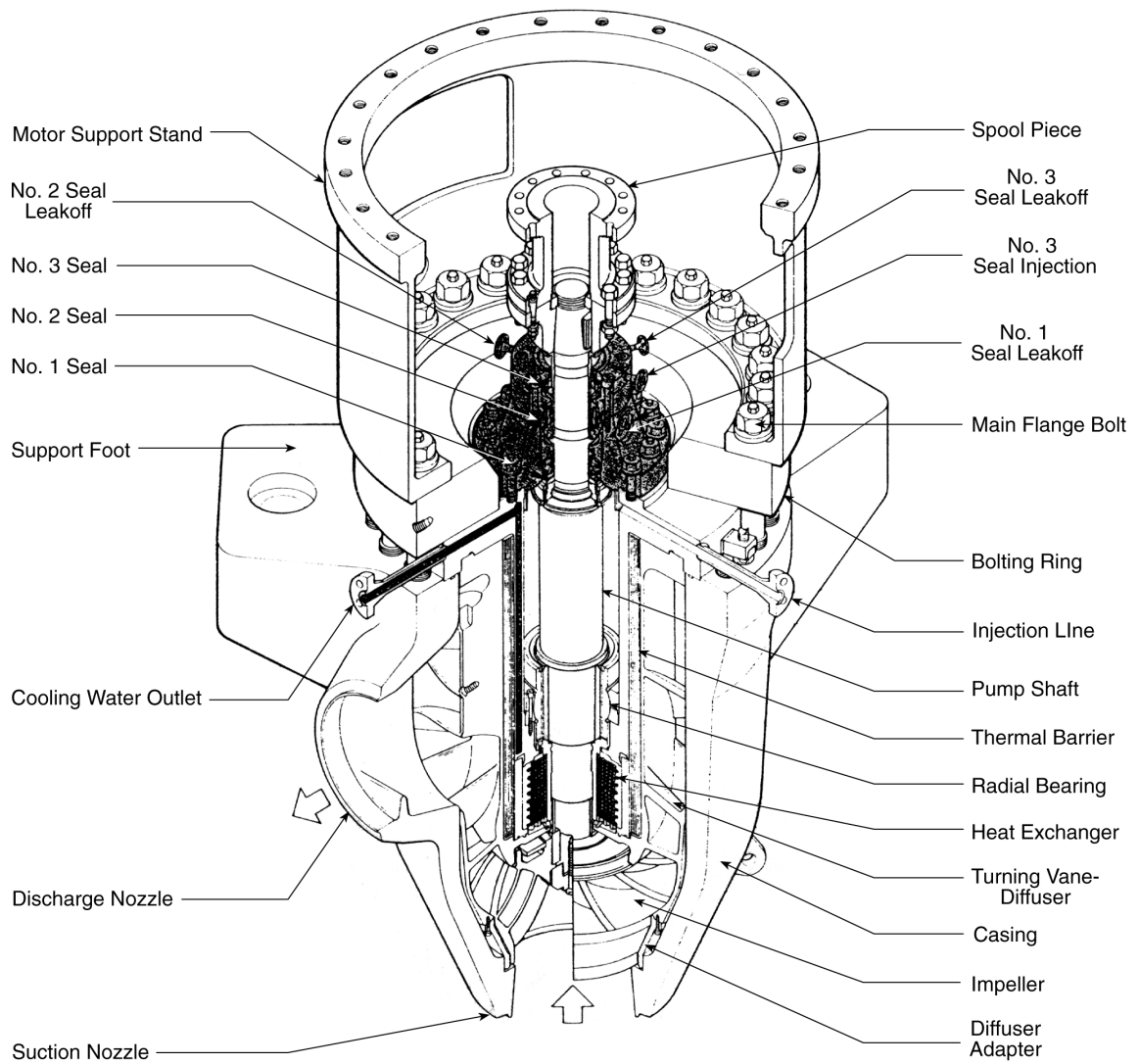


Figure A.2: Sectional View of Westinghouse RCP [4]

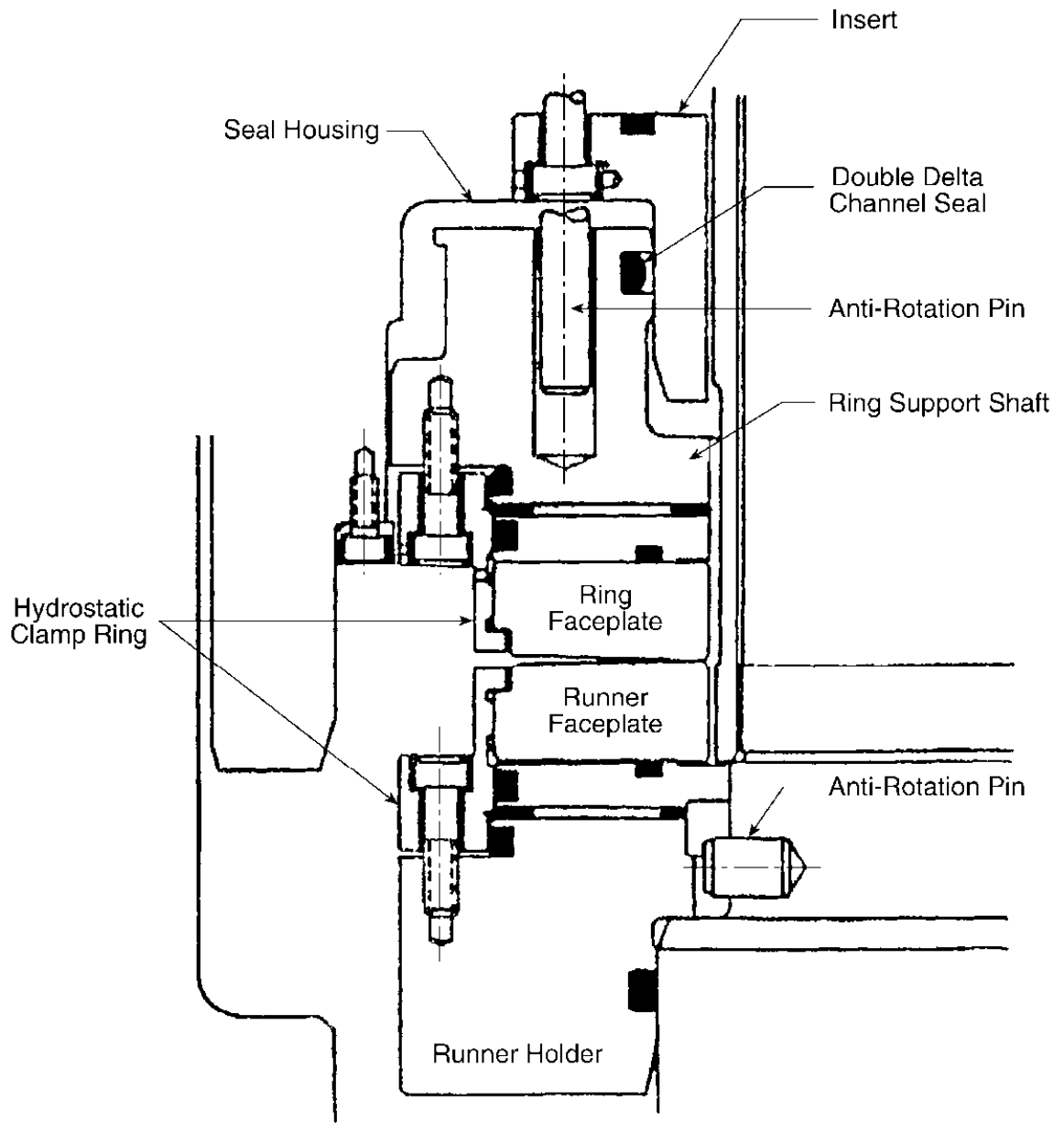


Figure A.3: Typical Westinghouse #1 Seal [4]

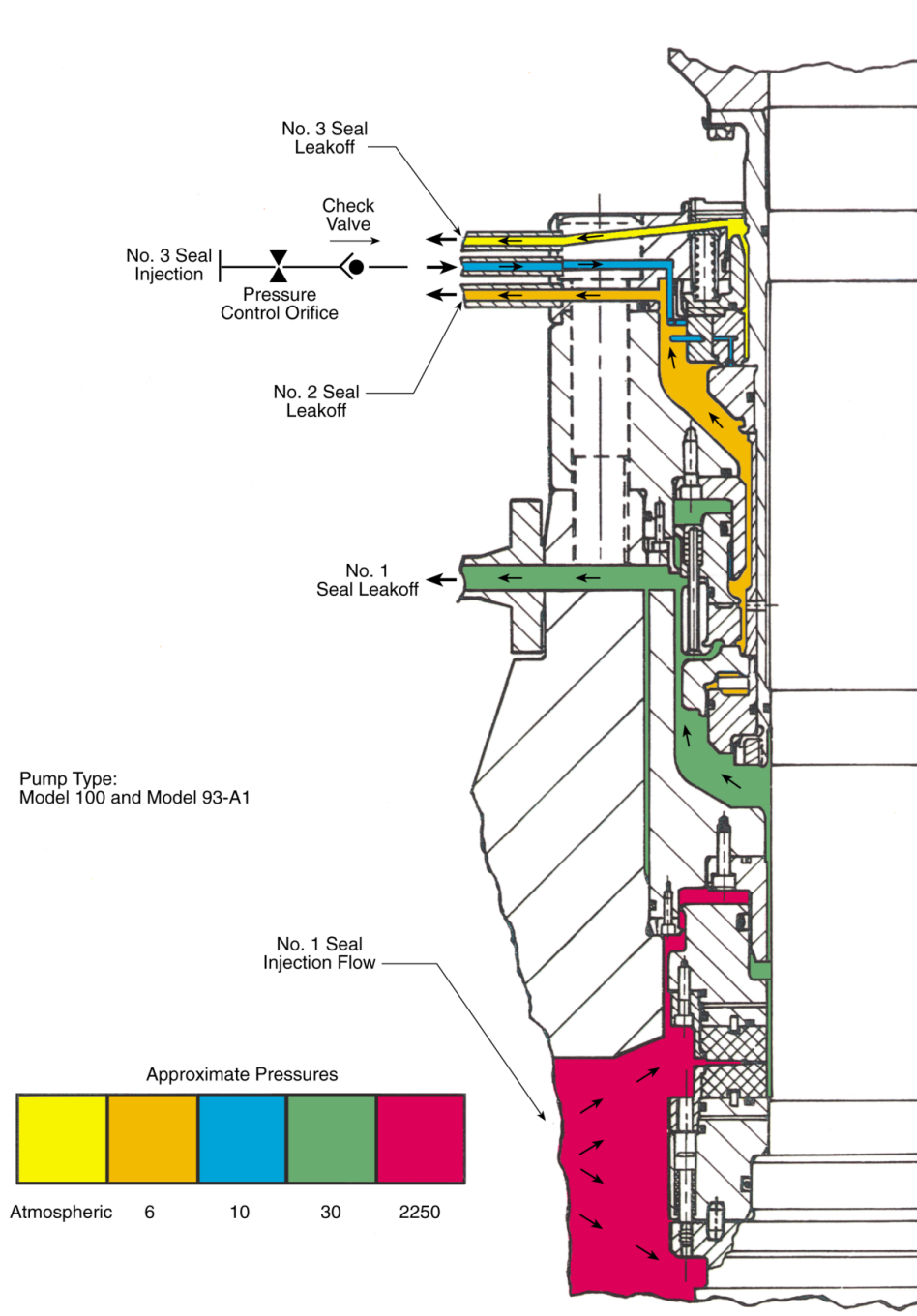


Figure A.4: Flow Diagram Sectional, RCP Models 93-A1 and 100 [4]

REFERENCES

- [1] “Manual reactor trip due to exceeding 21 rcp seal leak-off limits,” Tech. Rep. 70062042, INPO, Marietta, GA, 2006.
- [2] “Problem investigation process - failure number 946,” Tech. Rep. O-08-01940, INPO, Marietta, GA, 2008.
- [3] “Problem investigation process - failure number 693,” Tech. Rep. C-09-05242, INPO, Marietta, GA, 2009.
- [4] “Nuclear maintenance applications center: Westinghouse reactor coolant pump seal maintenance guide,” Tech. Rep. 1022315, EPRI, Palo Alto, CA, 2010.
- [5] “Nuclear maintenance applications center: The physical basis of abnormal seal leakoff mitigation,” Tech. Rep. 1025765, EPRI, 2012.
- [6] eFUNDA, “Properties of piezoelectric material lead zirconate titanate (pzt-4),” February 2013.
- [7] ETSION, I., PALMOR, Z., and HARARI, N., “Feasibility study of a controlled mechanical seal,” *Tribology Transactions*, vol. 47, pp. 621–625, 1991.
- [8] GROUP, S. C., “Materials for mechanical applications, sgl group’s graphite specialties,” February 2013.
- [9] HAMROCK, B. J., SCHMID, S. R., and JACKSON, B. O., *Fundamentals of Fluid Film Lubrication*. Marcel Dekker, Inc., 2nd ed., 2004.
- [10] KEY, W. E., SALANT, R. F., PAYVAR, P., GOPALAKRISHNAN, S., and VAGHASIA, G., “Analysis of a mechanical seal with deep hydropads,” *Tribology Transactions*, vol. 32, pp. 481–489, 1989.
- [11] MATWEB, “410 stainless steel,” February 2013.
- [12] PATANKAR, S., *Numerical Heat Transfer and Fluid Flow*. Hemisphere Publishing Corporation, 1980.
- [13] RUAN, B., SALANT, R. F., and GREEN, I., “A mixed lubrication model of liquid/gas mechanical face seals,” *Tribology Transactions*, vol. 40, pp. 647–657, 1997.
- [14] SALANT, R. F., MILLER, A. L., KAY, P. L., KOZLOWSKI, J., KEY, W. E., W. E., ALGRAIN, M. C., and GILES, O., “Development of an electronically controlled mechanical seal,” in *Eleventh International Conference of Fluid Sealing, BHRA*, pp. 576–595, 1987.

- [15] SALANT, R. F., WOLFF, P., and NAVON, S., “Electronically controlled mechanical seal for aerospace applications - part i: Design, analysis and steady state tests,” *Tribology Transactions*, vol. 37, pp. 189–195, 1994.
- [16] WOLFF, P. and SALANT, R. F., “Electronically controlled mechanical seal for aerospace applications - part ii: Transient tests,” *Tribology Transactions*, vol. 38, pp. 51–56, 1995.
- [17] WOLFF, P., “Development of an actively controlled mechanical seal,” Master’s thesis, Georgia Institute of Technology, June 1991.
- [18] ZOU, M. and GREEN, I., “Clearance control of a mechanical face seal,” *Tribology Transactions*, vol. 42, pp. 535–540, 1999.